


BRIDGING ARCTIC PATHWAYS: INTEGRATING HYDROLOGY,
GEOMORPHOLOGY AND REMOTE SENSING IN THE NORTH

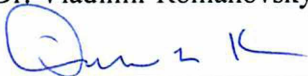
By

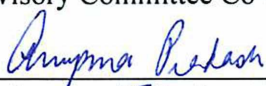
Erin D. Trochim

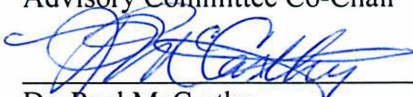
RECOMMENDED:


Mr. M. Torre Jorgenson


Dr. Vladimir Romanovsky

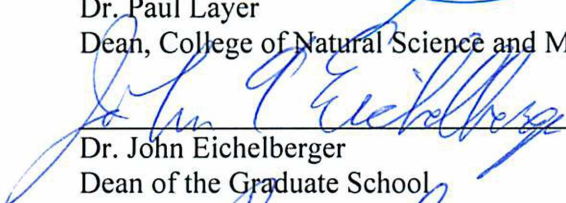

Dr. Douglas Kane
Advisory Committee Co-Chair


Dr. Anupma Prakash
Advisory Committee Co-Chair


Dr. Paul McCarthy
Chair, Department of Geosciences

APPROVED:


Dr. Paul Layer
Dean, College of Natural Science and Mathematics


Dr. John Eichelberger
Dean of the Graduate School


Date

BRIDGING ARCTIC PATHWAYS: INTEGRATING HYDROLOGY,
GEOMORPHOLOGY AND REMOTE SENSING IN THE NORTH

A
DISSERTATION

Presented to the faculty
of the University of Alaska Fairbanks

in Partial Fulfillment of the Requirements
for the degree of

DOCTOR OF PHILOSOPHY

By

Erin D. Trochim, M.S., B.S.

Fairbanks, Alaska

December 2015

Abstract

This work presents improved approaches for integrating patterns and processes within hydrology, geomorphology, ecology and permafrost on Arctic landscapes. Emphasis was placed on addressing fundamental interdisciplinary questions using robust, repeatable methods.

Water tracks were examined in the foothills of the Brooks Range to ascertain their role within the range of features that transport water in Arctic regions. Classes of water tracks were developed using multiple factor analysis based on their geomorphic, soil and vegetation characteristics. These classes were validated to verify that they were repeatable. Water tracks represented a broad spectrum of patterns and processes primarily driven by surficial geology. This research demonstrated a new approach to better understanding regional hydrological patterns.

The locations of the water track classes were mapped using a combination method where intermediate processing of spectral classifications, texture and topography were fed into random forests to identify the water track classes. Overall, the water track classes were best visualized where they were the most discrete from the background landscape in terms of both shape and content. Issues with overlapping and imbalances between water track classes were the biggest challenges. Resolving the spatial locations of different water tracks represents a significant step forward for understanding periglacial landscape dynamics.

Leaf area index (LAI) calculations using the gap-method were optimized using normalized difference vegetation index (NDVI) as input for both WorldView-2 and Landsat-7 imagery. The study design used groups to separate the effects of surficial drainage networks and the relative magnitude of change in NDVI over time. LAI values were higher for the WorldView-2 data and for each sensor and group combination the distribution of LAI values was unique. This study indicated that there are tradeoffs between increased spatial resolution and the ability to differentiate landscape features versus the increase in variability when using NDVI for LAI calculations.

The application of geophysical methods for permafrost characterization in Arctic road design and engineering was explored for a range of conditions including gravel river bars, burned tussock tundra and ice-wedge polygons. Interpretations were based on a combination of Direct-current resistivity - electrical resistivity tomography (DCR-ERT), cryostratigraphic information via boreholes and geospatial (aerial photographs & digital elevation models) data. The resistivity data indicated the presence/absence of permafrost; location and depth of massive ground ice; and in some conditions changes in ice content. The placement of the boreholes strongly influenced how geophysical data can be interpreted for permafrost conditions and should be carefully considered during data collection strategies.

Table of Contents

	Page
Signature Page.....	i
Title Page.....	iii
Abstract.....	v
Table of Contents.....	vii
List of Figures.....	xi
List of Tables.....	xv
Acknowledgements.....	xvi
Introduction.....	1
Chapter 1 Geomorphic and biophysical factors affecting water tracks in northern Alaska	8
1.1 Abstract.....	8
1.2 Background.....	8
Water tracks in the Arctic.....	10
Study area.....	11
Problem definition and motivation.....	13
1.3 Materials and methods.....	13
Sampling design and data collection.....	13
Data analysis.....	14
1.4 Results.....	16
MFA classification.....	16
Reliability of water track classes.....	17
1.5 Discussion.....	18
Usefulness of the classification methodology.....	18
Factors affecting occurrence/distribution of water track classes....	19
Definition of water tracks within periglacial environments.....	22
1.6 Conclusions.....	23

1.7 Acknowledgements.....	24
1.8 References.....	24
Chapter 2 Remote sensing of water tracks.....	47
2.1 Abstract.....	47
2.2 Introduction.....	47
2.3 Study area	50
2.4 Methods	51
Field data	51
Remotely sensed data	51
Intermediate clustering.....	52
Machine learning and post-processing.....	54
2.5 Results.....	55
Indicator species for water tracks and MESMA classification	55
Random forest results.....	56
2.6 Discussion.....	57
Applicability of the water track classification.....	57
Implications for permafrost research.....	58
Factors affecting classification performance.....	59
Alternative approaches	60
2.7 Conclusions.....	62
2.8 Acknowledgements.....	62
2.9 References.....	63
Chapter 3 Optimizing LAI estimates in the Arctic using remote sensing	85
3.1 Abstract.....	85
3.2 Introduction.....	85
3.3 Study area	87

3.4 Methods	88
Field data	88
Remotely sensed data	88
Calculation of fractional cover and LAI.....	89
Statistical and Spatial Examination of LAI.....	89
3.5 Results.....	90
NDVI versus derived LAI	90
Optimization of gap probability LAI estimates.....	91
3.6 Discussion.....	93
Usefulness of gap-method optimization for calculating LAI.....	93
Variation in LAI values.....	93
Effect of spatial resolution on LAI.....	95
3.7 Conclusions.....	96
3.8 Acknowledgements.....	97
3.9 References.....	97
Chapter 4 Geophysical and cryostratigraphic investigations for road design in northern Alaska	113
4.1 Abstract.....	113
4.2 Introduction.....	113
4.3 Methods	116
Regional setting and identification of terrain units	116
Site selection.....	117
Electrical resistivity tomography.....	117
Borehole and geospatial data.....	118
Permafrost description.....	118
4.4 Results.....	119

Site – AL2	119
Site – AR6	121
4.5 Analysis	123
Terrain units and permafrost properties	123
Combined cryostratigraphic and geophysical interpretations	124
Suitability of cryostratigraphic and geophysical methods for Arctic road construction and alternatives	127
4.6 Conclusions.....	129
4.7 Acknowledgements.....	129
4.8 References.....	130
Conclusion	149
References.....	152

List of Figures

	Page
Figure 1.1: Mechanisms of water transport in cold-region environments.	34
Figure 1.2: Water tracks are found extensively on hillslopes in the northern foothills of the Brooks Range, Alaska.	35
Figure 1.3: Location of the study which was centered on the Toolik Lake long-term ecological research (LTER) area.	36
Figure 1.4: Study design for dividing the water tracks into classes and replicating the results. ..	37
Figure 1.5: Hierarchical clustering for MFA dimensions 1 and 2 showing the five resulting water track classes.	38
Figure 1.6: Comparison of groups in different factors and their associated correlations for the MFA.	39
Figure 1.7: Conditional inference tree showing characteristics of water track classes after AUCRF variable selection where all splits are statistically significant ($p < 0.001$).	40
Figure 1.8: Final water track classes for the study area summarized including soil stratigraphy, soil texture, vegetation and geomorphology.	41
Figure 1.9: Water track class distributions over the study area. Insets show specific class examples.	42
Figure 1.10: Development of thermal erosion in water track.	43
Figure 1.11: Examples of features and processes influencing water tracks.	44
Figure 2.1: Comparing the affects between feature levels and feature size / scale for mapping water track properties on the North Slope of Alaska.	71
Figure 2.2: Water track classes in the Toolik Lake LTER.	72
Figure 2.3: Flowchart of input data and methodology.	73
Figure 2.4: Study area location showing locations of training and test plots overlaid on WorldView-2 imagery bands 5,4,2 and RGB input.	74
Figure 2.5: Vegetation and species identified for each water track class by calculating indicator values.	75
Figure 2.6: Input spectra used for MESMA classification.	76
Figure 2.7: Final water track classes overlaid over ASTER DEM with hillshade.	77

Figure 2.8: Inset examples of the water track classes which were majority filtered to aid interpretation.	78
Figure 2.9: Area of water track classes for the Toolik Thermokarst, Imnavait and Upper Kupuark watersheds.	79
Figure 2.10: Analysis of mineral-flark water tracks.	80
Figure 2.11: Water track classes compared to channels derived via DEM.	81
Figure 3.1: Development of groups to quantify effects of water tracks in the study area on the North Slope of Alaska.	104
Figure 3.2: Study area location showing WorldView-2 imagery (Bands 431 as RGB) used as input and the location of LAI ground-based measurements.	105
Figure 3.3: Summary of experimental design including input imagery and climatic variables.	106
Figure 3.4: Comparing median values of ground-derived LAI and NDVI between different groups by data acquired from Landsat-7 and WorldView-2 satellites.	107
Figure 3.5: Analysis of gap probability LAI results by group.	108
Figure 3.6: Residual results divided by group.	109
Figure 3.7: Location of each group compared to satellite-derived LAI values from each image date.	110
Figure 4.1: Stream meandering along ice wedges of high center ice-wedge polygons with the high bank of the Colville River in the background.	136
Figure 4.2: Study area showing field sites AR6 and AL2 with inset versions of aerial photographs and surficial geology.	137
Figure 4.3: Drilling with SIPRE corer at site AL4-2 in burned tussock tundra.	138
Figure 4.4: AL2 transect 1, 3 and 4 showing aerial photograph draped with 2 times vertical exaggeration and site photographs.	139
Figure 4.5: Cryostratigraphy and gravimetric water content (%) of frozen soils, site AL2.	140
Figure 4.6: Draped aerial photographs of AL2 transects 1, 3 and 4 with their corresponding DCR-ERT modeled resistivity (Ω m) below each.	141
Figure 4.7: AR6 transect 1, 2 and 3 showing aerial photograph draped with 2 times vertical exaggeration and site photographs.	142
Figure 4.8: Cryostratigraphy and gravimetric water content (%) of frozen soils, site AR6 (Bridge).	143

Figure 4.9: Draped aerial photographs of AR6 transects 1, 2 and 3 with their corresponding DCR-ERT modeled resistivity (Ω m) below each	144
Figure 4.10: Top surface of the small ice wedge, borehole AR6-2	145
Figure 4.11: : Comparison of subsurface characteristics derived from cryostratigraphic analysis (A, C & E) vs. geophysical interpretation (B, D & F) for AL2 transects 1, 3 and 4	146
Figure 4.12: Comparison of subsurface characteristics derived from cryostratigraphic analysis (A, C & E) vs. geophysical interpretation (B, D & F) for AR6 transects 1, 2 and 3	147

List of Tables

	Page
Table 1.1: Qualitative properties of clustered MFA classes	45
Table 1.2: Quantitative properties of clustered MFA classes (mean \pm standard deviation).	46
Table 2.1: Radiometric, spatial, and spectral resolutions of the WorldView-2 satellite imagery used for this study for each band.	82
Table 2.2: Final stacked raster dataset layers (n = 39) used as input for random forest models. .	83
Table 2.3: Model results from random forests for each water track class.	84
Table 3.1: Radiometric, spatial, and spectral resolutions of the WorldView-2 and Landsat 7 satellite imagery used for this study.....	111
Table 3.2: Final NDVI _g and NDVI _{back} values for each group and sensor.	112
Table 4.1: Site characteristics and descriptions of DCR-ERT, active layer depths and ice	148

Acknowledgements

Nine years ago I was lucky to have great mentors who strongly recommended graduate studies at the University of Alaska Fairbanks. During my masters, enthusiastic conversations with Larry Hinzman provided the impetus for my first proposal to examine water tracks in the beautiful foothills of the Brooks Range in Alaska. My partner, Matt Sprau joined the initial scouting mission. He was instrumental in observing that there were significant vegetative differences in water tracks and helped plan out my first sampling scheme.

This project would not have been possible without all the help, support, laughs and guidance during the many field seasons from 2008-2012. Michelle Brosius made it much more satisfying to hike many miles, learn latin plant names, and play many games of Canasta in the Silver Bullet. I really appreciated all the assistance and time spent in the field with: Torre Jorgenson, Nicole Farnham, John Mumm, Bill Schnabel, Jens Monk and Mischa Kanevskiy. The concepts, feedback and examples provided by Donald Walker, Ronald Daanen, Chien-Lu Ping and Thomas Hamilton were also invaluable.

Many thanks to all my graduate student colleagues over the years at UAF; it was great to explore both research and Alaska with you. Like any event which takes years of your life, my friends and family provided much needed support, humor and perspective. Thank-you Laura for keeping me active, Emily for re-introducing me to skijoring and Jodi for providing endless opportunities for fun. I also appreciated the encouragement of our local outdoor community who helped keep me balanced.

Most importantly, I want to sincerely thank Matt, Itty and Tarsis. My puppy secretaries were supportive at any hour of the day. All the dishes, meals, snuggles, howls and love were always appreciated. It took a family to finish this up.

Introduction

It is astounding how much and how little we know about the Arctic environment. In Alaska, we can walk on landscapes that experienced the first human footsteps on the continent. Visit the North Slope where dinosaurs once roamed. We drive our vehicles on highways mirrored by pipelines where 40 years ago it was just tundra, and 10,000 years ago there were glaciers. In a single place, the amount of variation over time is staggering. And yet by crossing over a ridgeline to the next valley it can be completely different. Understanding and quantifying this variability over the landscape has been a central theme to all of my Arctic research. My original foray into Arctic hydrology began with a simple goal: model the discharge patterns for the 2.2 km² Imnavait basin in the foothills of the North Slope of Alaska over 20 years. The initial questions I asked were: a) if we are successful in this basin, how do we know it will be applicable in the adjacent basin, and b) do we know if the basins are similar? These were critical considerations given that the over-arching plan was to predict discharge that would form the basis for estimating costs related to highway infrastructure, such as bridges and culverts. There are tens of thousands of individual basins in the North Slope area; to design appropriate infrastructure ideally we would predict discharge at a scale consistent with the original watershed. Inaccurate predictions could lead to over- or under-engineering and produce undesirable structural integrity and fiscal concerns.

Digital elevation models (DEMs) provide a conventional solution for estimating basin-wide discharge where they can be used to examine the channel networks and confirm their similarity. In our study area we had a DEM with 5 m horizontal resolution. This is relatively unusual on the North Slope where higher-resolution DEM data is restricted to intensive long-term studies or areas of economic interest. In Alaska elevation information is generally limited to either the Advanced Spaceborne Thermal Emission and Reflection Radiometer (ASTER) global DEM with a 30 m pixel size, or the United States Geological Survey (USGS) topographic maps which are only now being slowly updated from the versions produced in the 1950s. However, even with a higher-resolution DEM it was not possible to capture all of the topographic features that carry water off hill slopes in the small basin on the North Slope that I studied (Schramm et al., 2007). These preferential paths are also regionally known as water tracks. Water tracks are linear-curvilinear stripes that transport water on hill slopes. In theory they are a feature simply moving

water down an inclined surface, in practice there are complicating interactions among many biophysical factors.

In a periglacial (French and Thorn, 2006; French, 2000; Slaymaker, 2011) region like the North Slope, continuous permafrost appears to enhance water track existence due to lack of infiltration into deeper groundwater layers. Even though water continues downhill via a water track, the flow within water tracks can be convoluted by micro-topographic features, such as strang and hummocks, related to ice degradation, ice aggradation and heave related to permafrost. This means that even a DEM produced with high-resolution airborne light detection and ranging (LiDAR) would have difficulties delineating the water tracks based on topography alone. There are currently no studies on ice aggradation and heave in water tracks, and only minimal work documenting ice degradation (Fortier et al., 2007; Jorgenson et al., 2008). While these are important questions, the limiting factor to studies on hillslope hydrology and more specifically water tracks is still the same as with the drainage basins, how do we adequately quantify the processes within a zone with enough confidence to extrapolate the results reliably to adjacent areas?

During my observations of water tracks on hillslopes in the Imnavait, it became rapidly apparent that they didn't all look the same. Walker et al. (1994) had classified water tracks in the area as one of three plant communities: 1) *Betula nana* – *Rubus chamaemorus*; 2) *Eriophorum angustifolium* or 3) *Salix planifolia* ssp. *pulchra* - *Eriophorum angustifolium*. Why was the vegetation different in some water tracks? In general, changes in vegetation reflect differences in the underlying surficial geology and geomorphology. There were no studies addressing the geomorphology of water tracks other than in terms of elevation (McNamara et al., 1999). Limited mapping suggested water tracks were more widespread on the older Sagavanirktok deposits versus the younger Ikillik surfaces (Munger et al., 2008). How did the interplay between vegetation, geomorphology and surficial geology affect the water tracks? And what were the implications for the hydrologic and thermal gradients? First, we needed to know where they were and how to get a grasp on the system as a whole. If we could develop a classification system for the patterns observed in water tracks based on their geomorphic and ecological properties, this would make it easier to understand the major processes driving the development

of the water tracks. This would also offer a solid base from which to conduct more complex analysis.

Water tracks in the foothills of the Brooks Range have a larger significance than their status as a drainage feature. Channelized water has been documented spurring thermokarst and thermal erosion on the Dalton (Walker et al., 2008) and Richardson (Ferrians et al., 1969) highways. In a warming climate the movement of water in hydrological regimes affected by permafrost is comprised of dynamic and complex processes (Hinzman et al., 2013). Potential interactions exist between the ground thermal regime, vegetation, atmosphere and water cycle that are multifaceted (Callaghan et al., 2004) and have both physical and biogeochemical components. The broader hydrologic system, of which water tracks area are a headwater component, is already responding with variations in river discharge, precipitation, soil moisture, glacier area and volume (White et al., 2007) due to climatic variations in the Arctic (Serreze et al., 2000).

Warming has been documented on the North Slope since the early 1900s in permafrost temperatures (Lachenbruch and Marshall, 1986) with the greatest increase in the coastal regions (3 to 4 °C) compared to moderate increases south in the foothills (1 to 2 °C), with the most pronounced increases during winter months (Osterkamp, 2007). Permafrost in the foothills region may be the most vulnerable to change because it is closer to 0 °C (Osterkamp, 2008), warming significantly at depth (Hinzman et al., 2008) and complicated by snow water equivalent decreasing with increases in elevation (Homan and Kane, 2015). In order to infer these affects to features like water tracks the first order of business would be to understand the underlying geomorphology of the tracks. If we could get a handle on where specific types of water tracks were located this would provide a significant improvement towards spatially extrapolating ground temperatures, modeling hydrological regimes and understanding landscape dynamics.

Undertaking research to address topics like those of what types of water tracks exist and where they are located is inherently an interdisciplinary problem. Fundamentally, addressing multi-faceted issues requires the same steps as conventional problems: 1) defining the scope of the problems; 2) collecting appropriate data; and 3) using robust and repeatable analysis. The main difference between complex interdisciplinary and conventional research is the way

knowledge is leveraged; both within the scope of a project and in the sequence of steps required for reaching the research goals. In conventional research in established fields a customary dogma provides clear boundaries for what is already known, the data and methods that are appropriate and how to define realistic results. In interdisciplinary research, each field brings its own paradigm that may or may not provide sufficient guidelines for solving the issue at hand. Researchers engaging in interdisciplinary research must find ways to address realistic project designs and outcomes. The two main approaches to interdisciplinary research are: a) developing the skills to expertly apply existing methods to new fields; or b) collaborating with other specialized researchers with the necessary skills (Golde and Gallagher, 1999). In both of these approaches, it is critical to address where the gaps in knowledge and data are and the sequence required to build intermediate products.

Interdisciplinary research that focuses on the intersections between hydrology, permafrost, geomorphology and ecology has a rich history in the Alaskan Arctic going back to identifying Alaskan vegetation in the 1940s (Stoeckeler, 1949), bog studies in the Upper Kuskokwim in the early 1950s (Drury, 1956), consideration of Project Chariot at Cape Thompson in the late 1950s (Hobbie, 1997) and tundra studies in Barrow in the 1970s (Bliss et al., 1981). Within my main study area of the Imnavait, the R4D project in the mid-1980s provided a myriad of multidisciplinary information that allowed future researchers including myself to ask more complex questions such as why and where water tracks are different on hillslopes. Technological advances have also bolstered this type of research including the improved availability of remotely sensed imagery and powerful statistical packages becoming easier to access and apply. However, increasing the complexity of questions, data and techniques can also make it more convoluted to analyze and interpret results. Engaging in research questions especially those that are interdisciplinary in scope benefits from using innovative methods that help balance between incorporating finer details and complexity vs. the reproducibility of these details and the benefit they offer to analysis. Given that every project has a finite amount of time and resources available; data and methods which provide the best foundations for both current and future projects are even more valuable for addressing interdisciplinary research problems of greater complexity.

The initial step to improving our knowledge of water tracks in the foothills of the Brooks Range was to use better methods of quantifying the geomorphology including the ties between surficial geology environments (i.e. colluvial, organic) and soil characteristics. These geomorphic properties could then be used as input for a spatial classification using satellite imagery. The order in which these studies could be successfully executed was critical; without first generating water track classes based on their geomorphology mapping, efforts would be limited to simple presence / absence or general vegetation characteristics. Also, the current method of mapping water tracks was inefficient and used manual delineation (tracing by hand). Incorporating semi-automated techniques would allow bigger areas to be mapped more effectively. This idea of framing interdisciplinary research questions using optimal techniques and coherent approaches became the driving force behind my dissertation. I focused on identifying issues where the addition of specific knowledge would address fundamental gaps in our holistic understanding of water tracks. The challenge was to identify short-comings and to devise logical ways of addressing them using insights from a variety of fields.

If we could figure out why there were differences in water tracks and where the different types of water track classes were located, we would be closer towards modeling the relationships between the movement of water in the tracks and the implications for the permafrost and the ground thermal regime. Although these were the most important knowledge gaps, there were additional areas which could benefit from more in-depth study to meet the ultimate goal of understanding water tracks and their role in landscape evolution in the Arctic. Evaporation (Prowse et al., 2006) and the distribution of ground ice are two key components in understanding the processes in modern and future periglacial environments. Evapotranspiration, or the combined processes of evaporation and transpiration in plants is known to be affected by changes in moss or shrub cover (Blok et al., 2011) in tundra ecosystems. In terms of both moss and shrub cover there were obvious differences between non-water track and water track areas, as well as between the different types of water tracks. With this in mind I expanded my focus to improve calculations for leaf area index (LAI). LAI is an important component for modeling evapotranspiration and calculated using vegetation indexes which are affected by surficial soil moisture.

The distribution of ground ice is an important consideration in water track landscape evolution because thawing of ice-rich permafrost can cause the surface to settle or liquefy, and the amount and type directly relate to the amount of settlement (Jorgenson et al., 2008). While boreholes provide a direct way to examine ice characteristics of permafrost, geophysical techniques including capacitively coupled and direct current electrical resistivity tomography (CCR- and DCR-ERT) offer substantial advantages to extrapolating to larger areas (Hauck and Kneisel, 2006). However, the best practices for these techniques are still being developed. An opportunity presented itself to use DCR-ERT to examine permafrost characteristics for a potential road corridor extending from the Dalton Highway to Umiat, located in the center of the North Slope. Establishing more effective methods for using geophysics to map ground ice properties would be very valuable for future studies of water tracks.

With these ideas in mind, my dissertation is comprised of four different chapters. The details are as follows.

The first focus of my dissertation was to understand how the interplay between vegetation, geomorphology and surficial geology affected surficial drainage networks known as water tracks in the Toolik long term ecological research (LTER) area. I hypothesized that there was a range of geomorphic characteristics that could be quantified for water tracks. In order to do this we had to address how the classes could be identified and if they were robust enough to be repeatable. I also wanted to identify the basic factors affecting water track development. This would allow evaluation of the definition of water tracks in the Arctic and whether it needed refinement.

My second topic built off this classification and addresses whether water track distribution can be accurately and efficiently mapped. As input data, I combined my knowledge about water track morphology from my first topic with field survey data, high-spatial-resolution multi-spectral images and digital elevation model (DEM) properties. I hypothesized that: (1) water tracks could be efficiently delineated using remote sensing; (2) that the individual water track classes could be mapped; and (3) there would be spatial variability between the water track classes over the landscape. The goal was to move towards a semi-automated methodology which could be applied over larger regions of the North Slope of Alaska.

The third topic addressed improving spatial estimations of LAI in the same study area which are critical for predicting evapotranspiration rates, which are the largest unknown in the Arctic hydrological cycle. The main objective was to optimize LAI calculations using NDVI for both WorldView-2 and Landsat-7 imagery. The optimization was repeated for different groups based on: satellite (WorldView-2 vs. Landsat-7); surficial drainage (water tracks vs. other), and whether the NDVI values changed within a 10-day period. My hypotheses included: (1) optimization would be a robust addition to the gap-method of calculating LAI; (2) subdividing the data into groups would improve the LAI calculations; and (3) specific vegetation characteristics could be associated with LAI variability.

The final chapter focused on refining geophysical methods for quantifying permafrost characteristics for Arctic road design and engineering. The goal of this project was to evaluate the effectiveness of DCR-ERT and cryostratigraphy in delineating significant permafrost characteristics for Arctic road construction. There are few published best practices with respect to optimizing geophysical interpretation with boreholes in continuous permafrost areas. I present an interdisciplinary approach to site selection and interpretation of ground properties using geophysics and cryostratigraphic data obtained from drilling. I examine how optimization of DCR-ERT properties such as electrode spacing can be used to find the best resolution for the landscape and phenomena under investigation.

Chapter 1 Geomorphic and biophysical factors affecting water tracks in northern Alaska¹

1.1 Abstract

A better understanding of water movement on hillslopes in Arctic environments is necessary for evaluating the effects of climate variability. Drainage networks include a range of features that vary in transport capacity from rills to water tracks to rivers. This research focuses on describing and classifying water tracks, which are saturated linear-curvilinear stripes that act as first-order pathways for transporting water off of hillslopes into valley bottoms and streams. Multiple factor analysis was used to develop five water tracks classes based on their geomorphic, soil and vegetation characteristics. The water track classes were then validated using conditional inference trees, to verify that the classes were repeatable. Analysis of the classes and their characteristics indicate that water tracks cover a broad spectrum of patterns and processes primarily driven by surficial geology. This research demonstrates an improved approach to quantifying water track characteristics for specific areas, which is a major step towards understanding hydrological processes and feedbacks within a region.

1.2 Background

Hillslope drainage networks play an integral role in controlling the rate and timing of water movement from a catchment. In continuous permafrost environments, our observation is the lack of systematic insight into drainage networks leads to the assumption that they are homogeneous over the landscape. This severely limits our ability to understand the linkages between how geomorphology and ecology are related to hydrology and the ground thermal regime. In the foothills of northern Alaska this issue is particularly critical where the mean annual ground temperature is predicted to be between -2 and -0 °C by 2099 (Jafarov et al., 2012) and warming significantly at depth (Hinzman et al., 2008). Shrub expansion in drainage networks and hillslopes (Tape et al., 2006) is known to affect the thermal regime by lowering the albedo and capturing snow that serves to increase insulation (Sturm et al., 2001; Sturm et al., 2005; Tape et al., 2006). Massive ground ice, such as ice wedges (Kanevskiy et al., 2011) and buried glacier ice (Jorgenson, 2013), can occur close to the surface on hillslopes and next to drainage networks,

¹ Trochim, E.D., Jorgenson, M.T., Prakash, A. & Kane, D.L., Geomorphic and biophysical factors affecting water tracks in northern Alaska, submitted to *AGU Earth and Space Sciences*.

raising their potential for rapid degradation (Bowden et al., 2008). Thermokarst and thermal erosion development is strongly affected by water movement on hillslopes (Bowden et al., 2008). These effects could be further amplified in the future as climatic scenarios predict an increase in snow water equivalent for the Alaskan North Slope by the end of the century (Brown and Mote, 2009). The complexity of these factors (shrub expansion, massive ground ice, thermokarst/thermal erosion and increasing SWE) necessitates development of a classification system for characterizing the variability in drainage networks and a cohesive framework for evaluating the biophysical factors controlling their patterns.

Water moves from headwater hillslopes downstream following a variety of pathways common in Arctic environments (Figure 1.1) where drainage networks are affected by a variety of factors. These include freeze-thaw processes, the presence of snow and ice, organic soil accumulation and differential thermal and hydraulic properties between unfrozen and frozen ground. As the amount of water increases (i.e. as surface runoff or storage) it impacts the amount of heat and mass transfer to the surrounding ground. Gravity and pore pressure gradients advect sensible heat and temperature gradients induce conduction, while phase change either releases or consumes latent heat (Kane et al., 2001). Mass fluxes associated with erosion and sediment transport also amplify with greater amounts of discharge. Seasonally varying conditions, such as the development of the active layer and changes in the hydraulic conductivity of the soil material through phase change, affect the downslope movement of water. These factors are related to soil moisture, organic material depth and degree of decomposition (Hinzman et al., 1996) and advective and radiant energy fluxes, which control end-of-winter snowmelt (Quinton and Carey, 2008). Permafrost acts as a barrier to deeper groundwater infiltration and affects soil moisture and drainage (Kane et al., 1989). The presence of a porous organic layer underlain by a mineral soil creates a distinct contrast in hydraulic conductivity, which can cause the majority of flow to occur within the organic layer (Hinzman et al., 1991; Zheng and Moskal, 2009). Uneven surface and frost table topography on a hillslope (Quinton et al., 2009) can cause preferential wetting of certain areas due to lateral water fluxes. This enhanced soil moisture affects the rates of ground thaw, where wetter areas have higher rates of active layer development (Guan et al., 2010a). Enhanced flow has also been documented between inter-hummock areas, where the connected tortuosity between inter-hummock areas determines the runoff time for water to leave the

hillslope (Quinton and Marsh, 1998). There are similarities between inter-hummock flow and the more distinct features known as water tracks.

Water tracks in the Arctic

The natural function of water tracks in Arctic environments is to move water off hillslopes. Water tracks are linear-curvilinear saturated stripes that comprise the majority of the effective drainage network (McNamara et al., 1999) in the northern foothills of the Brooks Range (Figure 1.2). In these features water is confined to the active layer ($< 1\text{m}$) due to the presence of impermeable continuous permafrost (McNamara et al., 1998). Previous studies also documented an increase in the depth of the active layer (Hastings et al., 1989; Walker et al., 1994) in the near vicinity of water tracks. Jorgenson et al. (2008) describe water tracks as shallow depressions that are associated with supra-permafrost groundwater movement where reticulate and ataxitic ice is found at the permafrost surface (Jorgenson et al., 2008). Reticulate ice begins as desiccation cracks with vertical or diagonal orientation formed in early winter and becomes ice-rich through sublimation or segregation (Ping et al., 2008). Horizontal lens development is dependent on availability of water in saturated soil during freeze-back directed from the permafrost table upward. Ataxitic or suspended ice occurs after water accrues during repeated freeze-thaw cycles during active layer thinning over time, where the volumetric ice content generally exceeds 50% and may be up to 90% (Ping et al., 2008). One explanation for enhanced thaw in water track features is due to saturation of the organic mat throughout the majority of the summer, which augments the thermal conductivity of the track compared to the surrounding area and modifies the boundary condition of the upper mineral layer allowing increased warming (Kane et al., 2001). Saturated stripes in permafrost have also been documented in other regions including Seward Peninsula, Alaska (Hopkins and Sigafoos, 1951), foothills of the Alaska Range (Osterkamp et al., 2009), northern Quebec (Nicholson, 1978) and the Canadian High Arctic (Williams et al., 2008). The term water track was originally coined in the peatlands of Minnesota by Heinselman (1963). The existing literature points to an inadequate designation of how the term water track compares to features in other Arctic areas. It is also unclear how gullies differ from water tracks.

Characteristics of water tracks and how they develop over time in permafrost environments are poorly understood. Functionally, drainage networks develop based on minimized energy expenditures in self-organizing networks as in growth of rill complexes (Berger et al., 2010). Water tracks typically occupy repeat parallel spacing which is different from dendritic, rectangular or deranged drainage networks. Spacing of drainage channels is responsive to the amount of water flux over the drainage area, stream incision (advective erosion) and soil creep (diffusion-like mass transport) (Perron et al., 2008). The transition to incised channels occurs when the sediment transport capacity is greater than the sediment supply (Bledsoe et al., 2002). Under permafrost conditions there is normally an expansion of the drainage networks due to an increase in sediment yield (Bogaart et al., 2003). In the Imnavait basin (located within the Northern foothills of the Brooks Range) McNamara et al. (1999) proposed that water tracks formed on hillslopes where channels should exist. They suggested maturation of the channel network was limited by permafrost inhibiting erosion rates. Incision as gully development has been reported within water tracks (Osterkamp et al., 2009) and drainage networks (Bowden et al., 2008; Gooseff et al., 2009) over time. This supports the hypothesis that some water tracks will undergo thermal erosion and begin to develop into a more mature drainage network (Hinzman and Kane, 1992; McNamara et al., 1999). The potential for this to occur is dependent on multiple factors including the amount of water and the presence of massive ice to thaw. At this time there are insufficient data to understand where these processes are more likely to occur.

Study area

This study focuses on the area around the Toolik Lake long-term ecological research area and includes the Imnavait and Upper Kuparuk basins and Slope Mountain area (Figure 1.3). Permafrost in the Imnavait basin has been documented to be 250 to 300 m in depth (Osterkamp and Payne, 1981). The glacial history in the region can be broken into at least four separate glacial events with the two earliest dating from late Tertiary to early Pleistocene (Hamilton, 2002). The middle event occurred during the middle Pleistocene as the Sagavanirktok glaciation covered the area with glacial till and formed the incised rolling hills of the Imnavait and Upper Kuparuk basins (Hamilton, 1986). The last period of glaciation during the late Pleistocene was simultaneous to the late Wisconsin advances in North America and contained at least two advances (Itkillik I and II). Water tracks are more commonly found on the older Sagavanirktok

deposits versus the younger Itkillik surfaces (Munger et al., 2008). Geomorphic features in the region include high and low centered polygons, non-sorted circles, stripes, upland turf hummocks, solifluction features, pond complexes, wetland micro-relief and poorly- and well-developed hillslope water tracks (Walker and Maier, 2008). Evolution of the landscapes across these glacial deposits of differing ages has led to large differences in patterned ground and vegetation (Jorgenson, 1984). Although these works concur on the existence of water tracks, they do not explain the range of variation within the water tracks and the localized environmental factors contributing to their development.

Water tracks in the study area show an association between the type of vegetation and soil moisture as documented by Walker et al. (1994). Water tracks were classified as one of three potential plant communities: 1) *Betula nana* – *Rubus chamaemorus*; 2) *Eriophorum angustifolium* or 3) *Salix planifolia ssp. pulchra* - *Eriophorum angustifolium*. This is in contrast to nonsorted stone stripes dominated by *Cassiope tetragona* - *Calamagrostis inexplansa* and stream channels with *Carex aquatilis* - *Eriophorum angustifolium*. Additional vegetation characteristics of water tracks include increased above ground primary productivity of *Eriophorum vaginatum* by up to tenfold compared to the surrounding area as a response to the increase in nutrient flux to the root due to flowing water (Tsuyuzaki et al., 2008). In general *Salix planifolia ssp. pulchra* was found in the larger water tracks (Walker et al., 1994) potentially as a result of being more sensitive to nutrient availability than comparable areas with *Betula nana* (Matthes-Sears et al., 1988) although there may be a range of interactions (Myers-Smith et al., 2011). Shrubby vegetation is documented in both poorly and well-developed water tracks. Water tracks also showed a 5 to 15 fold increase in growth rate of *Sphagnum* spp. compared to non-water track areas (Guan et al., 2010b). While these studies illustrate that there are some differences between vegetation in both water tracks and the adjacent area as well as between the tracks themselves, the differentiation is simplistic and does not encapsulate the range of heterogeneity over the landscape. They also provide only a snap-shot of current conditions, without investigating the interactions between past vegetation and geomorphic conditions. These interactions are required for realistic predictions of future scenarios.

Problem definition and motivation

In summary, our current understanding of water tracks within the study area is limited to: 1) knowing they exist to transport water off of hillslopes; 2) water tracks can be associated with specific vegetation communities; and 3) that the organic layer and unfrozen component of the track plays a role in moving water. As discussed, there are more complex relationships occurring within water tracks in terms of how the geomorphology and ecology are impacting the hydrological and thermal gradients. The main problem addressed in this study was quantifying how geomorphic and biophysical characteristics differ among the range of water tracks. Accordingly, we had to figure out what classes of water tracks could be identified and if they could be replicated. This would allow us to identify the basic factors affecting water track development and their role in landscape evolution. We could also address if the definition of water tracks in the Arctic needed refinement. The process of classifying the water tracks, as well as the classes themselves is critical for providing fundamental baseline knowledge for further studies and monitoring future changes.

1.3 Materials and methods

Sampling design and data collection

The sampling was designed to collect data across the full range of water track conditions identified on aerial photographs within the Toolik Lake region. Sampling sites were clustered to permit easier access and those closest to road networks were prioritized. Collection of data took place during the summers of 2008, 2009 and 2010. Differential GPS measurements were used to precisely locate a network of 283 ground-verification points distributed in water tracks (Figure 1.3). Our general strategy was to sample each water track twice to capture variations over the hillslope. Vegetation percent cover was quantified over plots with sides of 1 to 2 m using the Braun-Blanquet approach (Mueller-Dombois and Ellenberg, 1974). The percent cover classes used were: r, present <5% of records; +, 5 – 10 %; I, 11 – 20%; II, 21 – 40%; III, 41-60%; IV, 61 – <80%; and V, ≥80%. Plants were described to the species level when possible guided by community compositions generated by Walker et al. (1994). The species level data was summed into the following functional groups using the midpoint of each percent cover class: low shrubs; erect dwarf shrubs; prostate dwarf shrubs; forbs; graminoids; and moss. Directly adjacent to each plot a small pit was excavated to describe soil properties and interpret geomorphic units using

standard methods (Schoeneberger et al., 2002). The fibrous peat was examined and differentiated into one of three plant remains: sphagnum; woody; or sedge. Organic soils were described using the following descriptors: near-surface moss and fibrous horizons (live moss, Oi–fibric horizons) or deeper and more decomposed horizons (generally Oe–hemic and Oa–sapric horizons). Soil textures were aggregated to their dominant matrix (clay, silt, loam, sand or gravel) for the purposes of analysis. Distinct changes in the dominant matrix of the mineral soil were used for discriminating horizons. The depth of the pit was approximately equal to the depth of thaw for the collection date. Surficial geology was assigned at each plot based on mapping by Walker and Maier (2008). They defined the following classes: 1) alluvial: stream deposits on modern and ancient floodplains; 2) colluvial: hillslope deposits whose origin is due primarily to downslope movement of material under the force of gravity which can include forces due to water movement; 3) organic; organic deposits deeper than 50 cm. Alluvial and organic surficial geology can be associated with water tracks (Walker and Maier, 2008). Slope percent was calculated using Star3i digital elevation data collected in September 2001 with a horizontal resolution of 5 m and an absolute vertical resolution of 2.7 m.

Data analysis

Water tracks were classified using multivariate techniques and the classes were validated using recursive partitioning techniques as shown in Figure 1.4. The dataset contained explanatory variables made up of quantitative and qualitative data types. Multiple factorial analysis (MFA) using the package FactoMineR (Husson et al., 2014) in program R (R Core Team, 2014) was used to cluster the geomorphology data into classes (Bécue-Bertaut and Pagès, 2008) by using blocks of variables to quantify the same object (I-objects \times J_k -variables; $k=1$ to K , $K=6$) (Singh et al., 2007). MFA weights data from the blocks using a consensus matrix, decreasing the chance of one block dominating when the principal component analysis (PCA) is applied (Escofier and Pagès, 1994). PCA produces factors that represent an optimized summary of the quantitative association between blocks and eigenvalues, which indicate the variance of the characterized data. PCA was run on both the blocks of variables and individual variables generating factors common to both (Bécue-Bertaut and Pagès, 2008). Clustering was applied to the principal components using classical Euclidean distance based on the hierarchical method with the generalized Ward's criterion (Bécue-Bertaut and Pagès, 2008). The significance of the

cluster description was evaluated using the v.test for the quantitative variables and chi-square and hypergeometric tests for the categorical data types.

The blocks of variables were selected using four criteria: (1) qualitative versus quantitative data; (2) features that could be mapped on the landscape level or estimated via remotely sensed data (*Geomorphology1* and *Geomorphology2*); (3) general soil properties (*Soil1* and *Soil3*); and (4) detailed soil stratigraphic information (*Soil2* and *Soil4*). Variables were designated as either active or passive. Active variables were used in the calculation of factors, while passive ones were only visualized after creation of the factors. Different versions of MFA explored the existence of more subtly expressed classes. Only the geomorphology and soil data were used when creating these potential classes to focus the results primarily on the physical processes. The final MFA selected used only the active blocks of *Geomorphology1* and *Geomorphology2*, while the remaining quantitative and qualitative blocks were plotted as supplementary data in addition to a block containing *Vegetation* (Veg). The variables included in the block were low shrubs (LS); erect dwarf shrubs (EDS); prostate dwarf shrubs (PDS); forbs (FORB); graminoids (GRAM); and moss; and shrub height.

Data collection methods changed between 2008 (124 ground points) and 2009/10 (159 ground points) to include the detailed soil stratigraphic conditions, depth to water table, and presence of strangs or aligned hummocks and flarks. Strangs and flarks are wetland features, which form perpendicular to the flow path, where strangs are raised areas while flarks are wet-saturated areas of standing water. In areas where flarks are not present, the aligned hummocks take on a similar form as strangs. The MFA technique accounted for the differences by substituting a new level of not-available (NA) for the qualitative variables and using the mean value for the class in the quantitative data. Rather than engage in synthesizing these variables, after the MFA analysis the 2008 data was reserved from further analysis.

Validation of the classes was confirmed through the use of conditional inference trees on the plots from 2009 and 2010, which use binary recursive partitioning based on a regression relationship (Hothorn et al., 2006). Two different variations of the method were run in the “party” package in R using the “ctree” and “cforest” functions (Hothorn et al., 2006; Strobl et al.,

2008; Strobl et al., 2007). “Ctree” builds a singular tree in comparison to the bootstrapped version of “cforest”, which used 1000 different variations with at least 6 different terminal nodes. Both methods partitioned data into branches using explanatory variables that terminated into nodes, which maximized the homogeneity of the response variables and the differences between nodes to determine the class. The process began with the global null hypothesis of independence being evaluated between any of the input variables and the response. If the hypothesis could not be rejected the branch was stopped. The criterion used for hypothesis testing was multiplicity adjusted p-values of less than 0.05 using the Bonferroni test type. Alternatively, the variable with the greatest connection to the response was selected and a split was implemented. In order to determine the accuracy of the method, the model was initialized using 80% of the data and evaluated using the remaining 20%. Both the initialization and evaluation datasets had similar distributions for the different classes. Because this is an ensemble method of many different combinations of trees, visualizing single versions is not an ideal representation. In order to produce a more accurate “ctree” version, variable selection used the AUCRF package (Calle et al., 2011). AUCRF is comprised of random forests and area under the curve. Each class was run as a binary end variable so that cross validation could be used to create an optimal selection.

1.4 Results

MFA classification

Five classes of water tracks were established from the MFA analysis. Visualization of the classes along the first and second dimensions (Dim), which explained 21.2 and 18.7% of the variance, respectively, showed substantial overlap among classes 1, 2, and 4, while classes 3 and 5 had higher separation (Figure 1.5). In terms of blocks of variables, *Geomorphology1* explains the majority of the variability in the first and second dimensions, while *Geomorphology2* dominates the remaining dimensions (Figure 1.6). In contrast, *Vegetation* and the two *Soil* blocks all cluster in similar space regardless of the dimension. The next subplots show the circle of correlations between different quantitatively grouped variables in the different MFA dimensions. Slope and width have strong opposing effects along dimension 2 (B and C in Figure 1.6). When gravel was grouped with clay, and sphagnum peat was grouped with sedge peat thickness, these variables were opposing factors most evident along dimensions 3 and 4 (C and D in Figure 1.6). Graminoid cover was strongly associated with dimension 3. Moss, low shrubs (LS) and erect

dwarf shrubs (EDS) form one group while shrub height (SHRUB_H) and forbs make up a second along dimensions 1 and 2. Overall, the analyses indicate that environmental variables had the largest effect, while the variables in *Soil2* and *Vegetation* formed smaller sub-groups with similar trends along all dimensions.

The MFA produced qualitative (Table 1.1) and quantitative (Table 1.2) properties for each of the classes and assessed their significance ($\alpha = 0.05$) among classes. Class 1 was distinguished by significant association with colluvial deposits, very low surface runoff, buried sphagnum and sedge peat, thick mineral soils, strangs or aligned hummocks and flarks, and high moss cover. Class 2 had colluvial material, lacked strangs or aligned hummocks, had frequent ponding and wet soils, and were narrow with high cover of erect dwarf shrubs. Class 3 also had colluvial material, gravel in 50% of cases, steep slopes ($> 13\%$) and high covers of erect dwarf shrubs and moss. Class 4 was dominated by organic surficial geology, saturated conditions and often had sphagnum underlain by graminoid peat in surface organics. Class 5 contained the widest water tracks and was often characterized by alluvial material. They had the greatest amount of soil layers and low shrubs.

Reliability of water track classes

The reliability of the MFA classes was evaluated using conditional inference trees. The random forest method (“cforest”) using all variables predicted the classes with 88% accuracy. AUCRF variable selection was used to constrain the number of variables for the “ctree” version and identified controlling variables similar to those produced by the MFA. After variable selection, the MFA classes were predicted with 77% accuracy (Figure 1.7). These analyses confirmed the importance of many of the variables highlighted in the MFA. Class 1 had a very high prediction probability based on the presence of colluvial deposits, strangs or aligned hummocks, and flarks. Class 2 had modest prediction probability, and depended on presence of colluvial deposits, lack of strangs or aligned hummocks, low slopes, and variable widths. It was frequently confused with class 3. The probability of predicting class 3 was mainly based on high slope angle. Class 4 had a very high prediction probability based on organic thickness. Class 5 had a low prediction probability, and was associated with high slopes.

Based on the factors dominating the classification, the classes were assigned common names that help differentiate the classes and aid recognition. Hereafter, the classes are referred to as *mineral-flark* (class 1), *narrow* (2), *steep* (3), *organic-rich* (4) and *wide* (5) water tracks.

1.5 Discussion

Usefulness of the classification methodology

During the development of the water track classification, data selection was a primary consideration. The advantage of our statistical analysis was that it retained information in its original context, unlike physically-based modeling where many geomorphic characteristics must be reduced down to their primary components, such as texture, porosity or permeability. Examining both qualitative and quantitative attributes simultaneously also offers clear benefits. Qualitative data collected using distinct parameters can often provide data in a more time-effective manner (i.e. relative soil moisture, soil texture) allowing a greater number of samples to be acquired. Some information, such as surficial geology (colluvial, alluvial, etc.) lends itself inherently to simple qualitative classes. For this project, the inclusion of the soil stratigraphic data into the MFA using modest categories like thickness and order of layers shed highly relevant information on the conditions. This will be discussed in greater detail in the next section. There were a number of possible groupings for organizing the data, however, that influenced the final classification. As the classes were non-unique, the key to this process was validating the reliability of the water track classes using an independent methodology to verify that the extracted classes were repeatable.

The combination of MFA and machine learning (via random forests and conditional inference trees) provided an essential framework for organizing, analyzing and interpreting a complex dataset to produce various classes of water tracks. Often, analysis of periglacial geomorphic features is done by pre-specifying scenarios of landscape processes and then fitting the data to meet these interpretations. Our methodology delayed the analytic explanation until the classifications could be reproduced via machine learning. Multiple trial and errors of the process also allowed the driving variables to be narrowed down to the major geomorphic characteristics. By setting the other variables as passive in the MFA, their effects were derived without actively influencing the classification process. Results from the random forest and conditional inference

tree analyses indicate that the additional variables can increase the accuracy of the class prediction. They also confirm that it is a combination of features within a water track that create conditions that are predominant enough to be statistically identified. This combination must be abundant enough that it is meaningful for a classifier. In summary, the main advantage of this approach is that the dominant trends driving the differences in the water tracks could be identified to minimize bias and maximize reliability.

Factors affecting occurrence/distribution of water track classes

The most important factor controlling the distribution and development of water tracks was the surficial geology. The MFA and conditional tree analyses confirmed that significantly different environments create lasting geomorphological conditions that influence water transport mechanisms into the present day. Water tracks vary over time depending on the localized response of vegetation to the climate where the surficial geology creates the initial conditions. Below we discuss some of the relevant factors that are most important to the individual classes and summarized in Figure 1.8.

The *mineral-flark* class was characterized mainly by colluvial deposits, the presence of clay and gravel and high graminoid and moss cover. In half of the plots, very low runoff and ericaceous peat as the top soil layer were observed. In many cases these plots appear to represent a transition from previously shrubby to graminoid dominated water tracks. In the MFA analysis (Figure 1.6C), clay and gravel were near to the graminoid conditions in ordination space. Moss appeared to be an intermediate state. The woody organic matter was opposite to clay/gravel/graminoid cluster and was associated with silt. The statistical analysis points to a distinct shift within this class of water tracks. As shown in Figure 1.9 (Class 1), water tracks classified as mineral-flark could be clearly identified due to the strong presence of bright-green graminoids. Mineral-flark plots in this area were associated with documented thermokarst activity (Figure 1.10). In this case downslope from the active thermokarst the water tracks became significantly incised. Active thermal erosion was observed as ice-rich colluvial material with entrained gravel and cobbles was thawed by both conductive surface heat and convectively by channelized running water. The interplay between increased incision of the water track, snow

(seen in Figure 1.11(A)) and the effects on ground thermal regimes and ice development are an important area for further study.

The *narrow* class was dominated by colluvial material with occasional to frequent ponding as shown in Figure 1.11 (B). Gravel and silt soils were present in a significant amount of the plots and the vegetation was mainly comprised of erect dwarf shrubs. Differences in the type of peat suggest that past conditions were wetter and promoted sedge development. As seen in Figure 1.9, some of the narrow water tracks appear similar to the areas between non-sorted stripes, which are found on the tops of most hills in the region. Non-sorted stripes maintain the stripe pattern by alternating depressed vegetation troughs with non-sorted ground. The stripes generally orient to the steepest angle slope (Nekola, 2004). The narrow water tracks are typically 2 - 6 m wide, as evident from the distinctive vegetation component, and the slope angles vary from 3 to 20 degrees. Ice-accumulation in the active areas of non-sorted circles, which are horizontal equivalent of stripes, can prevent vegetation from colonizing (Daanen et al., 2007). Frost heave is generally greatest with the finest sediments and in the foothills the non-sorted circles can quickly be revegetated by an organic mat (Walker et al., 2004). Vegetation can have a significant role in stabilizing non-sorted circles (Daanen et al., 2007; Walker et al., 2004), and frost heave generally decreases as the vegetation shifts to shrubs (Ping et al., 2008). It is plausible that water tracks could form in the vegetated troughs or margins of stripes. This is supported by the idea that on a hillslope the vegetation troughs are a natural runoff system (Bertoldi et al., 2006). Most interestingly, sphagnum responds to the addition of water in weakly developed tracks with a rapid increase in growth (Guan et al., 2010a), which would feedback into the stabilization of a non-sorted stripe and the creation of narrow water tracks.

The *steep* class was made up of organic surficial material that was often near saturation. In this class, peat stratigraphy transitioned from sedge to sphagnum and may point to a shift in ground ice content or rates of solifluction. Solifluction has been examined in silty swales in the region during both the late Pleistocene and Holocene (Hamilton, 2002). Field investigations in 2010 focused on documenting solifluction characteristics and they were found to varying degrees in each of the water tracks examined. Hummocks were found in and around water tracks where solifluction was more prominent and occurred with greater regular periodicity down the slope

than the adjacent areas as seen in Figure 1.11 (C). Between hummock and interhummock areas there were differences in soil moisture and vegetation. The tops of hummocks were generally drier and contained rooted *Betula nana* or *Salix planifolia* ssp. *Pulchra*, while the interhummock areas had higher soil moisture and were dominated by mosses. In water tracks characterized by *Carex aquatilis* - *Eriophorum angustifolium* vegetation, hummock development was observed both in the main channel and also on the margins which were predominated by *Salix planifolia* ssp. *pulchra*. The hummocks appear to be diverting and concentrating flow in a similar fashion as observed by Quinton and Marsh (1998). Although they do not appear to play a primary role in the formation of water tracks they create micro-topography within the tracks, which alters the soil moisture and vegetation. Since water tracks have enhanced moisture compared to the surrounding area it seems logical that there is a greater potential for solifluction to occur as a result.

The *organic-rich* class was dominated by peat-rich alluvium with frequent ponding and saturated soil conditions and often found downhill from the *narrow* class. The *organic-rich* class exhibited a different vegetation signature, which was dominated by over 50% cover of graminoids. Visual examination of the sites showed surficial indications of ice-wedge polygon networks (Figure 1.9). There are few studies concerning the formation of hillslope ice wedges and their relationship to drainage networks in Arctic regions. The most substantial work was conducted by Mackay (1995) who found ice wedges have been found to develop epigenetically on hillslopes, after surface materials stabilized, whereas, syngenetic wedges have been found at the base of the slope where sediments have continued accumulating. Mackay (1995) also found that polygonal development did not reflect current topography as material movement within the active layer was documented from the center of the polygons to the troughs through thermally induced mass transport regardless of the slope angle. The development and role of ice-wedge polygons in and around water tracks is of particular interest as thermokarst and thermal erosion has been documented, including thermokarst gullies (Gooseff et al., 2009) adjacent or in close proximity to the *organic-rich* class sites. Our field sites also contained water tracks with thermal erosion that had later stabilized as a more incised drainage channel. Further exploration of the role of ice wedge polygons and their relationship to particular types of water tracks is an area of interest.

The *wide* class was dominated by water tracks with an average width of 28 m and tall shrubs, representing a unique environment where some of the characteristics may have been influenced by glacial and/or topographic elements differently than the other water track classes. The extensive glacial history in the study area during both the earlier Pleistocene and more recent Holocene produced glacial-fluvial drainage networks typically characterized by gravels, cobbles and boulders depending on the magnitude of flows. In the Upper Kuparuk region there are distinct second-order streams that are well-incised topographically and often represent individual drainage basins (Figure 1.3). They have been previously described as relicts of either the later Sagavanirktok or the Itkillik I advances (Hamilton, 2002). These channels contain large, well-rounded boulders that likely underwent fluvial transport during the glacial regimes. Some of the wide water tracks also contained boulders and their surficial geology was considered alluvial. Although the Itkillik I did not descend into the main Upper Kuparuk valley, there was glacial drift on both the western ridge and within the upper bowl of the basin which may have also had an influence in some cases.

Definition of water tracks within periglacial environments

The five water track classes all preferentially transport water down the hill-slopes. The geomorphic environment (alluvial, colluvial, organic or glacial) uniquely affects the resulting soil and organic layer stratigraphy. This both reflects and feeds-back into the overlying vegetation and underlying permafrost conditions. Water tracks differ from rills or gullies in that they should not be defined by incision alone in periglacial environments. While sections of water tracks may differently transport water due to their topographic gradients, in periglacial environments it is the combination of steepest-path and/or hydraulic conductivity of the surficial organic material (Hinzman et al., 1996) which contribute to enhanced water transport and nutrient availability. Water tracks can be associated with a range of other features and processes including: thermokarst, thermal erosion, non-sorted stripes, solifluction, inter-hummock flow, ice-wedge polygons and glacial-fluvial drainages. The use of water track as a broad term for preferential flow paths where there is a broad spectrum of patterns and processes associated with the features should be continued with the understanding that for specific regions they can be subdivided into classes to quantify the variability within that region

The stratigraphy of the organic layer clearly points to water tracks evolving as vegetation, nutrients, snow, active layer depth and ground ice respond over time. In this context, water tracks are associated with climate-driven, ecosystem-modified permafrost (Jorgenson et al., 2010). The transitions among sphagnum, ericaceous and sedge peat layers over time evident in the soil stratigraphy, and the spatial variation among the different classes, indicate that water tracks adjust to variations in temperature and precipitation. Changes in the organic layers also affect the type and amount of heat and moisture transfer. Permafrost and ground ice continue to persist in this region of continuous permafrost, as the overall summer heat flux within water tracks is not sufficient to overcome the larger winter heat losses. The permafrost helps water tracks persist by preventing infiltration into deeper groundwater system. The availability of water also allows ice to aggrade over time if the climatic or vegetation and soil organic matter accumulation permit. Sphagnum, in particular, may play an important role in affecting active-layer dynamics and ice aggradation.

Understanding how water tracks differ within a region in terms of their geomorphology is a critical factor for studies regarding hydrology, ecology and permafrost. In particular, the types and locations of water tracks need to be included in long-term monitoring projects. The evolution and response of water tracks to changing climatic conditions will vary depending on the type of water track and the interactions between the formative factors. This research points to a need to better understand the relationship between the surficial properties and the type and distribution of ground ice. Water tracks are most likely to rapidly evolve when in close proximity to the form of ground ice where thermal erosion is possible. Vegetation plays a key role in supplementing the identification of the geomorphic and hydrologic components in water tracks and will be crucial for remote quantification over larger scales in the Arctic.

1.6 Conclusions

Water tracks represent a range of preferential flow paths in periglacial landscapes. Understanding how water tracks differ within a region in terms of their geomorphology is a critical factor for studies regarding hydrology, ecology and permafrost. We differentiated five water track classes using robust statistical methods that effectively partitioned a wide range of

biophysical factors. This methodology minimized bias and maximized reliability of the classification system that can be used for organizing, analyzing and interpreting complex data associated with water track development. Our analyses revealed that water track patterns are controlled primarily by surficial geology, although we found interactions among a wide range of factors. Water tracks were connected with an assortment of other features and processes including: thermokarst, thermal erosion, non-sorted stripes, solifluction, inter-hummock flow, ice-wedge polygons and glacial-fluvial drainages. These features and processes are all fundamentally controlled by slope, climate and surficial geology. These factors in turn determine soil texture and control the type and amount of ground ice. Snow, vegetation and cracking/heave are all related to soil moisture. Together, these factors affect the hydrologic conductivity found in different types of water tracks, their ability to carry water in both the surface and subsurface and store or retain water. This classification of water tracks, and the recognition that the patterns respond to a wide range of interacting factors, complicates predictions of how they will response to projected climate change.

1.7 Acknowledgements

This project was supported by a National Aeronautics and Space Administration (NASA) Earth & Space Science Graduate Fellowship (NNX09AN42H), with additional resources provided by the Alaska Water Resources Association and the University of Alaska Fairbanks including the Center for Global Change, the Graduate School and Department of Geosciences. World-View 2 imagery was acquired through the National Geospatial Agency Commercial Data Archive. Symbols for figures courtesy of the Integration and Application Network (ian.umces.edu/symbols/), University of Maryland Center for Environmental Science. Field assistance was provided by Michelle Brosius, Nicole Farnham, John Mumm and Matt Sprau with additional support by the Toolik Lake Research Station. Special thanks to Donald Walker, Ronald Daanen, Chien-Lu Ping and Thomas Hamilton for their teaching and guidance.

1.8 References

Bécue-Bertaut, M., and Pagès, J., 2008, Multiple factor analysis and clustering of a mixture of quantitative, categorical and frequency data: *Computational Statistics & Data Analysis*, v. 52, no. 6, p. 3255-3268.

Berger, C., Schulze, M., Rieke-Zapp, D., and Schlunegger, F., 2010, Rill development and soil erosion: a laboratory study of slope and rainfall intensity: *Earth Surface Processes and Landforms*, v. 35, no. 12, p. 1456-1467.

Bertoldi, G., Rigon, R., and Over, T. M., 2006, Impact of watershed geomorphic characteristics on the energy and water budgets: *Journal of Hydrometeorology*, v. 7, no. 3, p. 389-403.

Bledsoe, B. P., Watson, C. C., and Bierdenharn, D. S., 2002, Quantification of incised channel evolution and equilibrium: *Journal of the American Water Resources Association*, v. 38, no. 3, p. 861-870.

Bogaart, P. W., Tucker, G.E. & de Vries, J.J., 2003, Channel network morphology and sediment dynamics under alternating periglacial and temperature regimes: a numerical simulation study: *Geomorphology*, v. 54, p. 257-277.

Bowden, W. B., Gooseff, M. N., Balser, A., Green, A., Peterson, B. J., and Bradford, J., 2008, Sediment and nutrient delivery from thermokarst features in the foothills of the North Slope, Alaska: Potential impacts on headwater stream ecosystems: *Journal of Geophysical Research-Biogeosciences*, v. 113, no. G2, p. G02026-G02038.

Brown, R. D., and Mote, P. W., 2009, The Response of Northern Hemisphere Snow Cover to a Changing Climate: *Journal of Climate*, v. 22, no. 8, p. 2124-2145.

Calle, M. L., Urrea, V., Boulesteix, A.-L., and Malats, N., 2011, Auc-rf: a new strategy for genomic profiling with random forest: *Human Heredity*, v. 72, no. 2, p. 121-132.

Carey, S. K., and Woo, M. K., 2000, The role of soil pipes as a slope runoff mechanism, Subarctic Yukon, Canada: *Journal of Hydrology*, v. 233, no. 1-4, p. 206-222.

Daanen, R. P., Misra, D., and Epstein, H., 2007, Active-layer hydrology in nonsorted circle ecosystems of the arctic tundra: *Vadose Zone Journal*, v. 6, no. 4, p. 694-704.

Dingman, S. L., 1973, Effects of permafrost on stream flow characteristics in the discontinuous permafrost zone of central Alaska, in *Proceedings Second International Conference on Permafrost*, Yakutsk, Siberia, National Academy of Sciences, p. 447-452.

Escofier, B., and Pagès, J., 1994, Multiple factor analysis (AFMULT package): *Computational Statistics & Data Analysis*, v. 18, no. 1, p. 121-140.

Gooseff, M. N., Balser, A., Bowden, W. B., and Jones, J. B., 2009, Effects of Hillslope Thermokarst in Northern Alaska: *Eos*, v. 90, no. 4, p. 29-36.

Guan, X. J., Spence, C., and Westbrook, C. J., 2010a, Shallow soil moisture - ground thaw interactions and controls - Part 2: Influences of water and energy fluxes: *Hydrology and Earth System Sciences*, v. 14, no. 7, p. 1387-1400.

Guan, X. J., Westbrook, C. J., and Spence, C., 2010b, Shallow soil moisture - ground thaw interactions and controls - Part 1: Spatiotemporal patterns and correlations over a subarctic landscape: *Hydrology and Earth System Sciences*, v. 14, no. 7, p. 1375-1386.

Hamilton, T. D., 1986, Late Cenezoic glaciation of the Central Brooks Range: *Alaska Geological Society*, 9-49.

Hamilton, T. D., 2002, *Glacial geology of the Toolik Lake and Upper Kuparuk River region*: University of Alaska Fairbanks, 26.

Hastings, S. J., Luchessa, S. A., Oechel, W. C., and Tenhunen, J. D., 1989, Standing biomass and production in water drainages of the foothills of the Philip Smith Mountains, Alaska: *Holarctic Ecology*, v. 12, p. 304-311.

Heinselman, M. L., 1963, Forest Sites, Bog Processes, and Peatland Types in the Glacial Lake Agassiz Region, Minnesota: Ecological Monographs, v. 33, no. 4, p. 327-374.

Hinzman, L. D., Gieck, R. E., and Kane, D. L., 2008, Spatial and temporal variation of soil temperatures and arctic hydrology in the Kuparuk River Basin, Alaska, in Proceedings Ninth International Conference on Permafrost, Fairbanks, AK, U.S., Volume 1, Institute of Northern Engineering, p. 711-716.

Hinzman, L. D., and Kane, D. L., 1992, Potential response of an Arctic watershed during a period of global warming: Journal of Geophysical Research-Atmospheres, v. 97, no. D3, p. 2811-2820.

Hinzman, L. D., Kane, D. L., Benson, C. S., and Everett, K. R., 1996, Energy balance and hydrological processes in an Arctic watershed, in Reynolds, J. F., and Tenhunen, J. D., eds., Ecological Studies; Landscape function and disturbance in Arctic tundra, Springer-Verlag; Springer-Verlag New York, Inc., p. 131-154.

Hinzman, L. D., Kane, D. L., Gieck, R. E., and Everett, K. R., 1991, Hydrologic and thermal-properties of the active layer in the Alaskan Arctic: Cold Regions Science and Technology, v. 19, no. 2, p. 95-110.

Hinzman, L. D., Kane, D. L., and Everett, K. R., 1993, Hillslope Hydrology in an Arctic Setting, in Proceedings Sixth International Conference on Permafrost, Beijing, China, p. 267-271.

Hopkins, D. M., and Sigafos, R. S., 1951, Frost action and vegetation patterns on Seward Peninsula, Alaska, in U.S. Geological Survey, ed., Volume Bulletin 974-C: Washington, D.C., p. 51- 100.

Hothorn, T., Hornik, K., and Zeileis, A., 2006, Unbiased recursive partitioning: A conditional inference framework: Journal of Computational and Graphical Statistics, v. 15, no. 3, p. 651-674.

Husson, F., Josse, J., Le, S., and Mazet, J., 2014, FactoMineR: Multivariate Exploratory Data Analysis and Data Mining with R.

Jafarov, E. E., Marchenko, S. S., and Romanovsky, V. E., 2012, Numerical modeling of permafrost dynamics in Alaska using a high spatial resolution dataset: The Cryosphere Discuss., v. 6, no. 1, p. 89-124.

Jorgenson, M. T., 1984, The response of vegetation to landscape evolution on glacial till near Toolik Lake, Alaska, in Proceedings Proceedings of an International Symposium on Inventorying Forest and Other Vegetation of the High Latitude and High Altitude Regions, p. 134-142.

Jorgenson, M. T., 2013, Thermokarst Terrains, in Schroeder, J., ed., Treatise on Geomorphology: San Diego, Academic Press, p. 313-324.

Jorgenson, M. T., Romanovsky, V., Harden, J., Shur, Y., O'Donnell, J., Schuur, E. A. G., Kanevskiy, M., and Marchenko, S., 2010, Resilience and vulnerability of permafrost to climate change: Canadian Journal of Forest Research, v. 40, no. 7, p. 1219-1236.

Jorgenson, M. T., Shur, Y. L., and Osterkamp, T. E., 2008, Thermokarst in Alaska, in Proceedings Ninth International Conference on Permafrost, Fairbanks, AK, Volume 4, Institute of Northern Engineering, p. 869-876.

Kane, D. L., Hinkel, K. M., Goering, D. J., Hinzman, L. D., and Outcalt, S. I., 2001, Non-conductive heat transfer associated with frozen soils: Global and Planetary Change, v. 29, no. 3-4, p. 275-292.

Kane, D. L., Hinzman, L. D., Benson, C. S., and Everett, K. R., 1989, Hydrology of Imnavait Creek, an arctic watershed: Holarctic Ecology, v. 12, p. 262-271.

Kanevskiy, M., Shur, Y., Fortier, D., Jorgenson, M. T., and Stephani, E., 2011, Cryostratigraphy of late Pleistocene syngenetic permafrost (yedoma) in northern Alaska, Itkillik River exposure: *Quaternary Research*, v. 75, no. 3, p. 584-596.

Mackay, J. R., 1995, Ice wedges on hillslopes and landform evolution in the late Quaternary, Western Arctic Coast, Canada: *Canadian Journal of Earth Sciences*, v. 32, no. 8, p. 1093-1105.

Matthes-Sears, U., Matthes-Sears, W. C., Hastings, S. J., and Oechel, W. C., 1988, The Effects of Topography and Nutrient Status on the Biomass, Vegetative Characteristics, and Gas Exchange of Two Deciduous Shrubs on an Arctic Tundra Slope: *Arctic and Alpine Research*, v. 20, no. 3, p. 342-351.

McNamara, J. P., Kane, D. L., and Hinzman, L. D., 1998, An analysis of streamflow hydrology in the Kuparuk River basin, Arctic Alaska: A nested watershed approach: *Journal of Hydrology*, v. 206, no. 1-2, p. 39-57.

McNamara, J. P., Kane, D. L., and Hinzman, L. D., 1999, An analysis of an arctic channel network using a digital elevation model: *Geomorphology*, v. 29, p. 339-353.

Mueller-Dombois, D., and Ellenberg, H., 1974, *Aims and methods of vegetation ecology*, New York, John Wiley & Sons.

Munger, C. A., Walker, D. A., Maier, H. A., and Hamilton, T. D., 2008, Spatial analysis of glacial geology, surficial geomorphology, and vegetation in the Toolik Lake region: Relevance to past and future land-cover changes, in *Proceedings Ninth International Permafrost Conference*, Fairbanks, AK, Institute of Northern Engineering, p. 1255-1260.

Myers-Smith, I. H., Forbes, B. C., Wilmking, M., Hallinger, M., Lantz, T., Blok, D., Tape, K., Macias-Fauria, M., Sass-Klaassen, U., Lévesque, E., Boudreau, S., Ropars, P., Hermanutz, L., Trant, A., Collier, L. S., Weijers, S., Rozema, J., Rayback, S. A., Schmidt, N. M., Schaepman-Strub, G., Wipf, S., Rixen, C., Ménard, C. B., Venn, S., Goetz, S. J., Andreu-Hayles, L., Elmendorf, S., Ravolainen, V., Welker, J. M., Grogan, P., Epstein, H. E., and Hik, D. S., 2011, Shrub expansion in tundra ecosystems: dynamics, impacts and research priorities: *Environmental Research Letters*, v. 6, no. 4, p. 045509.

Nekola, J. C., 2004, Vascular plant compositional gradients within and between Iowa fens: *Journal of Vegetation Science*, v. 15, no. 6, p. 771-780.

Nicholson, F. H., 1978, Permafrost distribution and characteristics near Schefferville, Quebec: Recent studies, in *Proceedings Third International Conference on Permafrost*, Edmonton, AB, p. 427-433.

Osterkamp, T. E., Jorgenson, M. T., Schuur, E. A. G., Shur, Y. L., Kanevskiy, M. Z., Vogel, J. G., and Tumskey, V. E., 2009, Physical and Ecological Changes Associated with Warming Permafrost and Thermokarst in Interior Alaska: *Permafrost and Periglacial Processes*, v. 20, no. 3, p. 235-256.

Osterkamp, T. E., and Payne, M. W., 1981, Estimates of permafrost thickness from well logs in northern Alaska: *Cold Regions Science and Technology*, v. 5, no. 1, p. 13-27.

Oswood, M. W., Everett, K. R., and Schell, D. M., 1989, Some physical and chemical characteristics of an Arctic beaded stream: *Holarctic Ecology*, v. 12, no. 3, p. 290-295.

Perron, J. T., Dietrich, W. E., and Kirchner, J. W., 2008, Controls on the spacing of first-order valleys: *Journal of Geophysical Research-Earth Surface*, v. 113, no. F4, p. F04016-F04037.

Ping, C. L., Michaelson, G. J., Kimble, J. M., Romanovsky, V. E., Shur, Y. L., Swanson, D. K., and Walker, D. A., 2008, Cryogenesis and soil formation along a bioclimate gradient in Arctic North America: *Journal of Geophysical Research-Biogeosciences*, v. 113, no. G3, p. G03S12-G03S26.

Quinton, W. L., Bemrose, R. K., Zhang, Y. S., and Carey, S. K., 2009, The influence of spatial variability in snowmelt and active layer thaw on hillslope drainage for an alpine tundra hillslope: *Hydrological Processes*, v. 23, no. 18, p. 2628-2639.

Quinton, W. L., and Carey, S. K., 2008, Towards an energy-based runoff generation theory for tundra landscapes: *Hydrological Processes*, v. 22, no. 23, p. 4649-4653.

Quinton, W. L., and Marsh, P., 1998, The influence of mineral earth hummocks on subsurface drainage in the continuous permafrost zone: *Permafrost and Periglacial Processes*, v. 9, no. 3, p. 213-228.

R Core Team, 2014, *R: A Language and Environment for Statistical Computing*: Vienna, Austria, R Foundation for Statistical Computing.

Schoeneberger, P. J., Wysocki, D. A., Benham, E. C., and Broderson, W. D., 2002, Fieldbook for describing and sampling soils, Version 2.0. , in *Natural Resources Conservation Service*, ed.: Lincoln, NE, National Soil Survey Center.

Singh, K., Malik, A., Sinha, S., and Singh, V., 2007, Multi-Block Data Modeling for Characterization of Soil Contamination: A Case Study: *Water, Air, & Soil Pollution*, v. 185, no. 1, p. 79-93.

Strobl, C., Boulesteix, A.-L., Kneib, T., Augustin, T., and Zeileis, A., 2008, Conditional variable importance for random forests: *BMC Bioinformatics*, v. 9, no. 1, p. 307.

Strobl, C., Boulesteix, A., Zeileis, A., and Hothorn, T., 2007, Bias in random forest variable importance measures: Illustrations, sources and a solution: *BMC Bioinformatics*, v. 8, no. 25, p. 21.

Sturm, M., McFadden, J. P., Liston, G. E., Chapin, F. S., Racine, C. H., and Holmgren, J., 2001, Shrub Interactions in Arctic Tundra: A Hypothesis with Climatic Implications: *Journal of Climate*, v. 14, no. 3, p. 336-344.

Sturm, M., Schimel, J., Michaelson, G., Welker, J. M., Oberbauer, S. F., Liston, G. E., Fahnestock, J., and Romanovsky, V. E., 2005, Winter biological processes could help convert arctic tundra to shrubland: *Bioscience*, v. 55, no. 1, p. 17-26.

Tape, K., Sturm, M., and Racine, C., 2006, The evidence for shrub expansion in Northern Alaska and the Pan-Arctic: *Global Change Biology*, v. 12, p. 686-702.

Tsuyuzaki, S., Sawada, Y., Kushida, K., and Fukuda, M., 2008, A preliminary report on the vegetation zonation of palsas in the Arctic National Wildlife Refuge, northern Alaska, USA: *Ecological Research*, v. 23, no. 4, p. 787-793.

Vandenberghe, J., and Woo, M. K., 2002, Modern and ancient periglacial river types: *Progress in Physical Geography*, v. 26, no. 4, p. 479-506.

Walker, D. A., Epstein, H. E., Gould, W. A., Kelley, A. M., Kade, A. N., Knudson, J. A., Krantz, W. B., Michaelson, G., Peterson, R. A., Ping, C. L., Reynolds, M. K., Romanovsky, V. E., and Shur, Y., 2004, Frost-boil ecosystems: Complex interactions between landforms, soils, vegetation and climate: *Permafrost and Periglacial Processes*, p. 171-188.

Walker, D. A., and Maier, H. A., 2008, Vegetation in the vicinity of the Toolik Field Station, Alaska: *Institute of Arctic Biology*.

Walker, M. D., Walker, D. A., and Auerbach, N. A., 1994, Plant communities of a tussock tundra landscape in the Brooks Range Foothills, Alaska: *Journal of Vegetation Science*, v. 5, p. 843-866.

Williams, M., Bell, R., Spadavecchia, L., Street, L. E., and Van Wijk, M. T., 2008, Upscaling leaf area index in an Arctic landscape through multiscale observations: *Global Change Biology*, v. 14, no. 7, p. 1517-1530.

Zheng, G., and Moskal, L. M., 2009, Retrieving Leaf Area Index (LAI) Using Remote Sensing: Theories, Methods and Sensors: *Sensors*, v. 9, no. 4, p. 2719-2745.

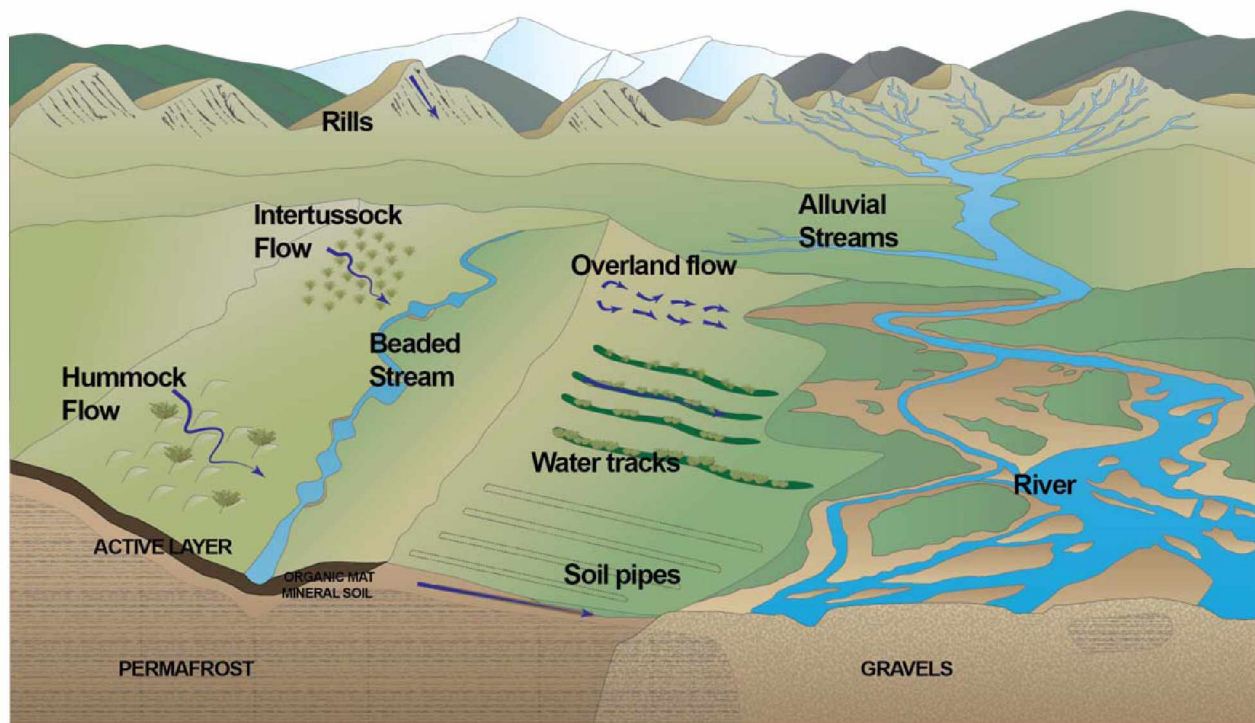


Figure 1.1: Mechanisms of water transport in cold-region environments.

Including overland flows (Bogaart et al., 2003), rills, intertussock (Dingman, 1973) and hummock flows (Quinton and Marsh, 1998), soil pipes (Carey and Woo, 2000), water tracks (Hinzman et al., 1993), beaded streams (Oswood et al., 1989) and larger alluvial streams and rivers (Vandenberghe and Woo, 2002).

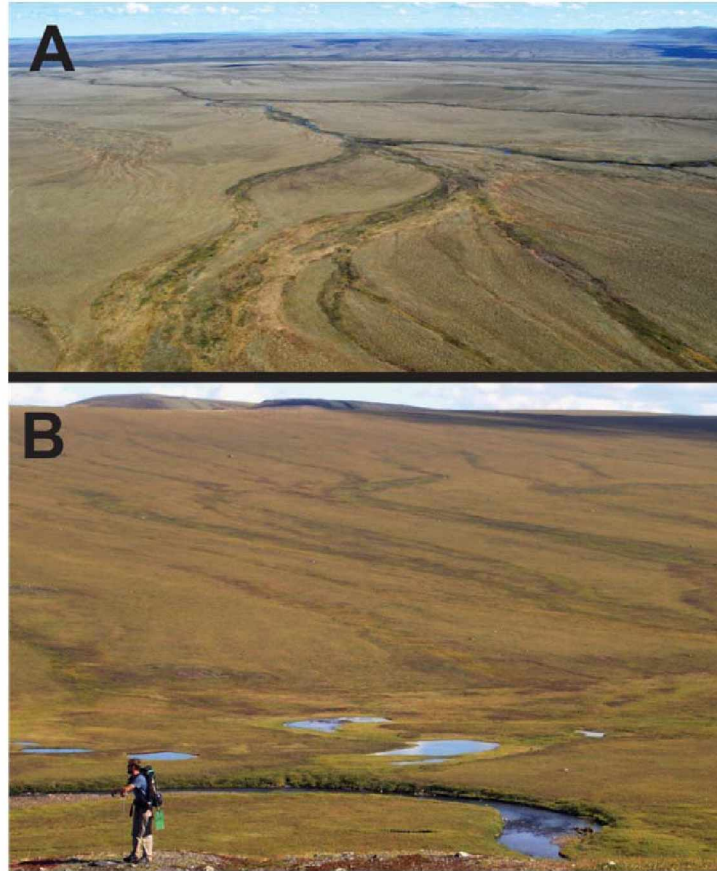


Figure 1.2: Water tracks are found extensively on hillslopes in the northern foothills of the Brooks Range, Alaska.

A) Variations occur between water tracks in terms of width, length, incision and vegetation. B) View of water tracks on the slope in the background looking east across the Upper Kuparuk River valley. Photos: E.D. Trochim, A) June 19, 2011, B) August 5, 2007.

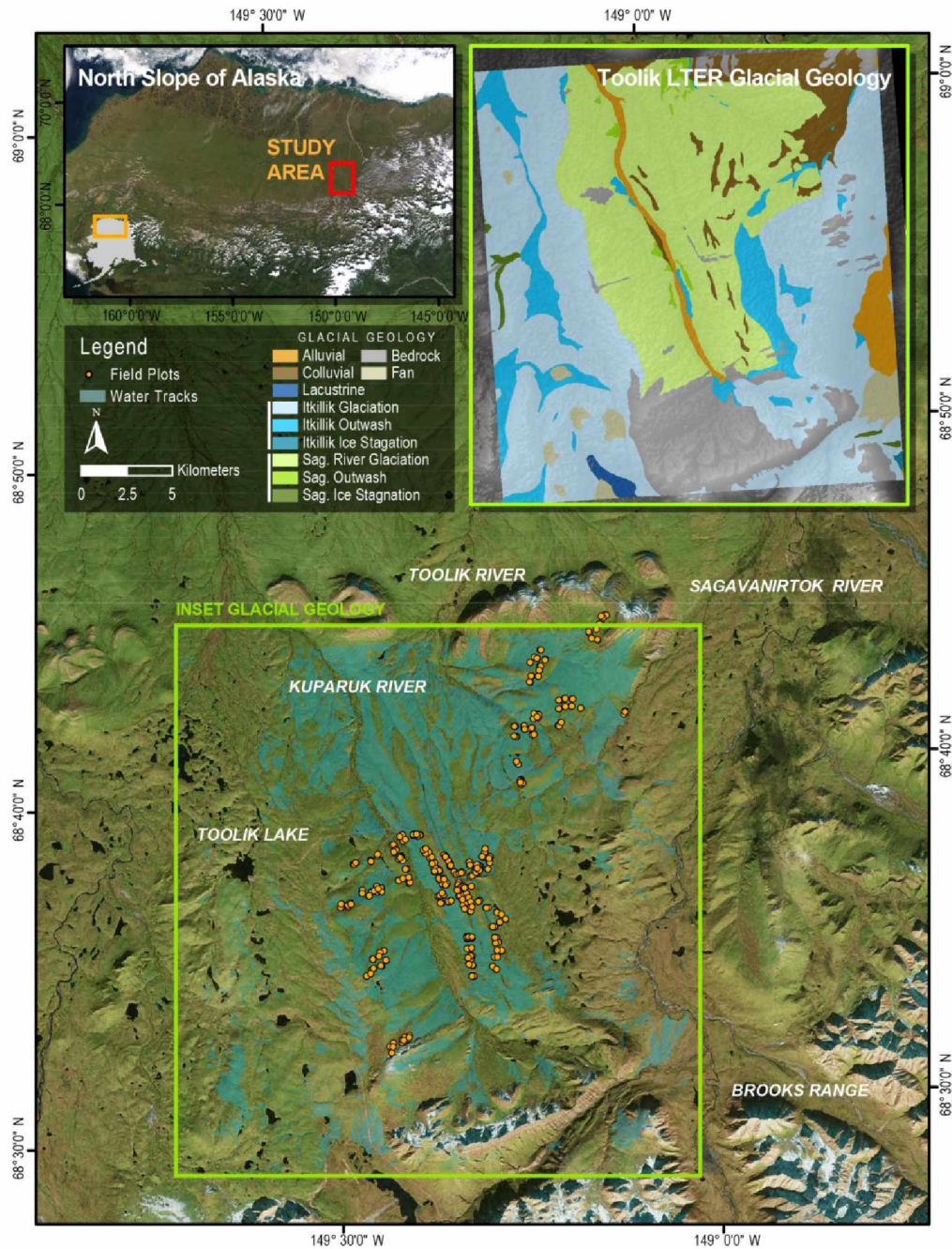


Figure 1.3: Location of the study which was centered on the Toolik Lake long-term ecological research (LTER) area.

The main panel shows the locations of the field sites (plots) in comparison to the generalized distribution of water tracks mapped by Walker and Maier (2008). The glacial geology of Toolik long-term ecological research (LTER) area (adapted from Hamilton, 2002) is shown in the top right, where the generalized water track distribution correlates to the Sagavanirtoq River Glaciation. *Imagery*: Main: SDMI Best Data Layer showing medium resolution Landsat imagery via Geographic Information Network of Alaska (GINA).

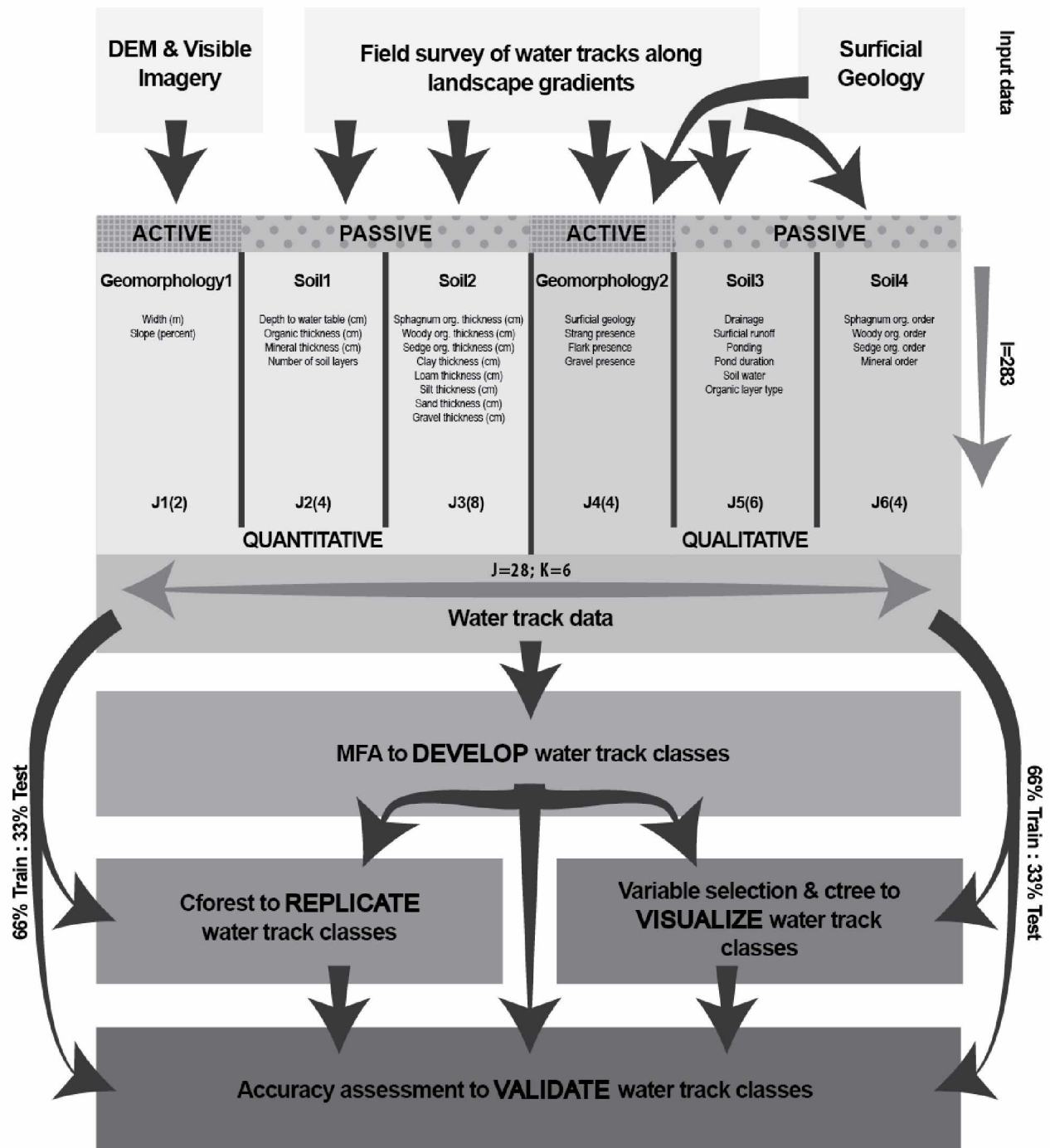


Figure 1.4: Study design for dividing the water tracks into classes and replicating the results.

The input data was divided into groups (K) of classes (J) for each plot (I). The active groups were used by the MFA to develop the water track classes, and the relationships to the passive groups were examined. This dataset was then divided into training and test subsets, based proportionally on the distribution of the water track classes. The training set was used to calibrate the cforest and ctree models. The test data was then used to validate the model predictions of the water track classes through an accuracy assessment.

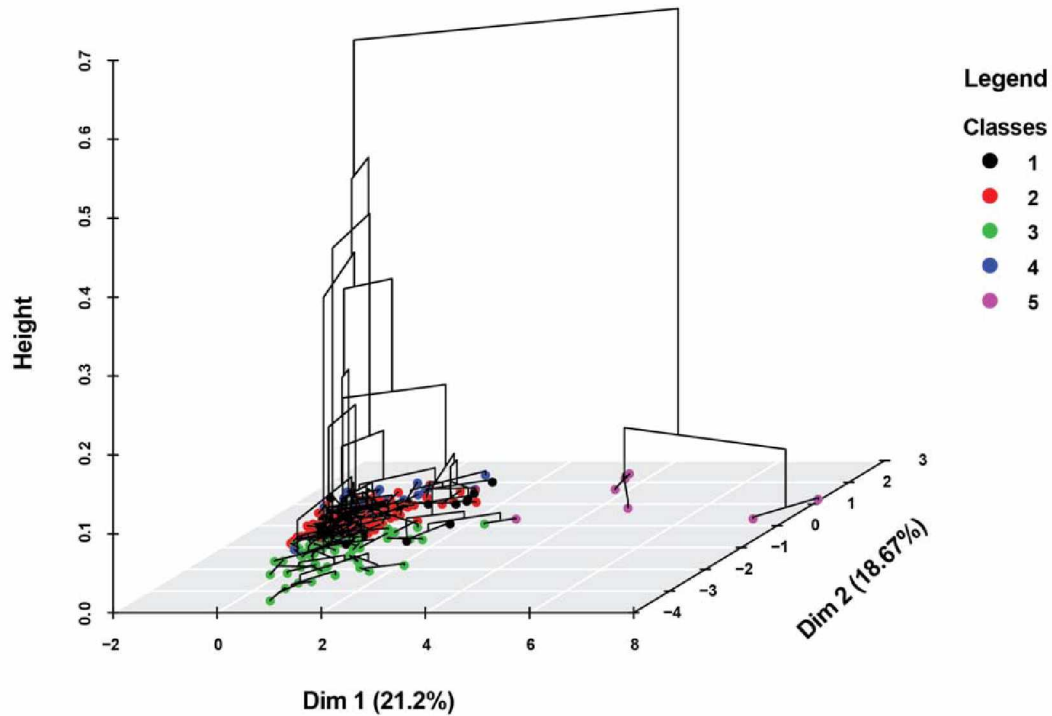


Figure 1.5: Hierarchical clustering for MFA dimensions 1 and 2 showing the five resulting water track classes.

Height demonstrates how separable the water track classes are within this dimensional space and the occurrence of overlap. Class 5 is the most distinct of all the classes in this dimension, while there is significant overlap between classes 1 and 2. Classes 3 and 4 occupy a similar, yet relatively unique area in this dimensional space.

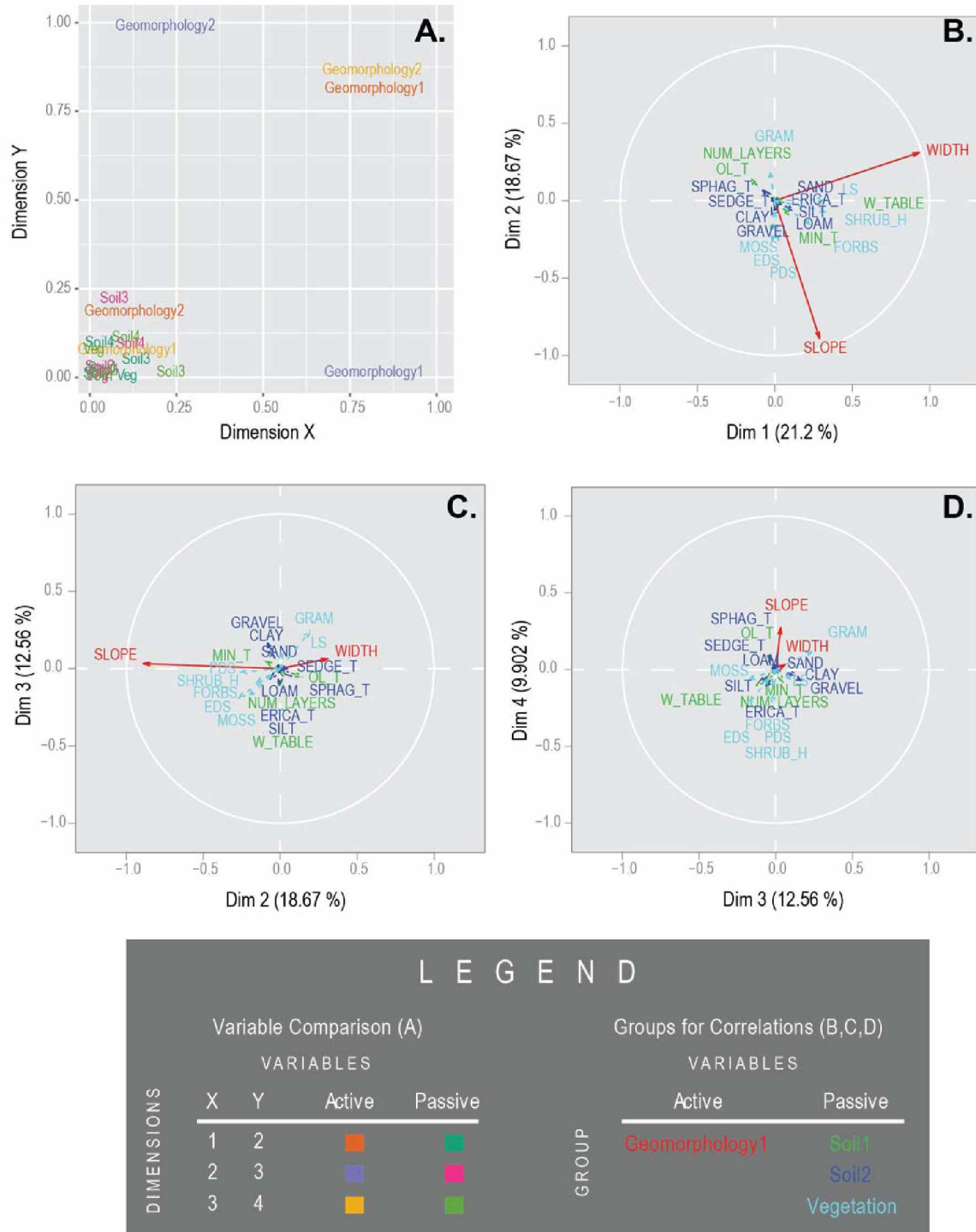


Figure 1.6: Comparison of groups in different factors and their associated correlations for the MFA.

A) Comparison of groups in each dimension (1 vs. 2, 2 vs. 3 and 3 vs. 4) where active and passive variables are indicated in the legend with different colors assigned to the pairs of each dimension; **B, C and D)** Correlations between MFA dimensions showing quantitative variables with color indicating group.

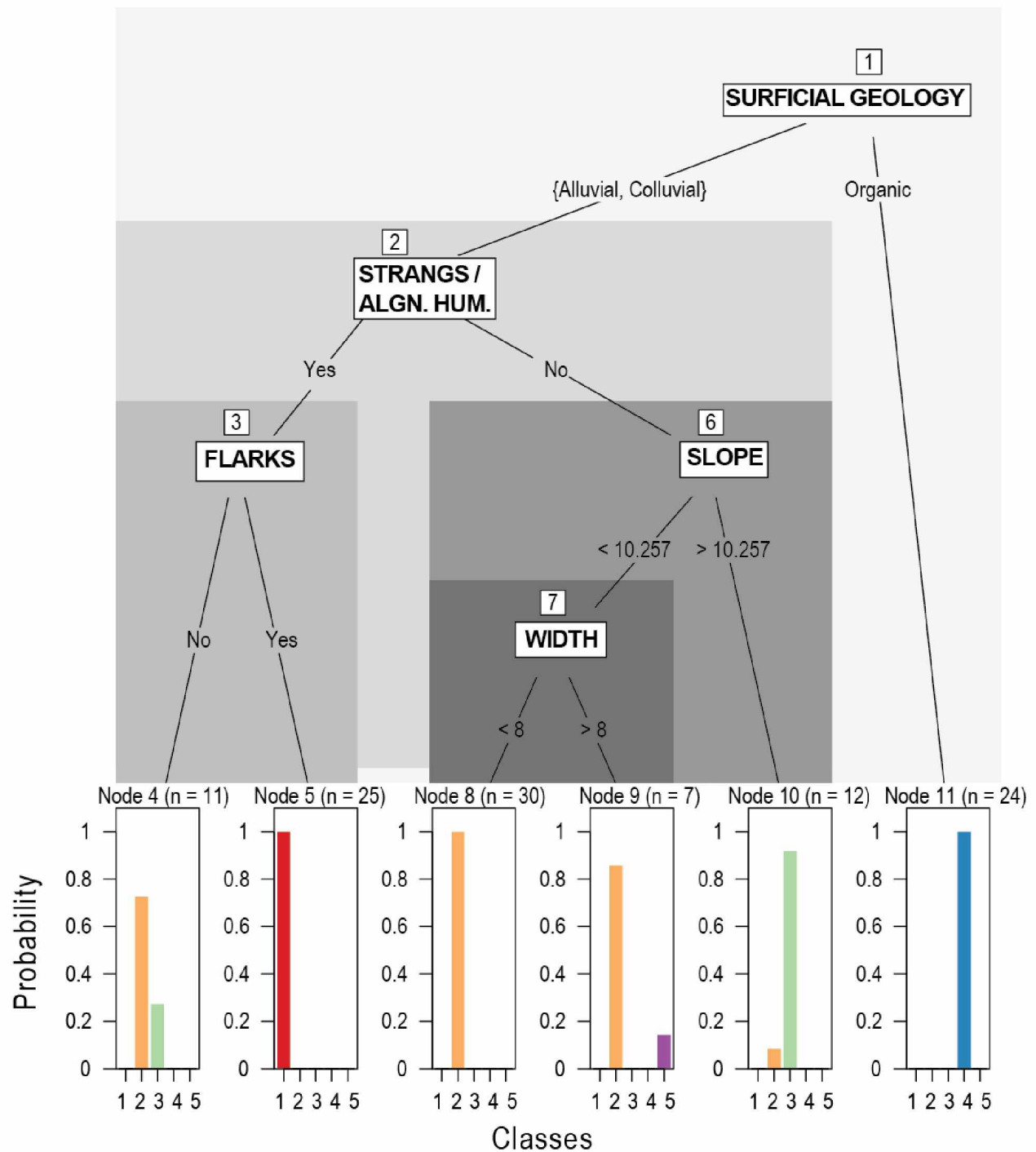


Figure 1.7: Conditional inference tree showing characteristics of water track classes after AUCRF variable selection where all splits are statistically significant ($p < 0.001$).

This classification tree has an overall accuracy of 77%. This decision tree demonstrates that there are numerous qualities which characterize the narrow (2) class, in comparison to the mineral-flark (1), steep (3) and organic (4) classes which have specific properties.

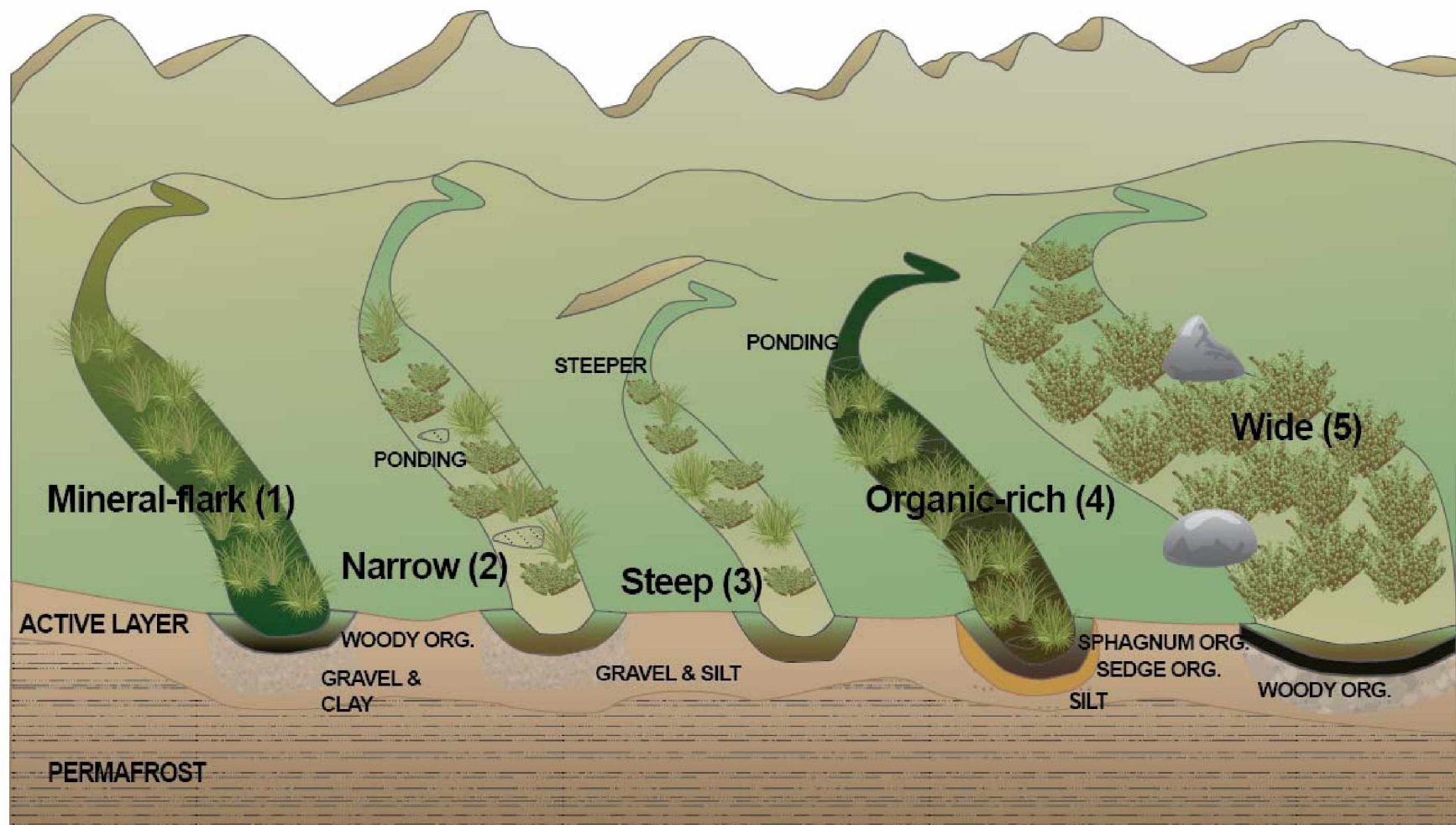


Figure 1.8: Final water track classes for the study area summarized including soil stratigraphy, soil texture, vegetation and geomorphology. The location of the active layer is approximate, and all water track classes are underlain by continuous permafrost.

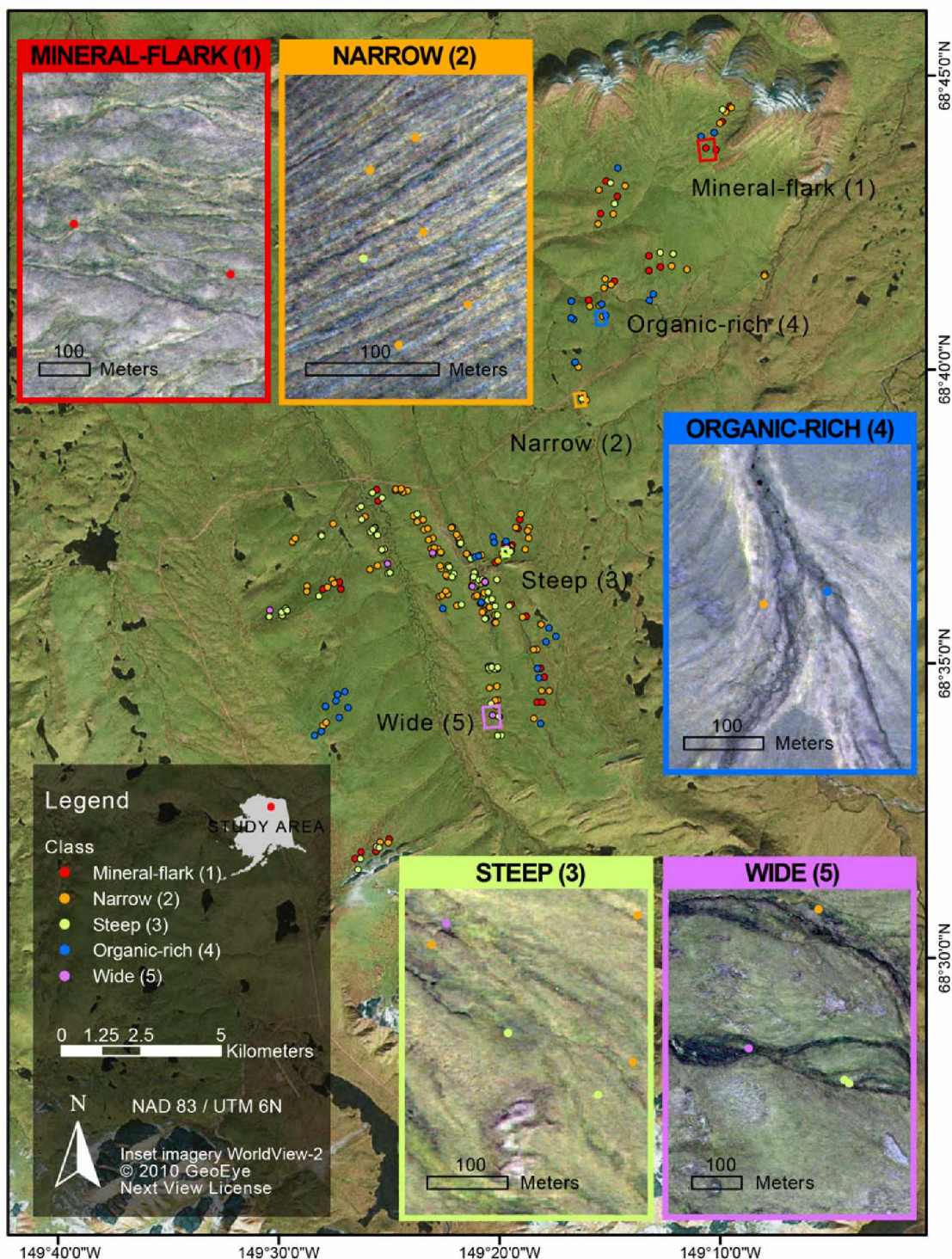


Figure 1.9: Water track class distributions over the study area. Insets show specific class examples.

In general, there is no obvious clustering of the water tracks in comparison to general topographic features. Imagery: Main: SDMI Best Data Layer showing medium resolution Landsat imagery via GINA, Insets: WorldView-2 acquired July 10, 2011 pan-sharpened with the panchromatic band and displayed using bands 542 as RGB.

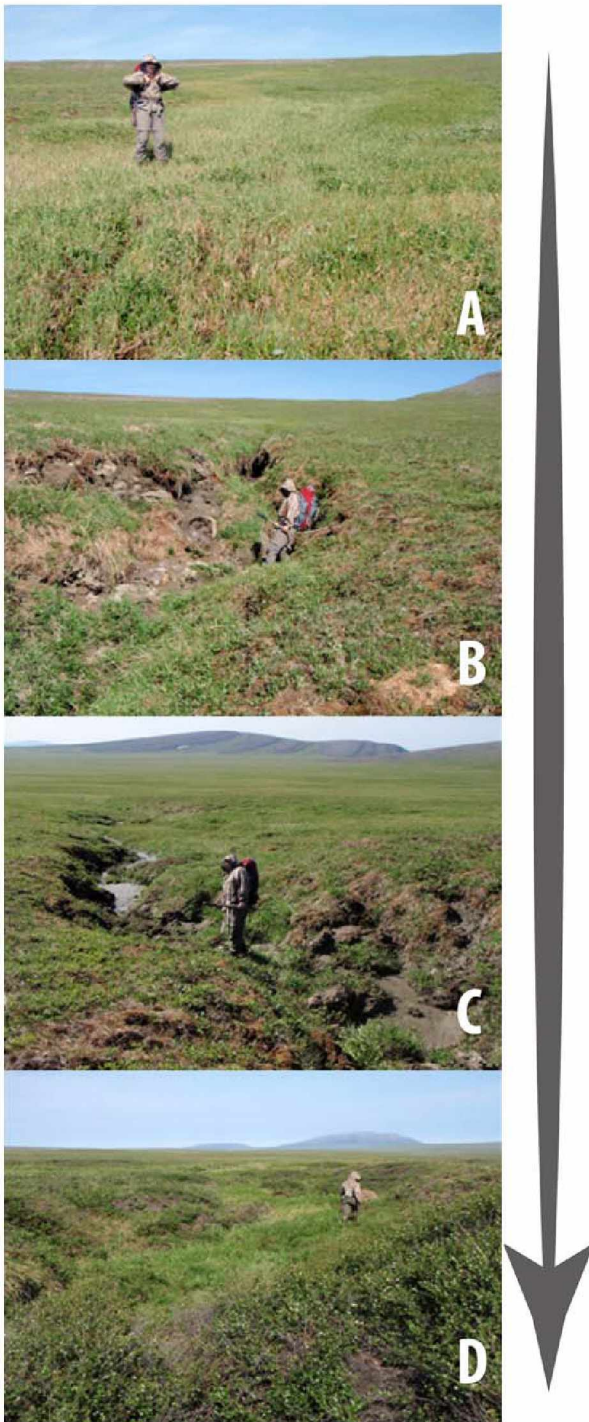
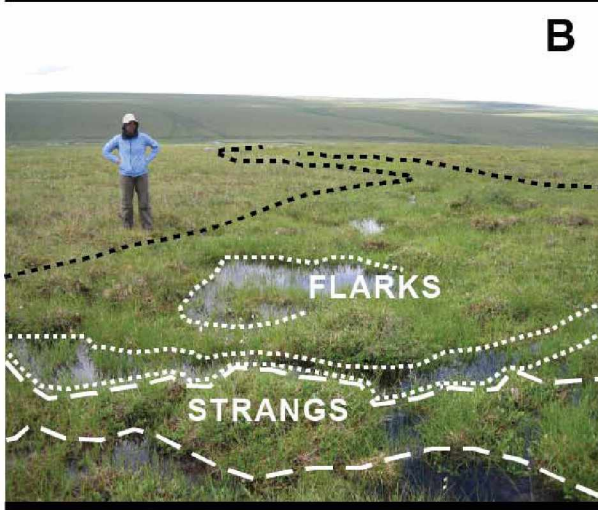


Figure 1.10: Development of thermal erosion in water track.

A) Uphill from thermal erosion (looking upstream) B) Active thermal erosion (looking upstream) C) Sediment and incision visible below (looking downstream) D) Thermal erosion stabilized by vegetation (looking downstream). *Photos: E.D. Trochim, July, 2009.*



A



B



C

Figure 1.11: Examples of features and processes influencing water tracks.

A) Snow remaining in an incised water track in early June 2010. **B)** Narrow (class 2) with flarks (occur in-between heaving ground and are wet-saturated areas which often contain standing water) and strangs (upraised areas between flarks) present. **C)** Steep (class 3) with hummocks in the Imnavait Basin. *Photos: E.D. Trochim, A) May, 2010 B & C) July, 2008.*

Table 1.1: Qualitative properties of clustered MFA classes

Significant $\alpha = 0.05$ in bold, Cla/Mod describes the percentage of individuals with the characteristic who belong to class X and Mod/Cla the percentage of individuals in class X who display the characteristic. Lines indicate groups of classes.

		CLASSES									
		1		2		3		4		5	
		<i>Cla/</i> <i>Mod</i>	<i>Mod/</i> <i>Cla</i>	<i>Cla/</i> <i>Mod</i>	<i>Mod/</i> <i>Cla</i>	<i>Cla/</i> <i>Mod</i>	<i>Mod/</i> <i>Cla</i>	<i>Cla/</i> <i>Mod</i>	<i>Mod/</i> <i>Cla</i>	<i>Cla/</i> <i>Mod</i>	<i>Mod/</i> <i>Cla</i>
Surficial geology	<i>Colluvial</i>	14	94	57	92	27	90				
	<i>Organic</i>							100	100		
	<i>Alluvial</i>									18	43
Strangs presence	<i>Yes</i>	49	100	16	8						
	<i>No</i>	0	0	67	43						
Flarks presence	<i>Yes</i>	50	97	21	10						
	<i>No</i>	1	3								
Gravel presence	<i>Yes</i>			32	22	40	57				
	<i>No</i>			58	78	16	43				
Drainage	<i>Poorly d.</i>							7	21		
	<i>Mod. d.</i>							16	74		
Surficial runoff	<i>Negligible</i>			56	57			8	32		
	<i>Very low</i>	23	41	31	14			24	44		
	<i>High</i>									67	29
Ponding	<i>None</i>									19	57
	<i>Occasionally</i>			60	42						
Soil water	<i>Frequently</i>	20	88	42	46			16	74		
	<i>Moist</i>					53	15				
	<i>Wet</i>			59	35						
	<i>Wet: satiated</i>							22	71		
Organic layer type	<i>Oa</i>					48	16				
	<i>Oe</i>					22	82				
Sphagnum order	<i>0</i>	36	44								
	<i>1</i>					12	18	25	74		
	<i>2</i>	36	15								
Woody order	<i>0</i>							35	65		
	<i>1</i>	34	47								
	<i>2</i>									8	57
Sedge order	<i>1</i>	40	12								
	<i>2</i>					10	10	24	47		
	<i>4</i>	60	9								
Mineral order	<i>2</i>	44	35	22	4						
	<i>3</i>	21	44			15	16				
	<i>5</i>	100	6								

Table 1.2: Quantitative properties of clustered MFA classes (mean \pm standard deviation).

Significant $\alpha = 0.05$ in bold. Lines indicate groups of properties.

	CLASSES					Overall
	1	2	3	4	5	
<i>Width (m)</i>	8 \pm 4	6 \pm 2	6 \pm 3	7 \pm 3	29 \pm 7	7
<i>Slope (%)</i>	7 \pm 3	6 \pm 2	12 \pm 3	6 \pm 3	8 \pm 5	8
<i>Depth to water table (cm)</i>	9 \pm 5	10 \pm 5	8 \pm 4	7 \pm 3	16 \pm 13	9
<i>Number of soil layers</i>	3 \pm 1	3 \pm 1	3 \pm 1	3 \pm 1	4 \pm 1	3
<i>Organic thickness (cm)</i>	19 \pm 6	21 \pm 6	20 \pm 6	24 \pm 6	19 \pm 13	21
<i>Mineral thickness (cm)</i>	10 \pm 7	8 \pm 7	10 \pm 7	6 \pm 4	7 \pm 4	8
<i>Sphagnum thickness (cm)</i>	5 \pm 6	7 \pm 7	6 \pm 6	13 \pm 3	7 \pm 7	8
<i>Woody thickness (cm)</i>	6 \pm 6	7 \pm 7	9 \pm 6	1 \pm 3	16 \pm 14	6
<i>Sedge thickness (cm)</i>	7 \pm 6	7 \pm 6	5 \pm 5	9 \pm 7	2 \pm 4	7
<i>Clay thickness (cm)</i>	1 \pm 3	0 \pm 2	0 \pm 0	0 \pm 0	0 \pm 0	0
<i>Silt thickness (cm)</i>	4 \pm 4	4 \pm 4	3 \pm 5	3 \pm 4	4 \pm 6	4
<i>Gravel thickness (cm)</i>	2 \pm 4	4 \pm 7	4 \pm 7	1 \pm 2	5 \pm 4	3
<i>Low shrubs (% cover)</i>	1 \pm 3	0 \pm 1	1 \pm 5	0 \pm 1	2 \pm 4	1
<i>Erect dwarf shrubs (% cover)</i>	2 \pm 4	1 \pm 2	2 \pm 4	1 \pm 3	0	1
<i>Prostrate dwarf shrubs (% cover)</i>	18 \pm 12	17 \pm 17	18 \pm 16	14 \pm 15	46 \pm 24	18
<i>Forbs (% cover)</i>	15 \pm 16	40 \pm 31	45 \pm 34	15 \pm 19	17 \pm 10	34
<i>Moss (% cover)</i>	5 \pm 17	5 \pm 8	7 \pm 12	0 \pm 1	2 \pm 4	5
<i>Graminoids (% cover)</i>	2 \pm 3	3 \pm 6	6 \pm 9	0 \pm 1	13 \pm 11	3
<i>Shrub height (cm)</i>	38 \pm 30	56 \pm 25	61 \pm 28	47 \pm 31	44 \pm 31	53

Chapter 2 Remote sensing of water tracks¹

2.1 Abstract

Water tracks are an intrinsic part of the surficial drainage network in the foothills of the Brooks Range, Alaska. They preferentially transport water off hill slopes and represent the interplay between hydrology, vegetation, geomorphology and permafrost characteristics. This research on mapping the location of water tracks builds on previous work which demonstrated that different types of water tracks exist due to difference primarily driven by geomorphology. We used a combination method where spectral classifications, texture and topography were fed into random forests to identify the water track classes. The most accurate distributions were obtained for the organic-rich and wide water track classes. The distinct linear shapes of the water tracks could also be visualized for many of the classes, especially in areas where the water track were particularly discrete. The biggest challenges to mapping the water tracks were due to class imbalances and high variability within and overlapping between classes. This research presents a significant step forward in understanding periglacial landscape dynamics.

2.2 Introduction

Delineating the composition and spatial extent of drainage networks on the North Slope of Alaska is an important step towards integrating these features to the hydrological system. Water tracks are the pathways for transporting water off of hillslopes in the region. They are linear-curvilinear saturated stripes (McNamara et al., 1998) where water is confined to the active layer (typically less than 1m in thickness) due to the underlying continuous permafrost acting as an impervious boundary. Water tracks in northern Alaska have multi-faceted characteristics related to their hydrological, vegetation and geomorphic components (Figure 2.1). Quantifying these inputs for the purpose of mapping water tracks is challenging because of the influence of scale. There is the initial challenge of connecting pan Arctic (Raynolds et al., 2008) and northern Alaska (Jorgenson and Heiner, 2008; Walker et al., 2003) remotely sensed ecosystem distribution with patch and community level vegetation data (Walker et al., 1994). Intensive geomorphic mapping in the region based on aerial photo interpretation has only been carried out

¹ Trochim, E.D., Prakash, A., Kane, D.L. & Romanovsky, V.E. Remote sensing of water tracks, submitted to *AGU Earth and Space Sciences*.

in key areas such as the Toolik Lake long-term ecological research (LTER) area (Hamilton, 2002).

Previous efforts to map water tracks in the area have been limited in the Toolik Lake LTER site. Walker and Maier (2008) used manual demarcation to map ecosystems and surficial geomorphology including water tracks in the 850 km² Upper Kuparuk River region at 1:25000 scale. Nested within this area, digital elevation models were used by McNamara et al. (1999) and Schramm et al. (2007) in the 2 km² Imnavait basin to detect the presence of water tracks. Given the prevalence of water tracks, the limited scope of these studies underscores the need for developing techniques which can efficiently map both the location of water tracks and their composition. This information is important for supplementing the sparse baseline ecology, hydrology and geomorphology data over large areas in the region and improving integration of the Arctic system (Hinzman et al., 2013).

A significant constraint has been the lack of knowledge about the underlying relationships between vegetation and geomorphology necessary to resolve the spatial patterns of water tracks. Recent work by Trochim (2015) laid the ground-work for enhanced mapping by delineating five main classes of water tracks in this study area: *mineral-flark* (class 1), *narrow* (2), *steep* (3), *organic-rich* (4) and *wide* (5) (Figure 2.2). Each class was associated with specific geomorphic features or phenomena including glacial-fluvial channels, ice-wedge polygons, solifluction, thermal and mechanical erosion. The classes were linked to significantly different vegetation distributions especially between low shrubs, erect dwarf shrubs and graminoids. Walker et al. (1994) also related vegetation and the approximate quantity of water as water tracks in the same area belonged to one of three plant communities: *Betula nana* – *Rubus chamaemorus*; *Eriophorum angustifolium*; and *Salix planifolia* ssp. *pulchra* - *Eriophorum angustifolium*. Recent availability of multispectral images from commercial satellites such as WorldView-2 (that has 8 spectral bands in the visible and near-infrared regions acquiring images at ~ 2 m spatial resolution) also increases the feasibility of using the vegetative structure of water tracks as a proxy for their respective geomorphic associations.

Previous approaches in Arctic regions used density slicing of panchromatic imagery to identify different geomorphic (Grosse et al., 2005) and vegetation (Tape et al., 2011) features. Spectral methods including on-site spectra acquisition and unmixing were used to identify periglacial units by Ulrich et al. (2009) in the Lena delta. Multiple Endmember Spectral Mixture Analysis (MESMA) is a spectral mixing technique which represents an opportunity to extend Spectral Mixture Analysis (SMA) where a series of known cover types are used as input. Each of the cover types has spectral endmembers corresponding to “pure” spectra which are unmixed as linear combinations. MESMA accounts for variability in pixel-scale spatial dimensions and sub-pixel mixing by allowing the number and type of endmembers to vary by pixel (Roberts et al., 1998). It has been applied in related studies including chaparral plant species mapping (Dennison and Roberts, 2003a; Dennison and Roberts, 2003b; Roberts et al., 1998; Roberts et al., 2003), arid land soil mapping (Okin et al., 2001) and improved LAI estimation for boreal forests (Sonnentag et al., 2007). Another strength of the MESMA technique is the development of indices for selecting optimal spectra to represent classes and the Count-based Endmember Selection (CoB) index (Roberts et al., 2003). These remote sensing techniques strongly benefit from the availability of ground-verified data specific to the desired target as both potential spectral targets and for accuracy assessment.

A significant issue in classifying geomorphic phenomena is variability both between and within factors which define the targets. Within each class there can be a range of surficial conditions due to variation in vegetation, surface composition and near surface moisture conditions. This is especially true when using data with the appropriate spatial and spectral resolution for the mapping the specific feature. Water tracks can vary from 2 meters to over 30 meters in width so while there are clear benefits to using imagery with spatial resolution comparable to the smallest features, there is a tradeoff due to the increase in data complexity. Statistical techniques such as random forests (Pal, 2005) have a history of being used to map geomorphic (Heung et al., 2014; Timm and McGarigal, 2012) and ecological (Crisci et al., 2012; Cutler et al., 2007) properties. In remote sensing, they are noted for their ability to handle non-parametric data while producing high accuracy classifications (Rodriguez-Galiano et al., 2012). Another advantage is that data from different sources like multispectral visible imagery can be combined with elevation properties like slope and aspect (Chasmer et al., 2014).

This work addresses whether water track distribution can be accurately and efficiently mapped by combining existing knowledge about water track morphology with field survey data, high-spatial-resolution multi-spectral images and digital elevation model (DEM) properties. We focus on the following questions: (1) can water tracks be delineated efficiently; (2) is it possible to map the water track classes of Trochim et al. (submitted); (3) what is the spatial variability of the water track classes; and (4) what are the main factors driving the model variability and errors. The main problems addressed in this study were to figure out what data would be necessary for mapping the water track classes and how to optimize the processing steps. This would require using both the MESMA technique to map various properties of the landscape including vegetation, surficial geology and geomorphology and other intermediate data to produce the final classifications using random forests. The goal was to move towards a semi-automated methodology which could be applied over larger regions of the North Slope of Alaska.

2.3 Study area

Moist acidic tundra covers the study area in the Imnavait and Upper Kuparuk basins in the Toolik Lake LTER area. The erosional topography on the landscape is created by Cretaceous sedimentary rocks forming east-west-trending open folds (Black, 1969). Elevation varies from 844 to 960 m. Glaciation in the middle Pleistocene during the Sagavanirktok advance created the incised rolling hills and covered the area with glacial till (Hamilton, 2002). Continuous permafrost in the area extends 250 to 300 m below the surface (Osterkamp and Payne, 1981). This forms a resistant surface for water percolation and restricts water movement to near-surface runoff or evapotranspiration (Hinzman et al., 1996). In this region of the Arctic strong seasonality restricts the annual cycle to warm ($>0^{\circ}\text{C}$) and cold ($<0^{\circ}\text{C}$) periods which go from May through September and October through April respectively. A continuous snowpack is typically present from late September to mid-May or early June although it can snow any day of the year. The topography influences the pattern in which the wind redistributes the snow in the study area (Evans et al., 1989). The discharge cycle follows a nival regime (Kane et al., 1989). Poorly- and well-developed hillslope water tracks, wetland microrelief (Walker and Maier, 2008) and beaded streams transport water to larger rivers. Greater amounts of snow and continuous discharge through the summer can be found in well-developed water tracks. In contrast poorly

developed water tracks generally have flow only during and after snowmelt and rain events. The five main vegetation communities found in the region include: dry exposed acidic sites, moist acidic shallow snowbeds, moist non-acidic snowbeds, moist acidic uplands, and moist nonacidic uplands (Walker et al., 1994).

2.4 Methods

This study used a diverse set of input data and a multistep process to delineate the spatial distribution of the water track classes as shown in Figure 2.3.

Field data

Ground information about water tracks and the adjacent areas was collected using a sampling design which identified cluster of water tracks on aerial photographs of the region. Priority was given to areas representing a range of gradients and proximity to the road networks. The data was collected the summers of 2008, 2009 and 2010. A network of 532 plots was precisely located using differential GPS measurements located in water tracks as seen in Figure 2.4. Each plot was 1 to 2 meter sq. and represented a homogenously mixed land cover. The Braun-Blanquet percent cover classes (Mueller-Dombois and Ellenberg, 1974) were used to describe vegetation, moss and lichen. Walker et al. (1994) community compositions were used as a principal key to identify plants found in the area to the species level. Directly adjacent to each vegetation plot a small soil pit was excavated to assess the geomorphic and soil properties using standard methods (Schoeneberger et al., 2002) which were analyzed in Trochim et al. (submitted). Surficial geomorphology, surficial geology, primary vegetation and plant communities were sampled at each point from vector data (Walker and Maier, 2008). Water track presence/absence and water track class were derived from the analysis of Trochim et al. (submitted) and used to proportionally divide the data into train and test (0.7/0.3) subsets.

Remotely sensed data

Panchromatic and multispectral data from the WorldView-2 satellite were collected on July 10, 2011. Three scenes were used for analyses which were acquired sequentially. The spectral, spatial and radiometric properties of the WorldView-2 satellite are listed in Table 2.1. Orthorectification was applied to the imagery in ENVI version 5.0 (Exelis Visual Information

Solutions, 2014) using the ASTER 30 meter digital elevation model. Atmospheric effects were resolved using the ATCOR 2 model (Richter and Schlapfer, 2011) and the data were converted to surface reflectance. Percent slope, aspect, plan convexity and profile convexity was calculated (Wood, 1996) from a Star3i digital elevation model collected in September 2001. The data had a horizontal resolution of 5 m and an absolute vertical resolution of 2.7 m. Using the multispectral WorldView-2 imagery, the Normalized Difference Vegetation Index (NDVI) (Richardson and Everitt, 1992) was calculated from reflectance using the multispectral imagery in the Near InfraRed (ρ_{NIR}) (band 7) and red (ρ_{RED}) (band 4) wavelengths. A mask was created from NDVI to remove gravel, roads and water from the multispectral imagery.

Intermediate clustering

The contribution of vegetation to the water track classes was isolated using the *labsv* package (Roberts, 2013) in R (Team, 2014) using the indicator value method (Dufrêne and Legendre, 1997). Indicator species and life-form groups were identified by detecting similarities within groups in sample compositions from different sites (McGeoch and Chown, 1998). A major advantage to this method is that each indicator value is calculated independently (Dufrêne and Legendre, 1997). A Monte Carlo method using 1000 permutation runs was used to generate p-values. P-values less than 0.05 were used to segregate the most important features. These properties were used as the target for the MESMA classification. If no significant property was found then the most important surficial geological property found in Trochim et al. (submitted) was substituted.

MESMA was applied using two different approaches to the WorldView-2 data where the information from the ground plots including the water track classes, vegetation and surficial geology were targeted. First, optimal endmembers were selected using the best CoB values for each subclass to classify: *surficial geology*, *primary vegetation*, *moss*, *forbs*, *prostrate dwarf shrubs*, and *low shrubs*. CoB values rank endmembers by optimizing the models chosen within the correct class, while constraining confusion with other classes (Roberts et al., 2003). Consideration was given to endmember average root mean square error (EAR) (Dennison and Roberts, 2003b) and minimum average spectral angle (MASA) (Dennison et al., 2004) as described by Quintano et al. (2013). Calculation of these parameters is automated within the

MESMA algorithm found in Visualization and Image Processing for Environmental Research (VIPER) tools software (Roberts et al., 2007) which was used for the analysis. Initially, a constrained square array using minimum and maximum allowable fractions of -0.05 and 1.05 and a maximum root mean square error (RMSE) of 0.025 was used for calculating the CoB values. The MESMA classification was repeatedly run using the spectral library specific to that class for the unmixing process. The minimum and maximum ElectroMagnetic (EM) fractions values used were identical to those of the square array. The maximum allowable RMSE used was 0.15 while the maximum shade fraction was 0.8. We used a larger RMSE value to ensure mapping over as much of the study area as possible. The MESMA process was run multiple times for each classification to identify the top spectra for each of the sub-classes which corresponded to wide-scale identification of modeled output. The accuracy of the classifications was evaluated and only those classes where it was greater than 65% were retained in order to preserve the most important characteristics.

The second MESMA classification process used the variables specific for each water track class including *Eriophorum angustifolium* (mineral-flark), *colluvial* and *alluvial surficial geology* (narrow), *erect dwarf shrubs*(steep), *graminoids* (organic-rich), *Carex aquatilis* (graminoids), *low shrubs* (wide), *forbs* (wide) and *Petasites frigidus* (wide). The same settings were used for constructing the square array and the spectra were selected based on the highest CoB values. Multiple spectra were used as input for each class if there were substantial differences. The MESMA classification was run for each class using up to three spectral libraries in the unmixing. The minimum and maximum EM fractions were again identical to the square array. A variety of maximum allowable RMSE limits were used starting with a value of 0.1 to a maximum of 0.5. Again, RMSE values were allowed to vary in order to visually confirm the results covered significant areas. As RMSE was used as an input to the random forest model, large errors were accounted for during that stage.

Next, a co-occurrence matrix (Anys et al., 1994; Haralick et al., 1973) was calculated for the panchromatic band. The *entropy* result was used to threshold the output into classes which indicated the presence of flarks and roughness. The *mean*, *variance*, *homogeneity* and *contrast* were also analyzed using a principal component analysis (PCA) where image noise was

minimized by retaining only the data found in the first three eigenvalues during the inverse rotation.

A final stacked raster dataset was created with a total of 39 layers including the original WorldView-2 imagery, MESMA results, co-occurrence products and topographic inputs as detailed in Table 2.2.

Machine learning and post-processing

The Classification And REgression Training (caret) package (Kuhn et al., 2013) was used to efficiently train random forest (Liaw and Wiener, 2002) models. For each water track class, two different binary random forest models were run to differentiate between water track and non-water track areas, and the specific water track class versus all the other water tracks. The model process started with determining the proportion of alternate (X0) versus desired (X1) classes. If the desired classes comprised less than 20% of the total classes then the dataset was sub-sampled using maximum dissimilarity (Willett, 1999). For the wide class, this approach was insufficient due to the low number of samples. Additional sites were selected in close proximity to those which had been ground verified. Next, an initial random forest model was trained using repeated cross-validation of 10 times and 5 repeats and 1000 trees. The number of predictor variables used as candidates for each split of the decision tree (mtry) was allowed to vary from 1 to 10. The area under receiver operator curve (ROC) was used to select the optimal model (DeLong et al., 1988). ROC compares sensitivity (true positive rate) against specificity (false positive rate). ROC values range from 0.5 (poor) to 1. Training accuracy was assessed using out-of-bag portion error (Breiman, 2001). Backward feature selection was then run to reduce the number of variables, and the random forest was rerun with the subset. Confusion matrices were calculated using the test datasets to assess accuracy and select either the original or variable-selected random forest model. Accuracy was calculated as a percentage (i.e. number of correctly classified pixels divided by the total of pixels). The final models were applied to the raster data stack.

Post-classification the presence/absence distribution for each water track was used to mask the class results specific to the type of water track. The water track classes were then overlaid, sieved and majority filtered to aid in interpretation. Zonal analysis was performed to examine the

differences between the water track classes in terms of area for three watersheds within the study area.

2.5 Results

Indicator species for water tracks and MESMA classification

Each of the water track classes had a significant associated vegetation species or group except steep as seen in Figure 2.5. The mineral-flark and organic-rich classes were both indicated by graminoid (GRAM) presence but there were differences between the specificity of vegetation and number of related samples. *Eriophorum angustifolium* (ERAN 6) was tied only to the mineral-flark water tracks. The steep class presence was tied to erect dwarf shrubs (EDS). The wide class was indicated by low shrubs (LS) and *Salix pulchra* (SAPU15), forbs (FORBS) and *Petasites frigidus* (PEFR5). Since the technique did not identify any related vegetation species for the narrow class, alluvial and colluvial surficial geology were used for the MESMA classification.

The spectra selected for each water track class demonstrated the robustness of the MESMA technique in systematically differentiating between many potential combinations as seen in Figure 2.6. For each water track class the spectra were relative similar within the visible (400 to 600 nm) region of the spectrum, with the largest differences in the near-infrared (> 800 nm) portion. For the MESMA classification that used all plots as potential input, there was more variation in the visible region. During the MESMA classification, vegetation which was less prevalent or patchier within the spatial resolution of 1.84 m required the allowable RMSE to be increased in order to produce diverse results. These classes included low shrubs, surficial geology, *Eriophorum angustifolium*, forbs and *Petasites frigidus*.

The entropy result from the co-occurrence matrix applied to the panchromatic band identified major channels. Many of these were related to ice-wedge polygon distribution or flarks. The ice-wedge polygons had a clear polygonal shape. Flarks occur in-between heaving ground and are wet-saturated areas which often contain standing water. A secondary class for roughness was developed to indicate areas which likely contain frost heaves and/or strang. Strang are raised areas perpendicular to the flow path in wetland regions.

Random forest results

The complete random forest results can be found in Table 2.3. Overall, the organic-rich water track class produced consistent results between the test and train datasets between both OOB error versus accuracy as well as in terms of the ROC values. In terms of accuracy, the next best classification was for the wide class. It should be noted that the high test ROC value is also somewhat sensitive to the low number of test plots for this class. The mineral-flark and narrow classes had moderate results, where the models generally appear to be performing slightly better on the training dataset than during the accuracy assessment. The narrow class was adequate only for discriminating between other types of water track classes.

For the mineral-flark class the texture (variance, contrast and flarks), the distribution of low shrubs and WorldView-2 band 1 were important variables in both random forest models. In discriminating the narrow class from the other water tracks, the MESMA RMSE of surficial geology had the largest overall contribution followed by the *Eriophorum angustifolium* EM distribution. The most important variables for both organic-rich class models were the RMSE of surficial geology, WorldView-2 band 5 and roughness. In the wide class four inputs (WorldView-2 band 2, colluvial surficial geology, the RMSE of graminoids / *Carex aquatilis* and WorldView-2 band 1) were selected by both models.

The water track class distribution for the entire study area can be seen in Figure 2.7. At this scale several patterns can be noted. First, wide water tracks are found primarily on east-facing slopes in the incised rolling hills of the Upper Kuparuk watershed and adjacent drainages. They can also be found in proximity to major drainages. The narrow class occurs on west-facing slopes, on the north-side of Slope Mountain and in the foothills adjacent to the Sagavanirtok River. The organic-rich class is more visible in areas where the topography is less incised. The narrow class is visible at steeper slopes in the mountain areas.

2.6 Discussion

Applicability of the water track classification

The range of accuracies between 60 and 85% for the various water classes was comparable to results from other studies quantifying wetland characteristics in discontinuous permafrost (Chasmer et al., 2014). Though the overall classification accuracies were not significantly better than the accuracies achieved from popular spectral classification approaches used in remote sensing studies, the classification scheme followed in this research has distinct advantages that the process (i) does not require the time-intensive step to ‘train’ the computer/classifier, (ii) minimizes the bias from user-interpretation, and (iii) is easier to scale-up. Spatially quantifying landscapes based on geomorphic properties is challenging due to variability and the role of scale. Features such as water track or wetland classes combine a multitude of vegetation, soil moisture, soil stratigraphy and surficial geology characteristics to form the individual classes. Ideally like in this study, these classes are based on ground-based data verified for the region. Many of these features may only be discernable at finer spatial and spectral scales such as through the use of WorldView-2 data with a pixel size of 1.84 m. The issue is that increasing our ability to identify the patterns also raises the variability and complexity of delineating the classes.

As can be seen in Figure 2.8, the curvilinear shape and pattern of water tracks can be discerned from the classification. In the areas such as those around Slope Mountain and on the east-facing slope of the Upper Kuparuk watershed where the water tracks are particularly distinctive the water track classes are adequately capturing the pattern. Within these slopes, clear variation between the mineral-flark, narrow and steep classes can be seen. The steep water classes in these situations may be more incised locally, rather than found on a greater angle slope. It should be noted that the connectivity of the water tracks is not identical to that found in the visible imagery. Given that this classification was mainly a spectral approach that did not focus on spatial relationships other than through texture, the ability to discern the shape of different water track classes is of significant relevance as it underscores their prevalence, on the landscape. Both the water tracks and their specific classes form a dominant geomorphic attribute which is complex and a blend of shape and composition.

The two classes which experience more clumping, or are less linear in nature are the narrow and wide classes. The poor performance of the narrow class which is closest to the World-View 2 pixel resolution is similar to that documented by Dronova et al. (2012) in their characterization of wetlands. The narrow class may also be comparable with hummock tussock tundra which can occur both as a type of water track and also as a poorly developed water transport mechanism on slopes. The wide water track class on many incised rolling hills occupies a large portion of the slope. This distribution is likely related to the vegetation which is high in chlorophyll and includes both shrubs and graminoids. WorldView-2 bands 1 and 2 (400 to 450 nm and 450 to 510 nm) have been documented to improve classification of bright green vegetation data in other studies (Tarantino et al., 2012).

Implications for permafrost research

Classifying the properties of water tracks over the landscape is a significant step towards understanding drainage features in the Arctic which have a multi-faceted effect on permafrost. Creating products like distribution of water track classes is useful because it provides a more detailed understanding of the specific properties and patterns on the landscape. This can be extrapolated to better infer processes and also tailor future studies more effectively. While this methodology did not capture every water track within the study area, it was able to successfully map the types which we had verified via ground point data. For thermal modeling, this is very useful as it improves our ability to delineate specific characteristics related to thermal conductivity and soil moisture. For instance, it would be useful to develop N factors for the different water track classes to take advantage of the similarities in the atmosphere-soil system which are important for predicting ground thermal regimes (Riseborough et al., 2008). Along these lines, the ability to lump characteristics together can increase the efficiency of running complex numerical models, as similar areas may be treated as a single area within a vector rather than repeating the same calculation multiple times over a raster format (grid points).

The distributions of the water track classes also provide a snapshot into how water is moving through a basin. By utilizing a raster-based methodology rather than vectorized-lines representing channels, the area of each water track class can be calculated. This was done for three different watersheds in the study area: the Upper Kuparuk, Imnavait and Toolik

Thermokarst (as seen in Figure 2.7). Figure 2.9 shows the differences in percent area between the water track classes for each watershed. The Toolik Thermokarst basin shows the highest proportion of organic-rich water tracks, and given the accuracy of this class there is reasonable confidence in this calculation. Both the Imnavait and Upper Kuparuk share similar proportions of mineral-flark and steep classes. Overall, the highest proportion of water tracks was identified in the Imnavait watershed with 32%. This is very close to the water track area of 34% estimated by McNamara et al. (1999) from a DEM derived from elevation contours generated from aerial photographs. Given the errors associated with some of the classes, this analysis is most useful in contiguous watersheds where the omission errors which are most common in the water track classes should be relatively consistent provided that the input conditions are within the modeled parameters.

Factors affecting classification performance

Analysis of the factors affecting the performance of the classifications can be grouped into the following areas: (1) General classification issues including insufficient separation between classes and errors of omission; (2) methods of spectra selection with the MESMA classification; and (3) the effects of class imbalance on the random forest models.

Separating the differences between water track and non-water track areas in both the MESMA and random forest techniques was problematic as there was overlap between the classes. While some water tracks are ecologically unique, others will be similar to non-water track areas as would be detectable from the World-View 2 multispectral imagery. This contributed to the dominant errors being those of omission, where the desired water track class could be misclassified as null. The complexity of this issue can be most effectively visualized in Figure 2.10. Along the analyzed transect, there is similarity between the water track classes and *Eriophorum angustifolium* values. This is in contrast to a filtered NDVI product which more clearly emphasizes the curvilinear shape. The issue is that depending on incision, soil moisture, and the distribution of shrubs versus graminoids water tracks can be found within the dominant linear feature in an area or directly adjacent to it. Over large areas, there does not appear to be a simple means for capturing this pattern/phenomenon.

In general the MESMA classification contributed critical information for the spatial quantification of the water track classes. Due to the variability both between water track and non-water tracks as well as discriminating between the classes themselves, a robust dataset was necessary to delineate the features. The MESMA process and the CoB statistic in particular provided a useful method for selecting spectra which are most likely to produce the desired subclass result. An increased number of available ground-verified points could potentially increase the accuracy of this approach. Alternatively, automated iterative selection can be used to isolate spectra for the MESMA classification (Roth et al., 2012).

The random forests were able to most effectively deal with issues of commission or overlap between classes through the use of multiple binary models. This is due to either overlapping and/or ecologically similar cover classes (Timm and McGarigal, 2012). Class imbalance (Chen et al., 2004; Evans and Cushman, 2009) can also lead to decrease in performance due to the sample size. This combined with the distribution between a number of classes can cause preferential training within the random forest model. Ideally, a dataset should be well-balanced through cross validation and class resampling. Variable reduction can be useful in some cases especially when one moves to hyperspectral data (Chan and Paelinckx, 2008). In this study cross-validation, class resampling and variable reduction were all used to assist with class imbalance in the random forest models.

Alternative approaches

The spatial context of water tracks and their trademark linear-curvilinear shape ultimately defines the connectivity of a water track and its ability to move water off hillslopes. Small scale topographic variation including frost heave and ponding can be concentrated in water tracks compared to the surrounding area. Theoretically, water tracks as drainage features should have an incised topographic profile which follows the least-cost path of decreasing elevation down the slope. In reality the influence of continuous permafrost creates a more complex scenario where parts of the water tracks are incised as seen in Figure 2.11. The propensity of linear channels share much similarity with both the validated water track classes and the majority filtered product, which was produced to make it easier for visual interpretation. In the field, incision was more common on the edges of the steep class and the centers of the organic-rich. Using a

topographic approach alone may classify many of the tracks; however it does not elucidate the differences between the different types of water tracks. Also, water tracks are not universally incised features due to thick organic mats and presence of shrubs. Water tracks may actually be convex in terms of the ground surface topography and slightly elevated in comparison to the adjacent environment.

Future improvements to classifying water tracks may include the development of multiple classification systems (Woźniak et al., 2014) i.e. the use of ensemble classification models versus multiple models best suited to answer a specific question. An additional approach would be to integrate geographically weighted errors instead of error matrices (Comber et al., 2012), as error matrices do not provide any indication of the spatial distribution of errors. The spatially explicit representation generated from geographically weighted approaches offers the prospect of creating improved land surface classes in a more explanatory fashion. The use of an object-orientated classification may offer limited improvement, as in comparable mapping of wetland plant functional types, advantages are generally related to scale (Dronova et al., 2012). The same study found the highest accuracies occurred at coarser object scales rather than those close-to-pixel resolution. However, future studies might be improved with pre-segmentation of images, as their use produces equal accuracy rates between random forests and object-orientated classification methods (Stefanski et al., 2013). In general, the advantage of the combined MESMA and random forest model approach is that model optimization process will improve through semi-automation. The approach also has the ability to efficiently handle iterative processing of large datasets.

Supplementary datasets such as polarimetric synthetic aperture radar (SAR) and high-resolution airborne light detection and ranging (LiDAR) potentially offer additional information necessary for accuracy improvement of water track classes. Polarimetric SAR has been used to estimate subsurface water in peat (Touzi et al., 2013), generalize landcover in Arctic coast regions (Banks et al., 2013) by approximating biomass (both above and below-ground) depending on type. Better discrimination of peat and subsurface water properties would be useful for water track descriptions. Acquisition of LiDAR using both bare-earth for more detailed topographic information, and first returns to estimate shrub height would be very useful. The

advantage to using machine learning methods such as random forests is that they allow the use of large, diverse datasets towards the application of complex issues like discriminating water track classes.

2.7 Conclusions

This study showed that both water track presence and different water track classes could be identified using primarily WorldView-2 imagery. The mineral-flark, steep and narrow water tracks displayed a curvilinear shape and repeating pattern perpendicular to the hill slope. The highest accuracy and best ROC values were found for the organic-rich and wide water track classes. The models performed better on the training set data which had a higher numbers of positive classes, and more equalized proportions between classes. In general, errors were primarily those of omission or the water track class being misclassified as null. This was due to insufficient separation between classes. The biggest underlying issue was the complexity of the water track classes. Although they represent the geomorphic properties, they were classified using a combination of variables including vegetation, soil moisture, and surficial geology. The use of high spatial resolution imagery also increased the variability within the data.

The comparison of different water track class percent area for different watersheds within the study area demonstrated that the classification was useful for illuminating differences in hydrology and geomorphology. This research has significant implications for understanding where water flows repeatedly in periglacial environments including future study designs of related phenomena including improving ground temperature predictions. The ability to map known water track geomorphic conditions provides a critical baseline for further investigations of landscape dynamics within a region. Given the complex interactions of these factors within the context of a changing Arctic climate, delineating, mapping, and quantifying different water track classes is a significant step forward.

2.8 Acknowledgements

This project was supported by a NASA Earth & Space Science Graduate Fellowship (NNX09AN42H), with additional resources provided by the Alaska Water Resources Association and the University of Alaska Fairbanks including the Center for Global Change, the

Graduate School and Department of Geosciences. This work was supported in part by a grant of HPC resources from the Arctic Region Supercomputing Center and the University of Alaska Fairbanks. WorldView-2 imagery was acquired through the National Geospatial Agency Commercial Data Archive. Symbols for figures courtesy of the Integration and Application Network (ian.umces.edu/symbols/), University of Maryland Center for Environmental Science. Field assistance was provided by Michelle Brosius, Nicole Farnham, John Mumm and Matt Sprau with additional support by the Toolik Lake Research Station.

2.9 References

Anys, H., Bannari, A., He, D. C., and Morin, D., 1994, Texture analysis for the mapping of urban areas using airborne MEIS-II images, in *Proceedings Proceedings of the First International Airborne Remote Sensing Conference and Exhibition*, p. 231-245.

Banks, S., Ullmann, T., Roth, A., Schmitt, A., Dech, S., and King, D., 2013, Classification of Arctic Coastal land covers with polarimetric SAR data, in *Proceedings Radar Conference (RADAR)*, 2013 IEEE on April 29 2013-May 3 2013, p. 1-6.

Black, R. F., 1969, Geology, especially geomorphology, of northern Alaska: *Arctic*, v. 22, no. 3, p. 283-295.

Breiman, L., 2001, Random forests: *Machine Learning*, v. 45, no. 1, p. 5-32.

Chan, J. C.-W., and Paelinckx, D., 2008, Evaluation of Random Forest and Adaboost tree-based ensemble classification and spectral band selection for ecotope mapping using airborne hyperspectral imagery: *Remote Sensing of Environment*, v. 112, no. 6, p. 2999-3011.

Chasmer, L., Hopkinson, C., Veness, T., Quinton, W., and Baltzer, J., 2014, A decision-tree classification for low-lying complex land cover types within the zone of discontinuous permafrost: *Remote Sensing of Environment*, v. 143, no. 0, p. 73-84.

Chen, C., Liaw, A., and Breiman, L., 2004, Using random forest to learn imbalanced data: University of California, , 666.

Comber, A., Fisher, P., Brunsdon, C., and Khmag, A., 2012, Spatial analysis of remote sensing image classification accuracy: *Remote Sensing of Environment*, v. 127, no. 0, p. 237-246.

Crisci, C., Ghattas, B., and Perera, G., 2012, A review of supervised machine learning algorithms and their applications to ecological data: *Ecological Modelling*, v. 240, no. 0, p. 113-122.

Cutler, D. R., Edwards, T. C., Beard, K. H., Cutler, A., Hess, K. T., Gibson, J., and Lawler, J. J., 2007, Random forests for classification in ecology: *Ecology*, v. 88, no. 11, p. 2783-2792.

DeLong, E. R., DeLong, D. M., and Clarke-Pearson, D. L., 1988, Comparing the areas under two or more correlated receiver operating characteristic curves: a nonparametric approach: *Biometrics*, p. 837-845.

Dennison, P. E., Halligan, K. Q., and Roberts, D. A., 2004, A comparison of error metrics and constraints for multiple endmember spectral mixture analysis and spectral angle mapper: *Remote Sensing of Environment*, v. 93, no. 3, p. 359-367.

Dennison, P. E., and Roberts, D. A., 2003a, The effects of vegetation phenology on endmember selection and species mapping in southern California chaparral: *Remote Sensing of Environment*, v. 87, no. 2-3, p. 295-309.

Dennison, P. E., and Roberts, D. A., 2003b, Endmember selection for multiple endmember spectral mixture analysis using endmember average RMSE: *Remote Sensing of Environment*, v. 87, no. 2-3, p. 123-135.

Dronova, I., Gong, P., Clinton, N. E., Wang, L., Fu, W., Qi, S., and Liu, Y., 2012, Landscape analysis of wetland plant functional types: The effects of image segmentation scale, vegetation classes and classification methods: *Remote Sensing of Environment*, v. 127, no. 0, p. 357-369.

Dufrêne, M., and Legendre, P., 1997, Species assemblages and indicator species: the need for a flexible asymmetrical approach: *Ecological Monographs*, v. 67, no. 3, p. 345-366.

Evans, B. M., Walker, D. A., Benson, C. S., Nordstrand, E. A., and Peterson, G. W., 1989, Spatial interrelationships between terrain, snow distribution and vegetation patterns at an arctic foothills site in Alaska: *Holarctic Ecology*, v. 12, p. 270-278.

Evans, J. S., and Cushman, S. A., 2009, Gradient modeling of conifer species using random forests: *Landscape Ecology*, v. 24, no. 5, p. 673-683.

Exelis Visual Information Solutions, 2014, ENVI version 5.0: Boulder, Colorado.

Grosse, G., Schirrmeister, L., Kunitsky, V. V., and Hubberten, H. W., 2005, The use of CORONA images in remote sensing of periglacial geomorphology: An illustration from the NE Siberian coast: *Permafrost and Periglacial Processes*, v. 16, p. 163-172.

Hamilton, T. D., 2002, Glacial geology of the Toolik Lake and Upper Kuparuk River region: University of Alaska Fairbanks, 26.

Haralick, R., Shanmugan, K., and Dinstein, I., 1973, Textural features for image classification: *IEEE Transactions on Systems, Man, and Cybernetics*, v. 3, no. 6, p. 610-621.

Heung, B., Bulmer, C. E., and Schmidt, M. G., 2014, Predictive soil parent material mapping at a regional-scale: A Random Forest approach: *Geoderma*, v. 214–215, no. 0, p. 141-154.

Hinzman, L. D., Deal, C. J., McGuire, A. D., Mernild, S. H., Polyakov, I. V., and Walsh, J. E., 2013, Trajectory of the Arctic as an integrated system: Ecological Applications, v. 23, no. 8, p. 1837-1868.

Hinzman, L. D., Kane, D. L., Benson, C. S., and Everett, K. R., 1996, Energy balance and hydrological processes in an Arctic watershed, in Reynolds, J. F., and Tenhunen, J. D., eds., Ecological Studies; Landscape function and disturbance in Arctic tundra, Springer-Verlag; Springer-Verlag New York, Inc., p. 131-154.

Jorgenson, M. T., and Heiner, M., 2008, Ecosystems of Northern Alaska: ABR Inc. and the Nature Conservancy.

Kane, D. L., Hinzman, L. D., Benson, C. S., and Everett, K. R., 1989, Hydrology of Imnavait Creek, an arctic watershed: Holarctic Ecology, v. 12, p. 262-271.

Kuhn, M., Wing, J., Weston, S., Williams, A., Keefer, C., Engelhardt, A., and Cooper, T., 2013, caret: Classification and regression training, R package version 5.17-7.

Liaw, A., and Wiener, M., 2002, Classification and regression by randomForest: R news, v. 2, no. 3, p. 18-22.

McGeoch, M. A., and Chown, S. L., 1998, Scaling up the value of bioindicators: Trends in Ecology & Evolution, v. 13, no. 2, p. 46-47.

McNamara, J. P., Kane, D. L., and Hinzman, L. D., 1998, An analysis of streamflow hydrology in the Kuparuk River basin, Arctic Alaska: A nested watershed approach: Journal of Hydrology, v. 206, no. 1-2, p. 39-57.

McNamara, J. P., Kane, D. L., and Hinzman, L. D., 1999, An analysis of an arctic channel network using a digital elevation model: Geomorphology, v. 29, p. 339-353.

Mueller-Dombois, D., and Ellenberg, H., 1974, Aims and methods of vegetation ecology, New York, John Wiley & Sons.

Okin, G. S., Roberts, D. A., Murray, B., and Okin, W. J., 2001, Practical limits on hyperspectral vegetation discrimination in arid and semiarid environments: *Remote Sensing of Environment*, v. 77, no. 2, p. 212-225.

Osterkamp, T. E., and Payne, M. W., 1981, Estimates of permafrost thickness from well logs in northern Alaska: *Cold Regions Science and Technology*, v. 5, no. 1, p. 13-27.

Pal, M., 2005, Random forest classifier for remote sensing classification: *International Journal of Remote Sensing*, v. 26, no. 1, p. 217-222.

Quintano, C., Fernández-Manso, A., and Roberts, D. A., 2013, Multiple Endmember Spectral Mixture Analysis (MESMA) to map burn severity levels from Landsat images in Mediterranean countries: *Remote Sensing of Environment*, v. 136, p. 76-88.

R Core Team, 2014, R: A Language and Environment for Statistical Computing: Vienna, Austria, R Foundation for Statistical Computing.

Raynolds, M. K., Comiso, J. C., Walker, D. A., and Verbyla, D., 2008, Relationship between satellite-derived land surface temperatures, arctic vegetation types, and NDVI: *Remote Sensing of Environment*, v. 112, no. 4, p. 1884-1894.

Richardson, A. J., and Everitt, J. H., 1992, Using spectral vegetation indices to estimate rangeland productivity: *Geocarto International*, v. 7, no. 1, p. 63-69.

Richter, R., and Schlapfer, D., 2011, Atmospheric/topographic correction for satellite imagery, ATCOR 2/3 User Guide.

Riseborough, D., Shiklomanov, N., Etzelmuller, B., Gruber, S., and Marchenko, S., 2008, Recent advances in permafrost modelling: Permafrost and Periglacial Processes, v. 19, no. 2, p. 137-156.

Roberts, D. A., Batista, G., Pereira, J., Waller, E., and Nelson, B., 1998, Change identification using multitemporal spectral mixture analysis: Applications in eastern Amazonia, in Elvidge, C., and Lunetta, R., eds., Remote Sensing Change Detection: Environmental Monitoring Applications and Methods: Ann Arbor, MI, Ann Arbor Press, p. 137-161.

Roberts, D. A., Dennison, P. E., Gardner, M. E., Hetzel, Y., Ustin, S. L., and Lee, C. T., 2003, Evaluation of the potential of Hyperion for fire danger assessment by comparison to the Airborne Visible/Infrared Imaging Spectrometer: IEEE Transactions on Geoscience and Remote Sensing, v. 41, no. 6, p. 1297-1310.

Roberts, D. A., Halligan, K., and Dennison, P., 2007, VIPER tools user manual. V1.5.

Roberts, D. W., 2013, labdsv: Ordination and multivariate analysis for ecology, R package version 1.7-0.

Rodriguez-Galiano, V. F., Ghimire, B., Rogan, J., Chica-Olmo, M., and Rigol-Sanchez, J. P., 2012, An assessment of the effectiveness of a random forest classifier for land-cover classification: ISPRS Journal of Photogrammetry and Remote Sensing, v. 67, no. 0, p. 93-104.

Roth, K. L., Dennison, P. E., and Roberts, D. A., 2012, Comparing endmember selection techniques for accurate mapping of plant species and land cover using imaging spectrometer data: Remote Sensing of Environment, v. 127, no. 0, p. 139-152.

Schoeneberger, P. J., Wysocki, D. A., Benham, E. C., and Broderson, W. D., 2002, Fieldbook for describing and sampling soils, Version 2.0. , in Natural Resources Conservation Service, ed.: Lincoln, NE, National Soil Survey Center.

Schramm, I., Boike, J., Bolton, W. R., and Hinzman, L. D., 2007, Application of TopoFlow, a spatially distributed hydrological model, to the Imnavait Creek watershed, Alaska: *Journal of Geophysical Research-Biogeosciences*, v. 112, no. G4, p. 1-14.

Sonnentag, O., Chen, J. M., Roberts, D. A., Talbot, J., Halligan, K. Q., and Govind, A., 2007, Mapping tree and shrub leaf area indices in an ombrotrophic peatland through multiple endmember spectral unmixing: *Remote Sensing of Environment*, v. 109, no. 3, p. 342-360.

Stefanski, J., Mack, B., and Waske, B., 2013, Optimization of object-based image analysis with random forests for land cover mapping: *IEEE Journal of Selected Topics in Applied Earth Observations and Remote Sensing*, v. 6, no. 6, p. 2492-2504.

Tape, K. D., Verbyla, D., and Welker, J. M., 2011, Twentieth century erosion in Arctic Alaska foothills: The influence of shrubs, runoff, and permafrost: *Journal of Geophysical Research-Biogeosciences*, v. 116, p. 1-11.

Tarantino, C., Adamo, M., Pasquariello, G., Lovergine, F., Blonda, P., and Tomaselli, V., 2012, 8-band image data processing of the worldview-2 satellite in a wide area of applications: *Earth Observation*, p. 137-152.

Timm, B. C., and McGarigal, K., 2012, Fine-scale remotely-sensed cover mapping of coastal dune and salt marsh ecosystems at Cape Cod National Seashore using Random Forests: *Remote Sensing of Environment*, v. 127, no. 0, p. 106-117.

Touzi, R., Omari, K., Gosselin, G., and Sleep, B., 2013, Polarimetric L-band ALOS for peatland subsurface water monitoring, in *Proceedings Synthetic Aperture Radar (AP SAR)*, 2013 Asia-Pacific Conference on 23-27 Sept. 2013, p. 53-56.

Trochim, E. D., 2015, Bridging Arctic pathways: Integrating hydrology, geomorphology and remote sensing in the north, Ph.D. diss., University of Alaska Fairbanks.

Ulrich, M., Grosse, G., Chabrillat, S., and Schirrmeister, L., 2009, Spectral characterization of periglacial surfaces and geomorphological units in the Arctic Lena Delta using field spectrometry and remote sensing: *Remote Sensing of Environment*, v. 113, no. 6, p. 1220-1235.

Walker, D. A., Epstein, H. E., Jia, G. J., Balser, A., Copass, C., Edwards, E. J., Gould, W. A., Hollingsworth, J., Knudson, J., Maier, H. A., Moody, A., and Reynolds, M. K., 2003, Phytomass, LAI, and NDVI in northern Alaska: Relationships to summer warmth, soil pH, plant functional types, and extrapolation to the circumpolar Arctic: *Journal of Geophysical Research-Atmospheres*, v. 108, no. D2, p. 1-18.

Walker, D. A., and Maier, H. A., 2008, Vegetation in the vicinity of the Toolik Field Station, Alaska: Institute of Arctic Biology.

Walker, M. D., Walker, D. A., and Auerbach, N. A., 1994, Plant communities of a tussock tundra landscape in the Brooks Range Foothills, Alaska: *Journal of Vegetation Science*, v. 5, p. 843-866.

Willett, P., 1999, Dissimilarity-based algorithms for selecting structurally diverse sets of compounds: *Journal of Computational Biology*, v. 6, no. 3-4, p. 447-457.

Wood, J., 1996, The geomorphological characterization of digital elevation models: Ph. D. diss., University of Leicester (United Kingdom).

Woźniak, M., Graña, M., and Corchado, E., 2014, A survey of multiple classifier systems as hybrid systems: *Information Fusion*, v. 16, no. 0, p. 3-17.

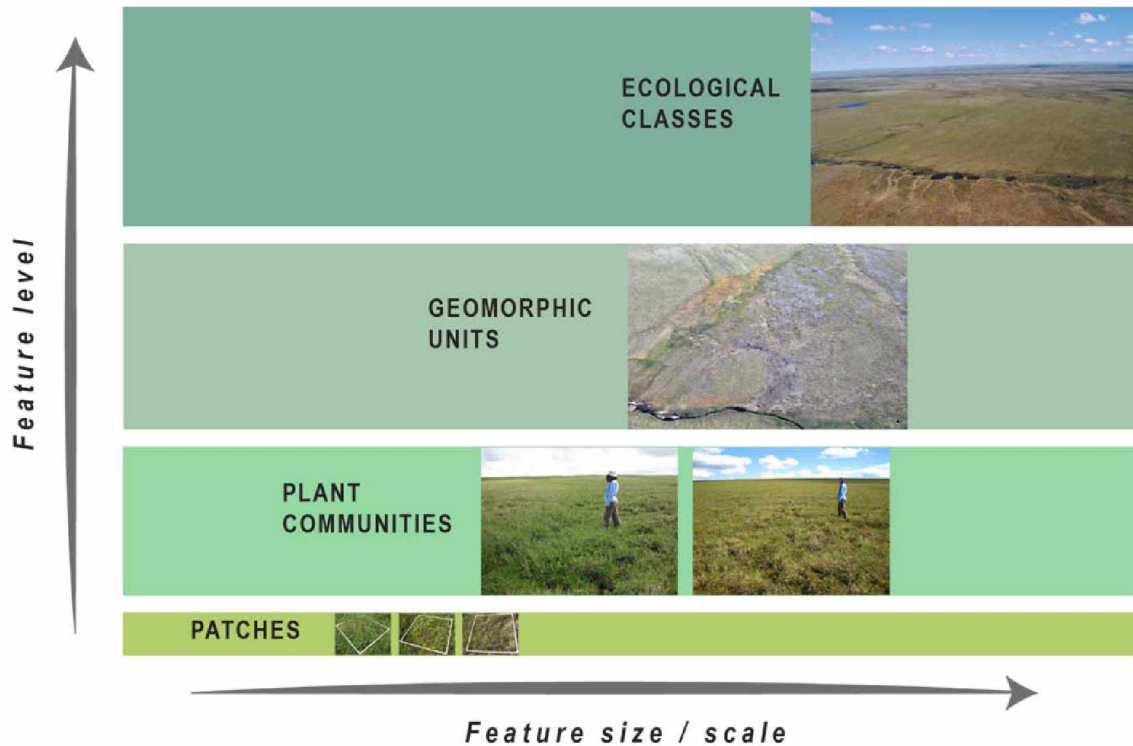


Figure 2.1: Comparing the affects between feature levels and feature size / scale for mapping water track properties on the North Slope of Alaska.

Vegetation is typically quantified by 1 m² plots or patches. These are extrapolated to estimate the plant communities. Between water tracks and the surrounding areas, plant communities typically vary. Substantial differences in plant communities are driven by underlying differences in geomorphology, which are quantified by mapping geomorphic units. Important changes in geomorphology such as the patterns of glaciation or significant climatic shifts control the location and range of ecological classes. Photos: E.D. Trochim.

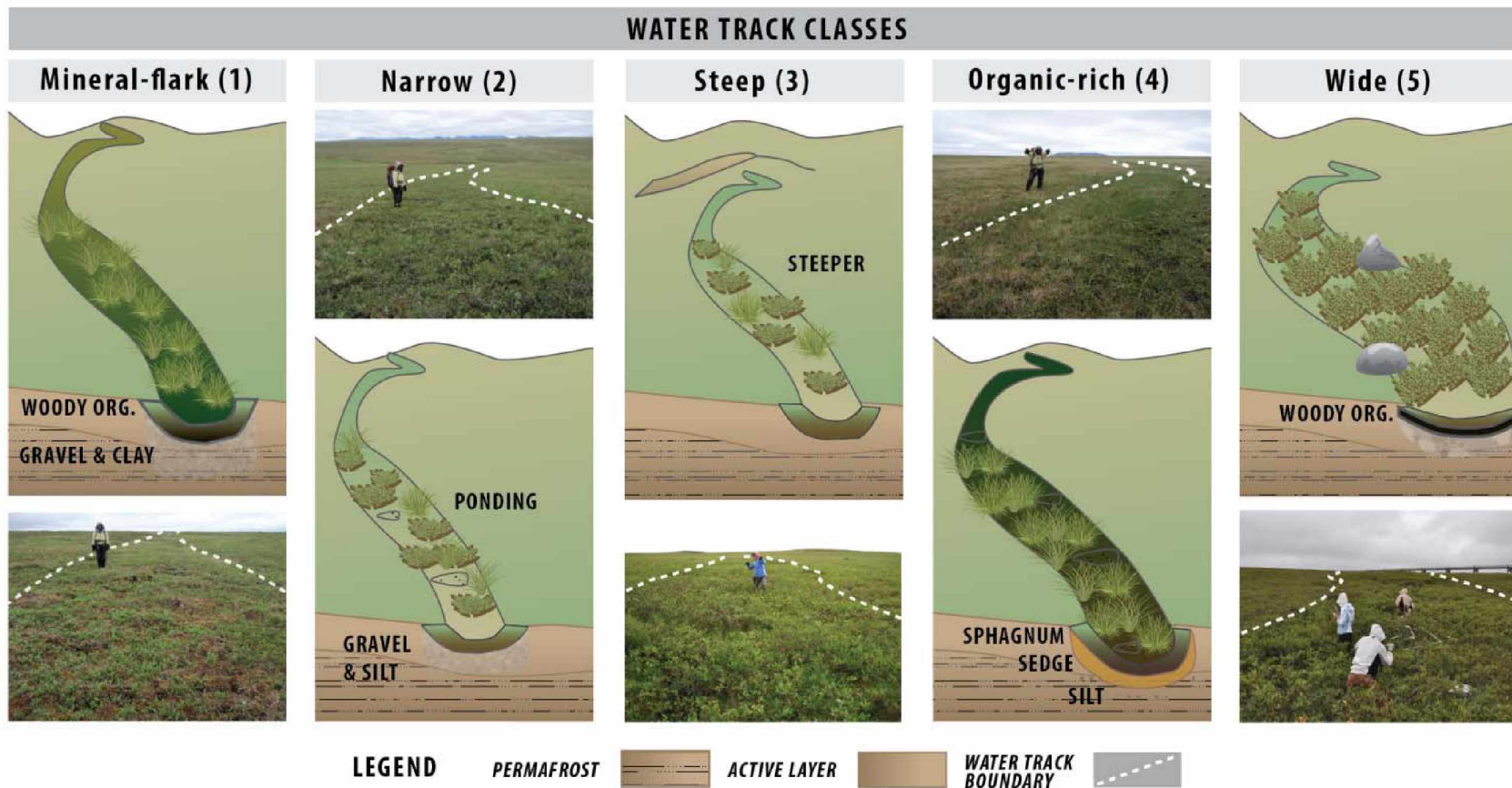


Figure 2.2: Water track classes in the Toolik Lake LTER.

Highlighted for the classes are the main characteristics in terms of vegetation, soil moisture and soil stratigraphy. A photographic example is also given for each class to assist in understanding the appearance of each class. The type of water track is ultimately controlled by the dominant surficial geological conditions, which affect the vegetation. Understanding and incorporating water tracks into hydrological and landscape-process models requires knowledge of both their locations and characteristics. Photos: E.D. Trochim.

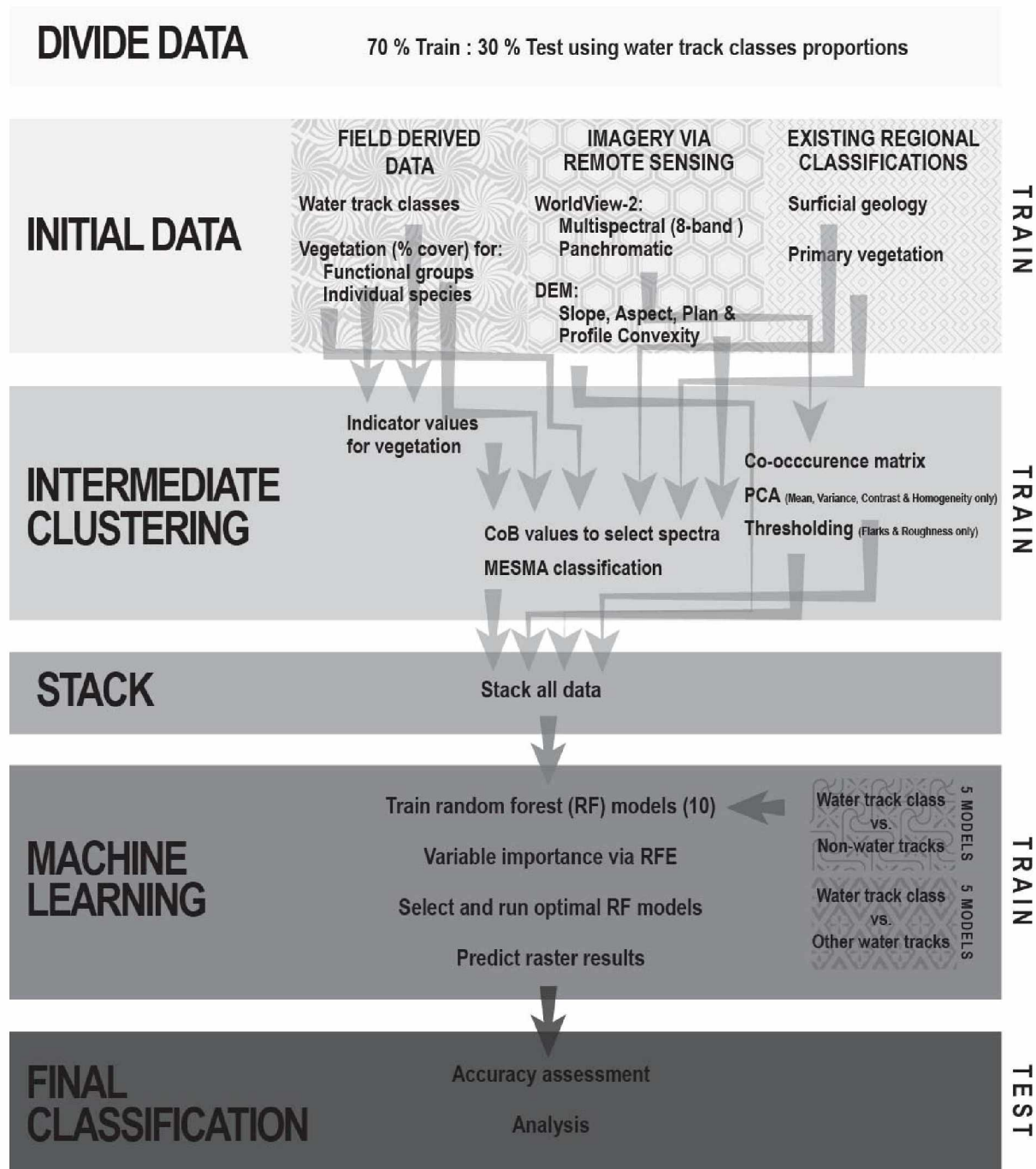


Figure 2.3: Flowchart of input data and methodology.

The plots were initially divided into train and test datasets while maintaining the proportions of the water track classes. A combination of field derived data, imagery and existing regional classifications were used as input data. After intermediate clustering, the final dataset was used to predict the classes using multiple random forest models. The final classification was evaluated using accuracy assessments derived using the test dataset.

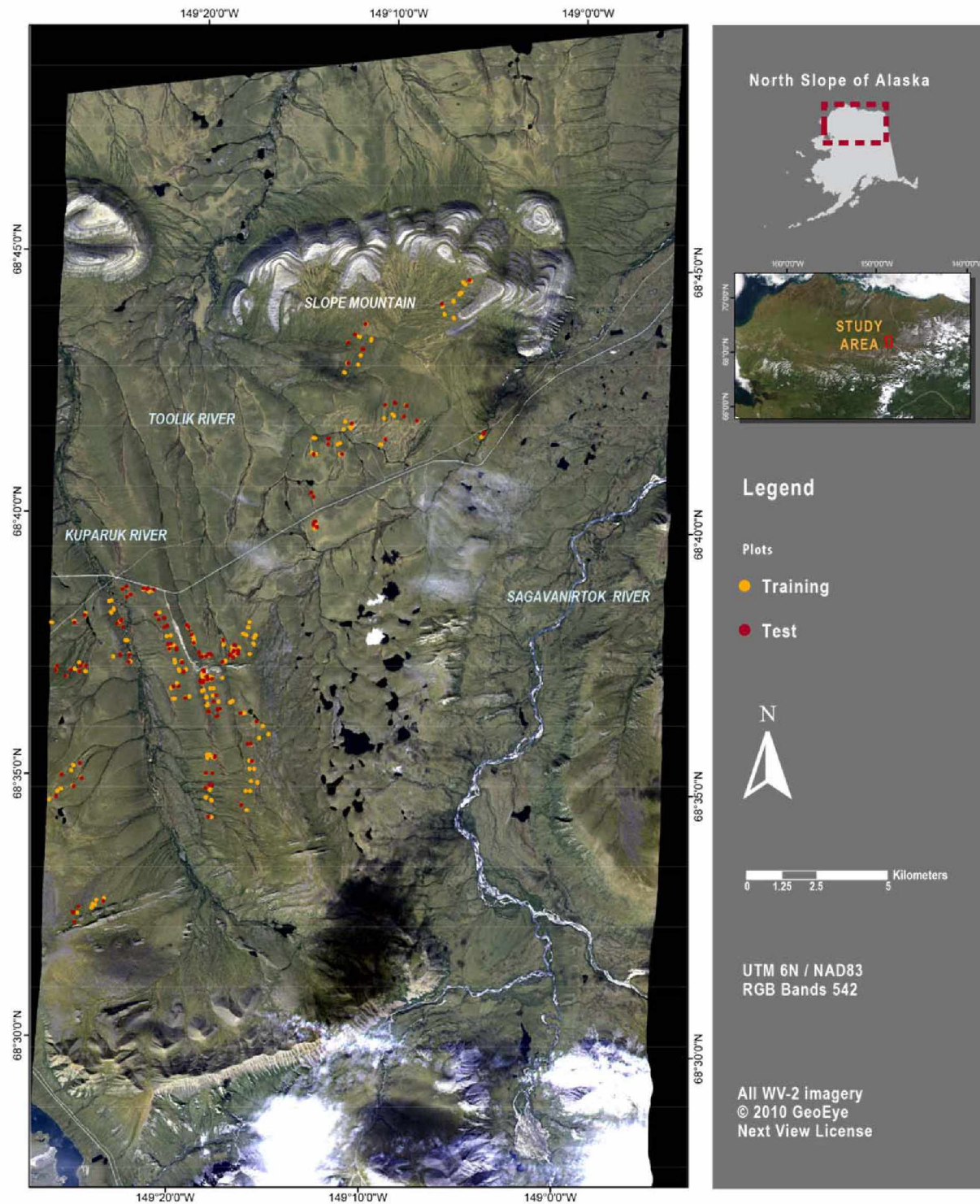


Figure 2.4: Study area location showing locations of training and test plots overlaid on WorldView-2 imagery bands 5, 4, 2 and RGB input.

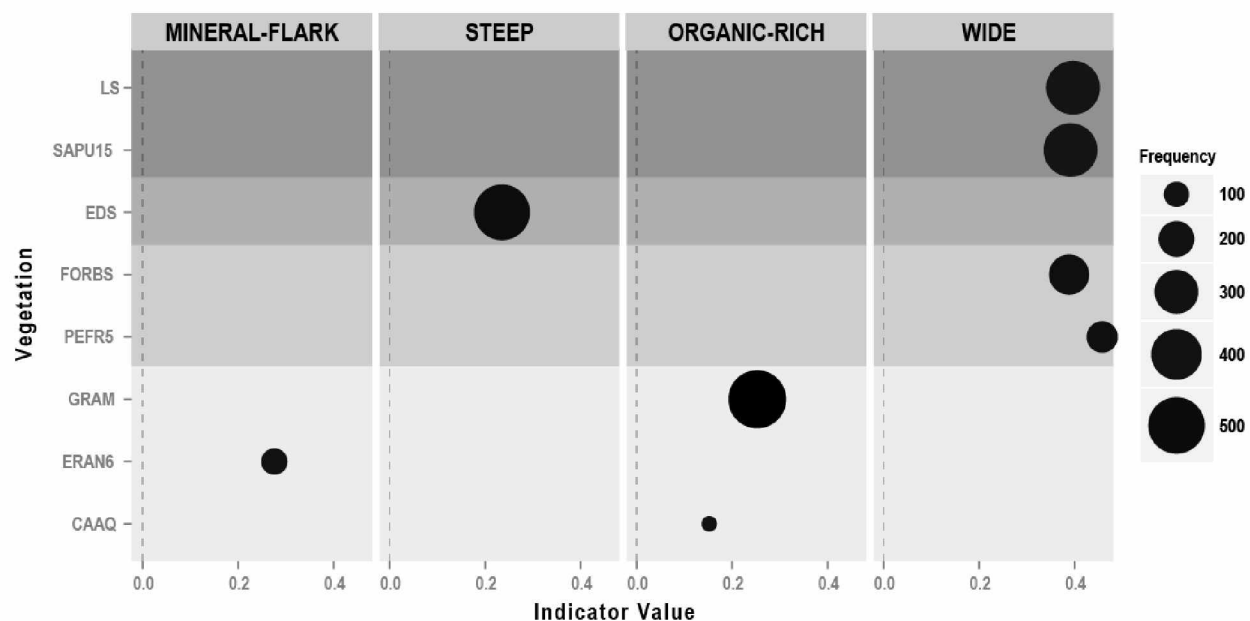


Figure 2.5: Vegetation and species identified for each water track class by calculating indicator values.

Shading indicates the type of vegetation class and the related species. The abbreviations are as follows: low shrubs (LS), *Salix pulchra* (SAPU15), erect dwarf shrubs (EDS), forbs (FORBS), *Petasites frigidus* (PEFR5), graminoids (GRAM), *Eriophorum angustifolium* (ERAN6) and *Carex aquatilis* (CAAQ). The indicator value represents the value of a species in relation to the type of site. Frequency indicates the number of times the species was found among the samples (not abundance).

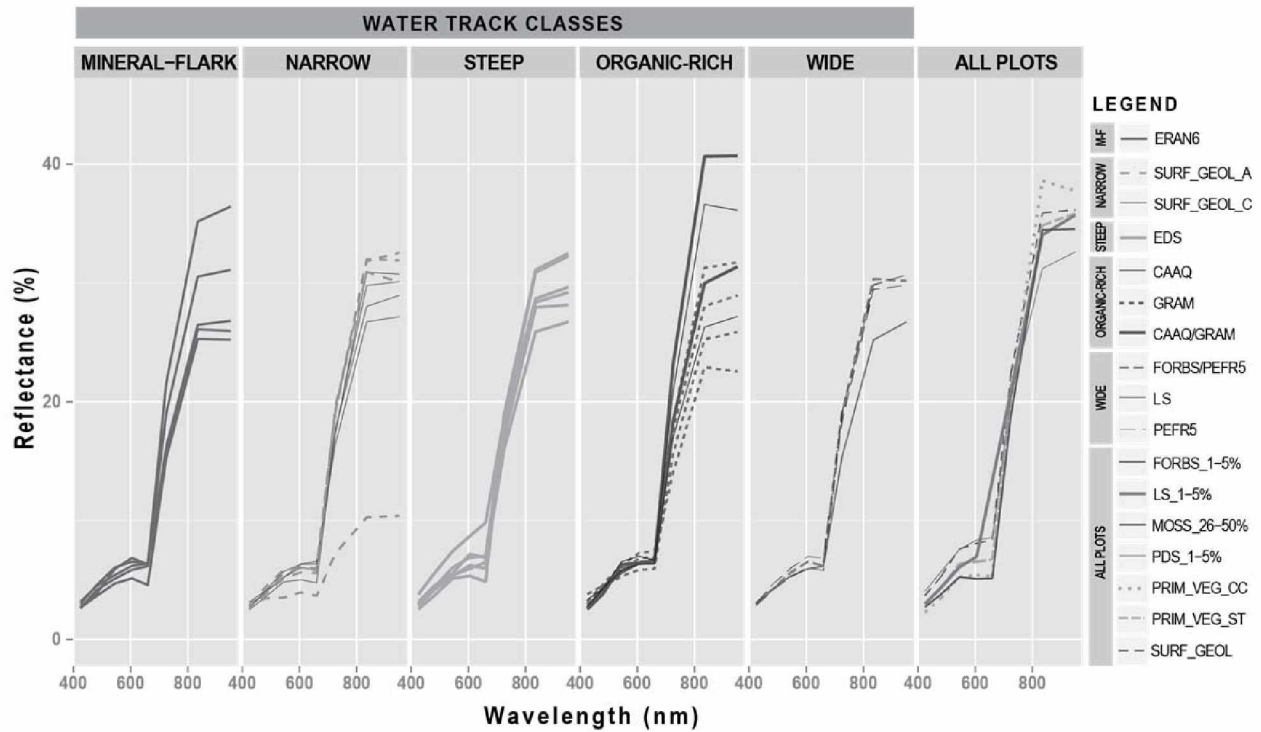


Figure 2.6: Input spectra used for MESMA classification.

Specific spectra were selected for each of the water tracks based on the indicator values clustering results or for the case of the narrow class the dominating surficial geology. Additional versions of the MESMA classification used spectra derived from all classes based on common types of vegetation and surficial geology.

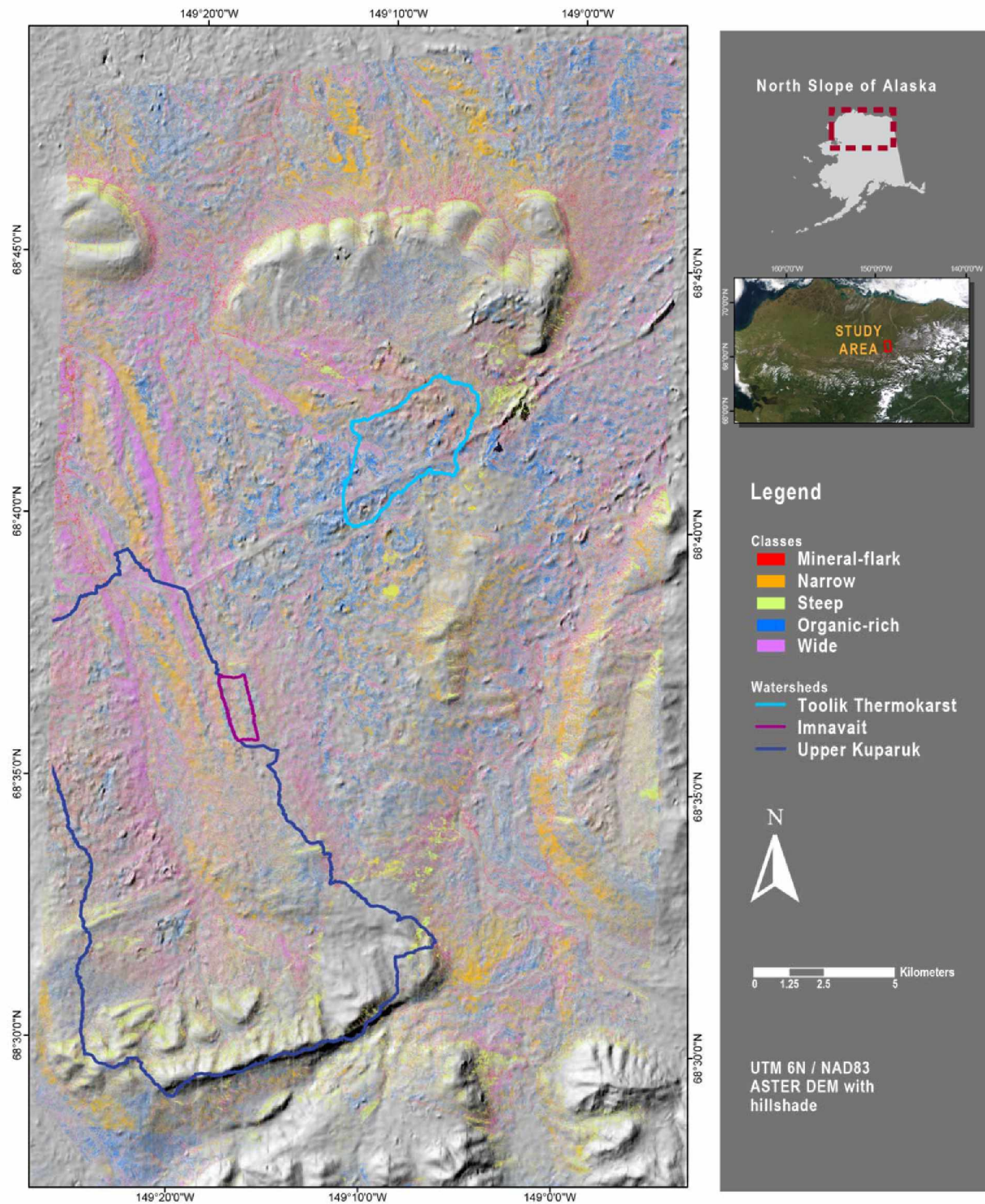


Figure 2.7: Final water track classes overlaid over ASTER DEM with hillshade.

The locations of the Toolik Thermokarst, Imnavait and Upper Kuparuk watershed boundaries are indicated.

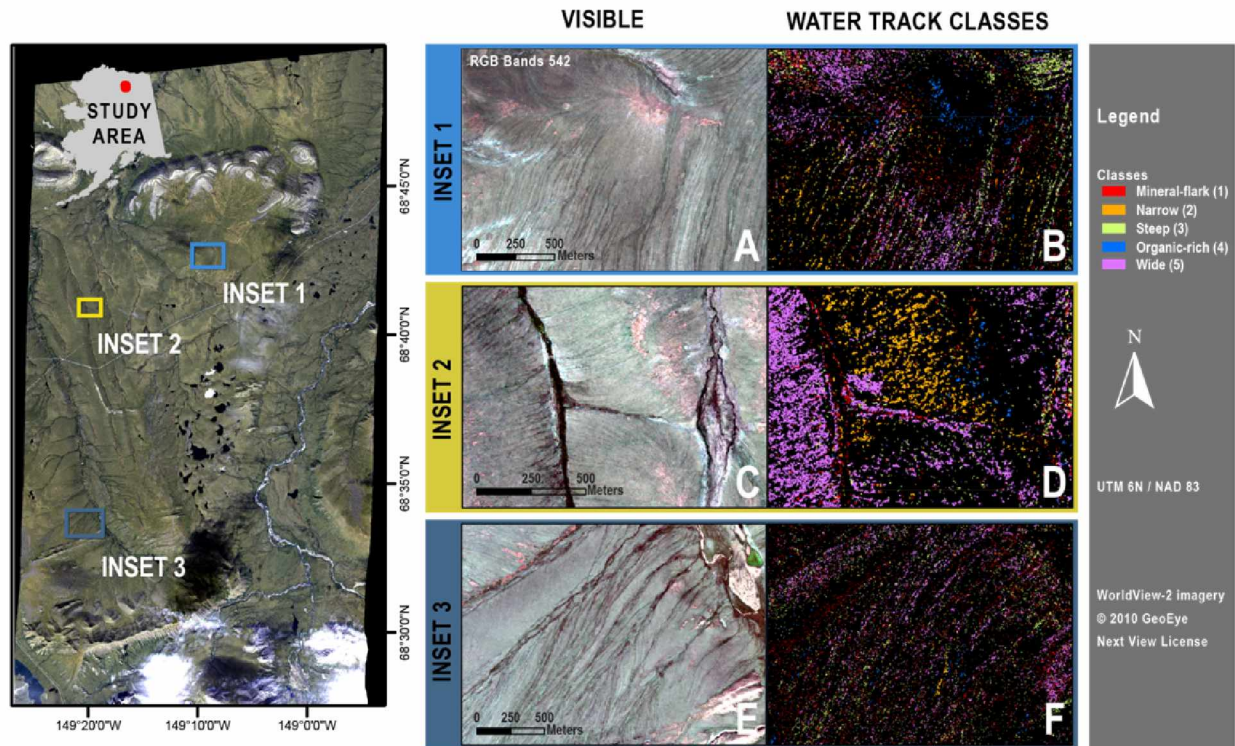


Figure 2.8: Inset examples of the water track classes which were majority filtered to aid interpretation.

A and B) show distinctive striped water tracks at the foot of Slope Mountain which are a mix of the narrow, steep and wide classes. C and D) show an incised drainage characterized by mineral-flark in the center and wide at the margins. On the west-facing slope are narrow water tracks versus the wide ones found on the east-facing. E and F) Show large wide water tracks on the east-facing slope of the Upper Kuparuk basin. These water tracks were also characterized by mineral-flark, steep and narrow areas.

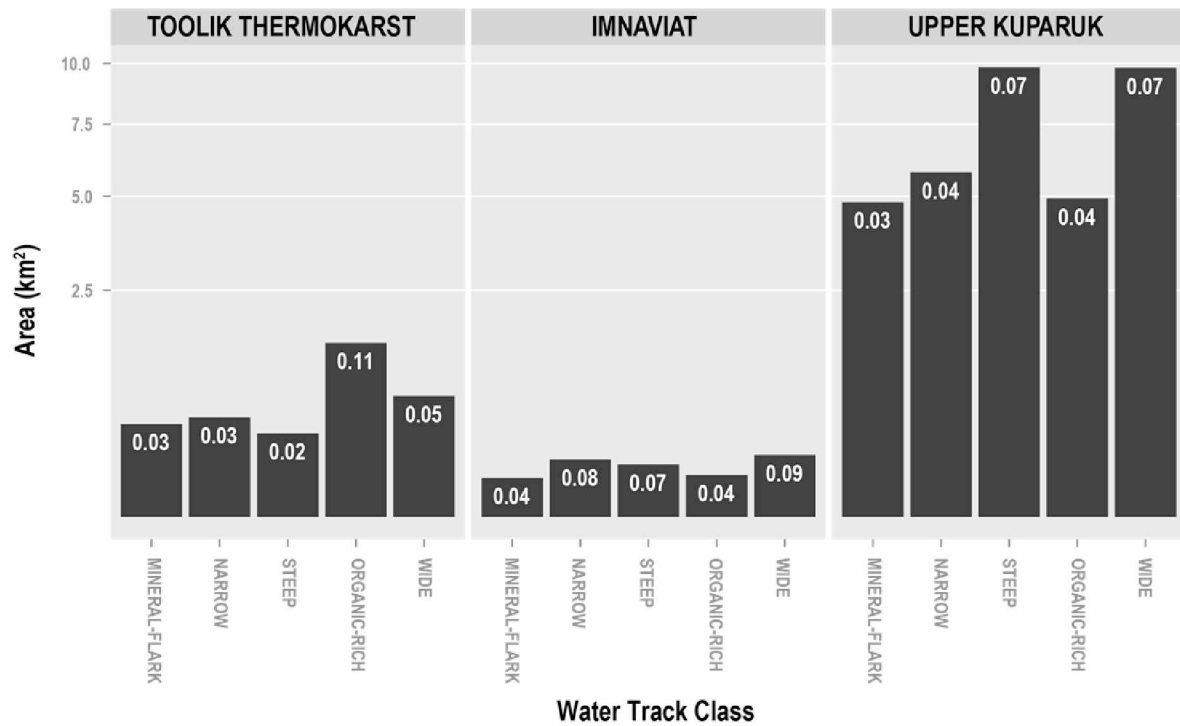


Figure 2.9: Area of water track classes for the Toolik Thermokarst, Imnavait and Upper Kuparuk watersheds.

The area is shown in square kilometers using a square root scale to enable visualization of all basins using the same notation. The percent area for each class versus the total watershed area is given. Note the similarities in proportions between the Imnavait and Upper Kuparuk basins in contrast to the Toolik thermokarst watershed.

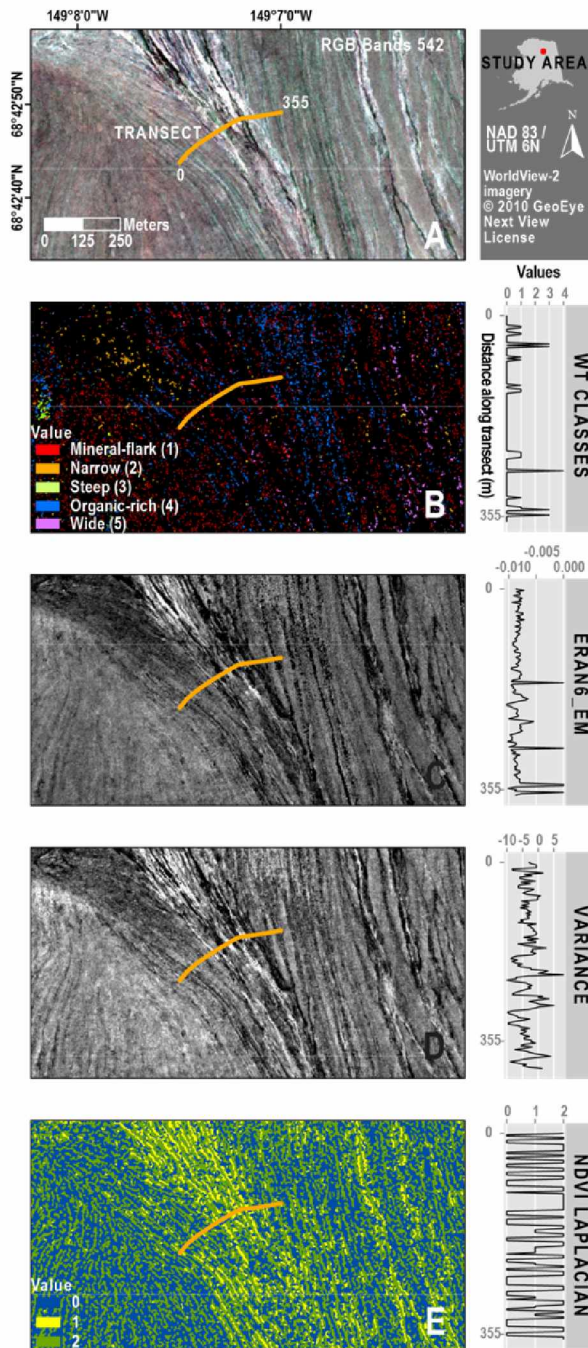


Figure 2.10: Analysis of mineral-flark water tracks.

A) Visible WorldView-2 imagery showing RGB 542. Location of the transect used for comparison is shown. B) Majority filtered water track classes where the mineral-flark class is shown in red. C) ERAN6 (*Eriophorum angustifolium*) ElectroMagnetic (EM) fraction where the water tracks are black. D) Variance from the co-occurrence matrix where the water tracks have a higher contrast to the landscape. E) NDVI (calculated the WorldView-2 data) filtered using a laplacian with density slicing, sieving and majority filtering applied.

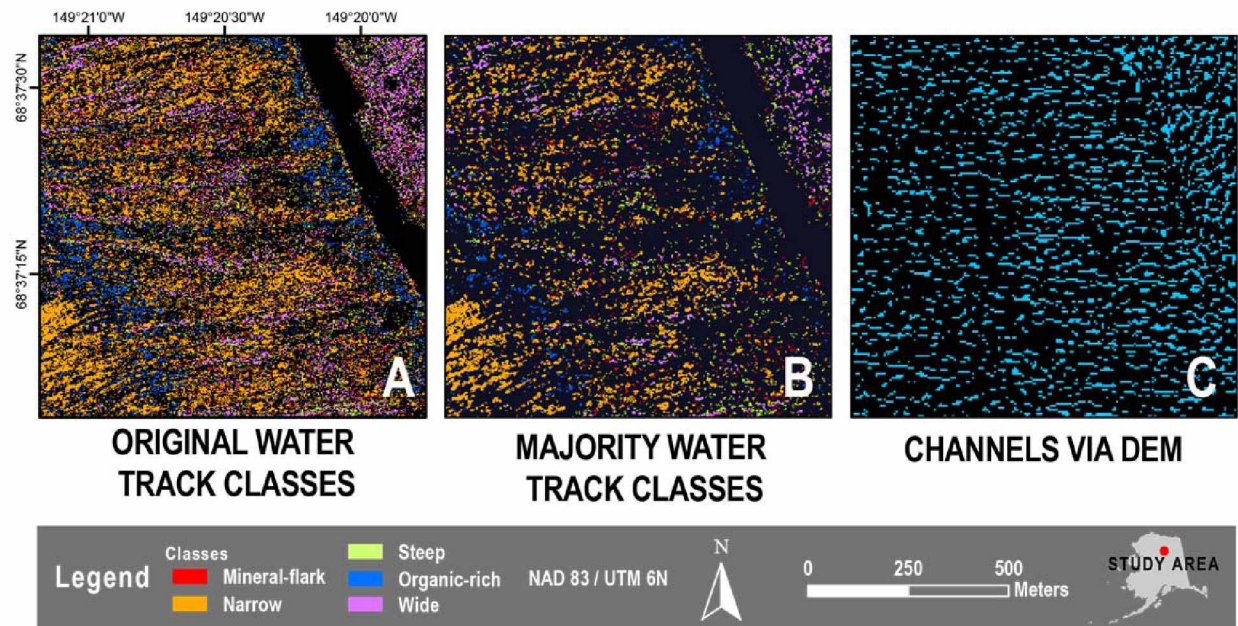


Figure 2.11: Water track classes compared to channels derived via DEM.

A) Illustrates the granularity of the original water track classes. B) Majority filtered water track classes which more clearly show that the slope is dominated by the narrow class. C) Alternatives to spectral approaches include extraction of channels via a 5 meter Star3i DEM which was low-passed filtered before topographic analysis.

Table 2.1: Radiometric, spatial, and spectral resolutions of the WorldView-2 satellite imagery used for this study for each band.

The data was acquired July 10, 2011.

Sensor	Radiometric resolution	Spatial resolution (m)	Spectral bands	Band name	Band range	Band centers	Band widths
					(nm)		
WorldView-2	11-bit	0.50	1	B-Pan	450 – 800	632	285
		1.84	8	B1	400 – 450	427	47.3
				B2	450 – 510	478	54.3
				B3	510 – 580	546	63
				B4	585 – 625	608	37.4
				B5	630 – 690	659	57.4
				B6	705 – 745	724	39.3
				B7	770 – 895	831	98.9
				B8	860 – 1040	908	99.6

Table 2.2: Final stacked raster dataset layers (n = 39) used as input for random forest models.

For Classes / Type, the following abbreviations were used: Presence - Absence (P-A); ElectroMagnetic (EM) fractions; and Root Mean Square Error (RMSE).

Layer	Abbreviation	Classes / Type	Processing	Input imagery
Band 1	B1	Reflectance	Converted via ATCOR to at-surface reflectance	WorldView-2: Multispectral
Band 2	B2			
Band 3	B3			
Band 4	B4			
Band 5	B5			
Band 6	B6			
Band 7	B7			
Band 8	B8			
Surficial geology	SURF_GEOL	P-A Colluvial	Best CoBI values from MESMA	
Primary vegetation	PRIM_VEG	P-A Caline-Castet (CC), Subass. Typicum (ST)		
Forbs	FORBS	P-A 1-5%		
Prostrate dwarf shrubs	PDS	P-A 1-5%		
Low shrubs	LS	P-A 1-5%		
Moss	MOSS	P-A 26-50%		
Eriophorum angustifolium	ERAN6	EM RMSE	MESMA: Mineral-flark WTs	
Surficial geology: colluvial	SURF_GEOL_C	EM	MESMA: Narrow WTs	
Surficial geology: alluvial	SURF_GEOL_A	EM		
Surficial geology: colluvial / alluvial		RMSE		
Erect dwarf shrubs	EDS	EM RMSE	MESMA: Steep WTs	
Graminoids	GRAM	EM	MESMA: Organic-rich WTs	
Carex aquatilis	CAAQ	EM		
Graminoids / Carex aquatilis		RMSE		
Low shrubs	LS	EM RMSE	MESMA: Wide WTs	
Forbs	FORBS	EM		
Petasites frigidus	PEFR5	EM		
Forbs / Petasites frigidus		RMSE		
Roughness		P-A	Co-occurrence matrix & thresholding	WorldView-2: Panchromatic
Flarks				
Mean		Values 0 – 1.0	Co-occurrence matrix & PCA	
Variance				
Homogeneity				
Contrast				
Slope		Percent	Topographic analysis	Star3i DEM
Aspect		Degrees		
Profile convexity		Convex positive, concave negative		
Plan convexity				

Table 2.3: Model results from random forests for each water track class.

Each water track class had two binary models: one for presence of the water tracks (vs. non water tracks) and the second to differentiate the specific class of water track (vs. other water tracks). The number (N) of the alternate (X0) versus desired (X1) class is given for both train and test datasets. If the variable selection produced a better model, the number of selected variables is given. The out of bag (OOB) error is given for the training set while the accuracy refers to the final model results on the tests data.

Water Track Class	Type	N Train X0 / X1	OOB Error	Train ROC	Number of Variables Selected	N Test X0 / X1	Test Accuracy	Test ROC
<i>Mineral- Flark (1)</i>	Presence	60 / 24	30.95%	0.70	5	76 / 10	0.7674	0.67
	Classes	60 / 24	28.57%	0.72	5	70 / 10	0.7125	0.56
<i>Narrow (2)</i>	Presence	180 / 97	35.38%	0.58	--	76 / 41	0.6667	0.47
	Classes	98 / 97	43.59%	0.64	9	39 / 41	0.6	0.64
<i>Steep (3)</i>	Presence	90 / 45	37.04%	0.62	--	76 / 18	0.7234	0.53
	Classes	90 / 45	37.78%	0.63	--	62 / 18	0.7125	0.59
<i>Organic- Rich (4)</i>	Presence	48 / 24	36.11%	0.71	11	76 / 10	0.8023	0.77
	Classes	60 / 24	26.19%	0.75	19	70 / 10	0.85	0.70
<i>Wide (5)</i>	Presence	28 / 14	28.57%	0.81	11	76 / 1	0.7792	0.95
	Classes	35 / 14	26.53%	0.84	5	79 / 1	0.8	0.92

Chapter 3 Optimizing LAI estimates in the Arctic using remote sensing¹

3.1 Abstract

Calculations of Leaf Area Index (LAI) in Arctic regions using remotely sensed imagery are important given increases in the Normalized Difference Vegetation Index (NDVI) and shrub cover. The purpose of this study was to optimize LAI calculations using the gap-method with NDVI as input for both WorldView-2 and Landsat-7 imagery. This method of estimating LAI was repeated for different groups based on the presence/absence of water tracks and changes in NDVI over time which confound estimates of greenness. Changes in surficial moisture conditions are a known confounding factor in NDVI measurements and the study design helped to isolate this affect. Ground-based measurements of vegetation cover and type were used to understand sub-pixel variability and supplement the analysis. The results showed that NDVI values were higher for the WorldView-2 data than the Landsat-7 imagery and for both sensors the distributions were unique to their groups. After the LAI calculations were developed for each group and satellite, overall the Landsat-7 results had lower RMSE values while those from the WorldView-2 had greater variability. The variability in Landsat-7 LAI for some groups was linked to the interaction between NDVI and either graminoids or erect dwarf shrubs. In contrast the WorldView-2 LAI results showed significant interactions between NDVI and moss for water tracks with high amounts of change in the NDVI values over time. This study showed that even though higher resolution images may be superior for identifying and mapping landcover classes (such as different types of water tracks), a coarser resolution image that averages some of the variability in spectral signatures may be superior for estimating the LAI.

3.2 Introduction

In tundra ecosystems remotely deriving canopy cover is critical for predicting the effects of climate change on vegetation cover and related processes. This information is a key component for computing primary productivity (Stoy et al., 2009), energy balance, evapotranspiration (Anderson and Kustas, 2008) and biogeochemical cycling. Canopy cover is defined by the dimensionless Leaf Area Index (LAI) which is the total one-sided area of leaves per unit ground

¹ Trochim, E.D., Mumm, J.P., Prakash, A. & Kane, D.L. Optimizing LAI estimates in the Arctic using remote sensing, submitted to *Remote Sensing*.

area (Watson, 1947). Calculating LAI can be challenging due to variability in spatial (horizontal and vertical dimensions) and temporal dimensions in addition to the issues of stratification and heterogeneity (Breda, 2003). In the Arctic, previous efforts have concentrated on tying direct methods of calculating LAI with indices that can be derived through remotely sensed imagery including the Normalized Difference Vegetation Index (NDVI) and Enhanced Vegetation Index (EVI) (Rocha and Shaver, 2009; Stenberg et al., 2004; van Wijk and Williams, 2005; Williams et al., 2008). These studies compared LAI calculated at the plot scale (0.1 m^2 to 1 m^2) to NDVI and/or EVI derived either via plot scale measurements or from satellite imagery with a pixel size of at least 30 m. This study builds on previous work by utilizing remotely sensed imagery collected in similar space and time dimensions. Data was acquired from the WorldView-2 satellite during field collections and compared to images obtained from Landsat 7.

Canopy cover, and by definition LAI, reflect plant and vegetation community composition. Previous work by Shippert et al. (1995) demonstrated that plant functional types with specific moisture contents could be used as groups to better predict LAI. The independent variable in this study was NDVI. This approach was an indirect method to limiting the effects of soil moisture and its interaction with moss, which are the two largest unknowns in terms of its influence on NDVI and thus LAI. Hallik et al. (2009) showed spectral reflectance from within an herb-moss layer was related to its mass bulk properties in the visible spectrum and the above ground water content in the near infrared portion. Differentiating the effects of pixel mixing from the vegetation components is also an issue in relating LAI to NDVI values derived at different spatial resolutions. Dividing the landscape into similar groups based on vegetation and hydrologic characteristics is one way to gage the impact of pixel mixing in different areas.

Surficial water drainage is a key consideration in continuous permafrost environments as illustrated by Engstrom et al. (2008) as variations in vascular vegetation greenness and wetness are associated with microsite topography. On the northern side of the Brooks Range in Alaska, drainage networks are comprised of linear-curvilinear saturated stripes known as water tracks (McNamara et al., 1999). They can easily be identified by the differences in vegetation between the track and surrounding area. Water is confined to the active layer ($< 1\text{m}$) due to continuous permafrost (McNamara et al., 1998) and the immediate water track area shows high amounts of

the shrubs *Betula nana* and *Salix planifolia ssp. pulchra* (Walker et al., 1994) and increased amounts of *Sphagnum spp.* (Guan et al., 2010). Given these characteristics, water tracks are areas where greening may differentially occur. They represent an important area to quantify NDVI characteristics as the increased moss, shrubs and soil moisture are important components for quantifying both LAI and error associated with LAI measurements (Figure 3.1).

These issues are especially pertinent given documented increases in NDVI throughout northern Alaska (Jia et al., 2006; Stow et al., 2003; Verbyla, 2008) and the pan-Arctic (Raynolds et al., 2008). Increases in NDVI values have been attributed to increases in shrub cover over time in the foothills of the Brooks Range (Tape et al., 2006; Tape et al., 2011). The availability of high-resolution satellite imagery in this area multiple times per growing season provides a useful resource for understanding how NDVI values vary over the landscape and what effects this has on LAI calculation. The main objective of this study was to optimize LAI calculations using NDVI for both WorldView-2 and Landsat-7 imagery. In order to facilitate this process, the data was grouped based on: satellite (WorldView-2 vs. Landsat-7); surficial drainage (water tracks vs. other), and whether the NDVI values changed within a 10-day period. The goals were to: a) examine whether optimization was useful for developing robust method of calculating LAI using the gap-method using NDVI for the different groups; and b) examine if specific vegetation characteristics could be associated with LAI variability.

3.3 Study area

This study area is comprised of moist acidic tundra within the Imnavait and Upper Kuparuk basins (68°37' N, 149° 19' W; elevation 900 m) in the Toolik (Figure 3.2) Lake long-term ecological research (LTER) area. Continuous permafrost is present and documented in the Imnavait basin to extend 250 to 300 m below the surface (Osterkamp and Payne, 1981). Seasonality is limited to warm and cold periods which go from May through September and October through April in this region of the Arctic. The average temperature is approximately 10 °C in July while the average annual rainfall is around 220 mm (Trochim, 2009). Water only has two paths out of the basins: as near-surface runoff or evapotranspiration as the permafrost forms a resistant block (Hinzman et al., 1996). Water is transported downslope through poorly- and well-developed hillslope water tracks and wetland microrelief (Walker and Maier, 2008). Well-

developed water tracks can have discharge all summer and contain deeper snow accumulation in the winter. Flow is restricted to the snowmelt period and following rain events in poorly developed water tracks. The period of vegetation activity is from early to mid-June through early September. Vegetation communities found in the region include: dry exposed acidic sites, moist acidic shallow snowbeds, moist non-acidic snowbeds, moist acidic uplands, and moist non-acidic uplands (Walker et al., 1994).

3.4 Methods

Field data

Fieldwork was completed between July 6 and 14 in 2010. The sampling design consisted of transects constructed perpendicular to the slope angle across water tracks. Each transect consisted of four to six plots of 2 m² located at positions where the characterization of heterogeneity could be maximized. Nadir-looking color and near infrared (NIR) digital camera images were acquired over each plot. The color camera was a Nikon D5000 with a 12.3 megapixel CMOS image sensor with 4288 by 2848 pixel format and 35 mm focal length lens. The NIR imagery was acquired using a red-blocking filter (Hunt et al., 2010) on a Canon EoS Rebel XT. The measurements were performed with the exposure set manually. Color and NIR images were mosaicked separately and georeferenced using differential GPS co-ordinates from the field plots which had accuracy on the order of < 0.25 meters.

Remotely sensed data

Satellite data including WorldView-2 and Landsat 7 imagery was collected during the same time period as seen in Figure 3.3. The details of each satellite (Chander et al., 2009) are listed in Table 3.1. The WorldView-2 data was orthorectified using the ASTER 30 meter digital elevation model. All of the Landsat 7 and WorldView-2 scenes were converted to surface reflectance using the ATCOR 2 model (Richter and Schlapfer, 2011). In order to maximize spatial resolution the Landsat 7 multispectral imagery was pan-sharpened to 15 meters using the hyperspherical color sharpening (HCS) method (Te-Ming et al., 2012) which maximizes preservation of spectral characteristics and does not alter values for vegetation indices (Johnson, 2014). The Normalized Difference Vegetation Index (NDVI) was calculated from reflectance in the Near InfraRed (ρNIR) and red (ρRED) wavelengths (Richardson and Everitt, 1992).

Calculation of fractional cover and LAI

LAI was calculated using gap probability (Jonckheere et al., 2004) to determine the contribution of vegetative and non-vegetative components as observed from above (Tang et al., 2007). This was based on the definition of fractional cover (f_c) by Gonsamo et al. (2011) where f_c is the ratio of pixels recorded as canopy versus the total number of pixels in a specific plot subscene. Fractional cover can also be calculated from NDVI using the maximum or saturated NDVI_g when vegetation occupies the complete field of view and non-vegetation NDVI (NDVI_{back}) as per Equation 3.1:

$$f_c = \frac{NDVI - NDVI_{back}}{NDVI_g - NDVI_{back}} \quad (3.1)$$

This produces a scaled version of NDVI (Carlson and Ripley, 1997). LAI was calculated from fractional cover through Beer-Lambert's law as per Equation 3.2:

$$LAI = -\frac{\ln(1 - f_c)}{k} \quad (3.2)$$

where k refers to the extinction coefficient (m^2 ground m^{-2} leaf). This study used a k value of 0.5 as suggested by Shaver et al. (2007). Fractional cover was derived from all available WorldView-2 and Landsat 7 scenes using NDVI. A similar approach was also used for the nadir-looking ground-based imagery. The red and NIR were stacked and georeferenced. NDVI was calculated from the red and NIR bands and a threshold based on trial-and-error was applied to obtain an estimate of percent area green vegetation which excluded moss.

Statistical and Spatial Examination of LAI

LAI values were analyzed in R (R Core Team, 2014) to isolate the most important factors affecting the prediction of LAI. The first step was to optimize the NDVI_g and NDVI_{back} values. Four different groups for each of the satellites were identified based on surficial drainage characteristics (water-tracks vs. non-water tracks from Trochim (2015)) and changes over time in NDVI values (high vs. low). The change quantiles were calculated based on the difference in NDVI values between the earliest and latest dates. For each group, the Nelder-Mead

optimization algorithm for derivative-free optimization in the dfoptim package (Varadhan et al., 2011) was used to estimate $NDVI_g$ and $NDVI_{back}$ values. Initial estimates of those values were made by minimizing the median absolute deviation between the ground and satellite-derived LAI values. Next, log weights were calculated using robust regression (Rousseeuw et al., 2014) to reduce the influence of outliers. The $NDVI_g$ and $NDVI_{back}$ values were optimized a second time using the weights so that plots with higher accuracy had a greater contribution. Root Mean Square Error (RMSE) and correlations using the spearman method were calculated for each group between the ground and satellite-derived LAI values.

A Kruskal-Wallis test was performed on the satellite-derived LAI values to assess whether they were unique to each sensor. The lme4 package (Bates et al., 2013) was used to perform a linear mixed effects analysis of the relationship between LAI and group. The intercepts for plots and dates were tested as random effects, while the groups were set as the fixed effect. We then examined the random effects of by-plot and by-date random slopes for the effect of groups. P-values were obtained by likelihood ratio tests using parametric bootstrapping of the full model with the effect under investigation against the model without the effect under investigation. Linear mixed effect analysis was performed a second time to investigate the linkages between satellite-derived LAI and field measurements of percent cover which were significantly correlated with the residuals from the gap-method analysis. Percent cover for graminoids (sedges and grasses combined), erect dwarf shrubs and moss was factorized into the following classes: r, present in < 5% of records; +, 5 - 10 %; I, 11 - 20 %; II, 21 - 40 %; III, 41 - 60 %; IV, 61 - 80 %; V, ≥ 80 %. As fixed effects, NDVI and the corresponding percent cover were used with both interaction terms and main effects into the model. The repeated use of the same plots was assigned as a random effect. The p-values for the compared models were obtained as described earlier. If the interactions were significant, the t-test values were also analyzed.

3.5 Results

NDVI versus derived LAI

The initial relationship between NDVI and derived LAI values was examined by their group median and quartiles as seen in Figure 3.4. NDVI values for all dates were compared to each group. Overall, there were some clear differences between the Landsat-7 and WorldView-2

sensors; given that one of the group criteria was based on relative change in NDVI values over time this is expected. The WorldView-2 derived LAI values were lower for all groups except the high change water tracks than those derived from the Landsat-7 data. This indicates potential fundamental differences between the Landsat-7 and WorldView-2 groups in terms of input LAI values. The NDVI values follow different patterns for each sensor; where NDVI values in general were higher for the WorldView-2 satellite.

Optimization of gap probability LAI estimates

The final optimized $NDVI_g$ and $NDVI_{back}$ values for each group are found in Table 3.2. The accuracy of the satellite-derived LAI values can be seen in Figure 3.5. At the 0.05 significance level, the LAI gap-probability results from the WorldView-2 and Landsat-7 satellites are from non-identical populations. There was a significant difference in LAI overall based on date for both the Landsat-7 and WorldView-2 data with p values less than 0.05. The groups were also significantly different from each other for both sensors. However, there were no significant differences within the groups by date when the random effects of the interaction were examined. Overall, the Landsat-7 results were more accurate than those from the WorldView-2 satellite, as RMSE values were smaller and more positively correlated. In almost all cases, ground-derived values of LAI greater than 1.5 were underestimated in the satellite-derived values. In general, satellite-derived LAI values from June 30 from the Landsat-7 data were higher than those ground-derived. This was in contrast to the LAI values from July 9 which were under-estimated. The relationship was the most linear between the ground-derived and satellite-derived values for the other low-change group as it had the strongest positive correlation out of any group.

LAI values calculated from the WorldView-2 satellite were most similar to the Landsat-7 results in the water track high change group, where many of the same plots had similar values in between satellites. The water track low change group showed the most accurate LAI calculation for the WorldView-2 satellite. Overall, the WorldView-2 LAI results were more affected by outliers than the Landsat-7 data, as indicated by the larger RMSE. Generally, the LAI values for July 2 in all groups were higher than other dates. In the water track classes, the July 4 LAI values were the lowest for the range of dates. Both of the other groups were negatively correlated. For the high change other group this correlation was significant, meaning that both the

overestimation of LAI values less than 1.5 and underestimation of LAI values greater than 1.5 caused a substantial trend. The low-change other group is noteworthy as all of the LAI values derived from satellite data underestimate in comparison to ground-derived values. While half of the values from this group show a relatively good fit, outliers around the measured value of 2.0 are substantially underestimated at 0.5 by the predicted values and create considerable error.

Examining the residuals as seen in Figure 3.6 shows that there is variation between homoscedasticity and heteroscedasticity between the groups, especially those indicated with significant correlations. Of all the correlations, only three had significant interactions between LAI, NDVI and the percent-cover vegetation data derived from the plots. The water track high change group from Landsat-7 had a significant interaction effect between LAI and the combination of NDVI and graminoids ($\chi^2_{(1)} = 18.25$, $p=0.05$). The interactions model contained multiple significant t-values ($p<0.05$) in both the main effects and interactions between NDVI and graminoids. Examination of the residual plot shows lower values of graminoids were associated with under prediction of LAI while higher amounts resulted in over prediction. There was also a significant relationship between LAI and the interactions of NDVI and erect dwarf shrubs for the other low change Landsat-7 group ($\chi^2_{(2)} = 33.18$, $p=0.01$). The individual interactions of this model were not significant, so interactions between erect dwarf shrubs and NDVI on LAI are likely a combined effect not captured by the factors. In the WorldView-2 data the only significant interaction for LAI was found between moss and NDVI in the water track high change group ($\chi^2_{(3)} = 18.19$, $p=0.01$). The significant influence of moss and its interactions with NDVI are interesting for this group. The increase in moss from 5-10% to 10-20% was associated with a 0.17 increase in LAI with a standard error of ± 0.06 ($p<0.01$). In contrast, as moss increases from 61-80% to 81-100% it was related to a decrease in LAI of 0.42 with a standard error of ± 0.09 ($p<0.01$). When the interaction between NDVI was accounted for the increase in moss from 5-10% to 10-20% was associated with a decrease of 0.27 in LAI with a standard error of ± 0.10 ($p<0.01$). This also happened between the interaction of NDVI and moss from 61-80% to 81-100% as LAI increased by 0.63 with a standard error of ± 0.13 ($p<0.01$).

3.6 Discussion

Usefulness of gap-method optimization for calculating LAI

We assessed the usefulness of optimization within the gap-method of calculating LAI from NDVI derived via satellite imagery. Optimization was a more robust and repeatable method of calculating $NDVI_g$ and $NDVI_{back}$ than simply deriving the values from the images. It also allowed the error in the gap-method calculation to be reduced, as $NDVI_g$ and $NDVI_{back}$ are important parameters in the calculation of LAI. The use of optimization reduced the gap-probability method to be computationally similar to using linear regression to calculate LAI (Rocha and Shaver, 2009; Shippert et al., 1995). In this study, the gap-probability method of calculating LAI was also consistently used for both ground-based and satellite-based data. The advantage to this was the extinction coefficient ($k - m^2 \text{ ground } m^{-2} \text{ leaf}$) suggested by Shaver et al. (2007) that was regularly used in all LAI calculations, simplifying it as possible error source in all LAI calculations.

The use of groups with the gap-method also improved the overall accuracy of the LAI calculations. Since the study used WorldView-2 and Landsat-7 satellite imagery with different spatial resolutions, it was useful to examine if relatively simple characteristics could be useful in discriminating LAI values. The groups were based on the idea that there are regular wetting and drying cycles occurring on the landscape which are associated with different rates of greening. The first division was to separate out water track from non-water track areas, as water tracks represent areas of preferential surficial flow. The second division, both within water tracks and other areas was to separate whether there was change over time in terms of NDVI. This is a modified version of implementing LAI calculations using vegetation-community specific linear regression equations like Shippert et al. (1995).

Variation in LAI values

There were clear differences between the WorldView-2 and Landsat-7 LAI values which are ultimately driven by variations in NDVI. Overall the WorldView-2 NDVI values were higher in all groups than those derived from the Landsat-7 satellite, similar to what was found by Williams et al. (2008) at comparable scales. Even with the use of optimization, the Landsat-7 derived groups had lower RMSE values than the majority of those from WorldView-2. This means that

the increased averaging of a larger area due to the bigger 15 m pixels allowed the NDVI values derived from the Landsat-7 imagery to better estimate LAI. Fundamentally, this is an issue of spectral mixing at different scales. Within the Landsat-7 results the significant vegetation factors that were interacting with NDVI were graminoids and erect dwarf shrubs. Given the spatial resolution of the Landsat-7 data, this means that effects of graminoids and erect dwarf shrubs were perceptible in larger pixels, since the interaction was absent in the WorldView-2 results.

Both the graminoids and erect dwarf shrubs showed similar patterns when the LAI gap-model residuals were compared to their percent-area, underestimations of LAI were associated with lower percent covers while overestimations were linked to higher ones. Water tracks which are associated with high levels of graminoids tend to contain species that tolerate saturated conditions like *Carex aquatilis* and are essentially small fens in places. Variations in background moisture conditions in these areas may be related to higher variations in NDVI values over time. Another potential cause might be the flowering of *Eriophorum angustifolium*. Known as cotton grass it produces a distinctive fluffy white seed-head. Over a large area, it could raise NDVI values and also cause changes over time as it gains and sheds its seed-head. In comparison, some water tracks also contain tussocks. Plots could also be depressed as a result of the presence of tussocks of *Eriophorum vaginatum* where the presence of standing dead material may not only depress values but also lead to increased shadowing (McGuffie and Henderson-Sellers, 1986). Graminoids including grasses have also been shown to behave asymptotic more quickly in the visible portion of the spectrum in comparison to the NIR as a result of total wet biomass, total dry biomass, dry green biomass, chlorophyll content, and leaf water content (Tucker, 1977).

The erect dwarf shrubs like *Ledum palustre decumbens* and *Vaccinium uliginosum* may be experiencing similar flowering and shading effects respectively to those seen in the graminoids for the other low change group. If the magnitude of this effect is overall lower than the graminoids, perhaps the effect although discernable has an overall effect on NDVI as there was less variability in NDVI values over time. Chen et al. (2009) found that percent cover and mean height of *Vaccinium uliginosum* could be used to estimate LAI along with other common Arctic vegetation. Within this study area, NDVI has been shown to be significantly dominated by shrubs including live foliar and woody deciduous types in measurements with a spatial resolution

of 0.35 m^2 (Riedel et al., 2005), at other spatial scales this relationship is unclear. The literature supports the interaction of erect dwarf shrubs and NDVI for the calculation of LAI although additional attention on their effects over scales similar to Landsat-7 data would be useful.

In contrast, the WorldView-2 LAI results were only associated with the significant interaction between moss and NDVI for the water track high change group. In terms of spectral reflectance, common species of moss like *Sphagnum* are influenced by color, cell structure, morphology, water content and chemistry (Arkimaa et al., 2009). Water content, in particular, was shown to be one of the most confounding influences on spectra as increased moisture content suppresses reflectance from 500 to 700 nm while the response can be variable between 750 to 900 nm. This means that as moss increases in moisture content, NDVI would decrease through an intermediate stage before rising. In areas of high moss cover, increases in LAI and NDVI were asymptotically linked with moss water content and the thickness of the green moss layer (Douma et al., 2007). NDVI has also been linearly correlated with photosynthetic activity in mosses (Harris, 2008). This may be variable in the Arctic, where the abundance of brown-colored mosses (e.g., *Tomentypnum nitens*) can also influence greenness (Buchhorn et al., 2013). In summary, the interaction between moss, NDVI and LAI are complex. This is indicated in the results by the reversal of the trend between low and high percent covers of moss when the interaction of NDVI is considered versus the influence of percent cover alone on LAI.

Variability within LAI from the remainder groups for both sensors was likely due to a combination of the factors discussed above along with the influence of soil moisture (Weidong et al., 2002). The data collection period for this study represents an intermediate period in canopy development. Other potential sources of error include non-photosynthetic and photosynthetic plant material interacting to create nonlinear spectral mixing (Asner et al., 2007). Other studies found this period represents an intermediate stage when neither woody stem cover nor canopy leaf area strongly influences the spectral signature (Boelman et al., 2011).

Effect of spatial resolution on LAI

The spatial implications of using either Landsat or WorldView-2 data to calculate LAI are clearly demonstrated in Figure 3.7. There are noticeable contrasts in the locations of the groups

and variations between the groups based on the spatial resolution of the data. Curvilinear features on the landscape as either water tracks or frost stripes are readily apparent in the WorldView-2 data and lacking in the Landsat-7. Since a conservative distribution of water tracks was used, many water tracks appear as stripes in the high change other group. Overall, Landsat-7 LAI values were lower than those from the WorldView-2 imagery even when similar dates were compared. In the Landsat-7 results the highest LAI values were found on the hillside. In comparison, the highest LAI values in the WorldView-2 results were found in the centers of the water tracks with elevated LAI values within the tracks. The WorldView-2 data also made it possible to discern areas of low LAI values including the frost-stripes on the hillslope and within the peat ice-wedge polygons and wetlands between the two hillslopes. Future studies should weight their study criteria carefully when selecting the spatial resolution of imagery used for LAI analysis and craft their methodologies appropriately.

3.7 Conclusions

This study showed that LAI could be calculated using satellite-derived NDVI values by using optimization in the gap-probability model. Emphasis was placed on analyzing hillslope patterns, which were described by the presence/absence of water tracks and the magnitude of variation in NDVI over time. The results indicated these simple characteristics created groups where the groups of LAI values are distinct from each other even with variability over time. The effects of the groups were compared between WorldView-2 and Landsat-7 imagery where the LAI values were higher in the WorldView-2 results. This did not result in more accurate LAI estimates, as the Landsat-7 imagery had lower RMSE values. We conclude that the spatial resolution had an overall effect on the LAI values by substantially changing the nonlinear spectral mixing inputs. This was supported by different vegetation factors (erect dwarf shrubs, moss and graminoids) significantly interacting with the NDVI and LAI depending on which sensor was used.

While there has been a push towards higher resolution spatial data, future studies should be cognizant of the advantages and limitations offered by the increased spatial resolution on LAI calculations based on NDVI. Although the use of WorldView-2 imagery allowed comparisons to be made using data collected using the same footprint as field measurements, the number of field observations necessary to validate the increase in variability also increases. Future projects

should be cognizant of these issues and modify their project design accordingly. Given increases in NDVI values over time in the Arctic and the role of LAI computing ecological and hydrological characteristics, utilizing remotely sensed data effectively will remain important over time.

3.8 Acknowledgements

This project was supported by a NASA Earth & Space Science Graduate Fellowship (NNX09AN42H), with additional resources provided by the Alaska Water Resources Association and the University of Alaska Fairbanks including the Center for Global Change, the Graduate School and Department of Geosciences. World-View 2 imagery was acquired through the National Geospatial Agency Commercial Data Archive. Field assistance was provided by Nicole Farnham with additional support by the Toolik Lake Research Station.

3.9 References

- Anderson, M., and Kustas, W., 2008, Thermal remote sensing of drought and evapotranspiration: *Eos*, v. 89, no. 26, p. 233-234.
- Arkimaa, H., Laitinen, J., Korhonen, R., Moisanen, M., Hirvasniemi, T., and Kuosmanen, V., 2009, Spectral reflectance properties of Sphagnum moss species in Finnish mires, in *Proceedings 6th EARSeL SIG IS workshop, Imaging Spectroscopy: Innovative tool for scientific and commercial environmental applications*, p. 16-19.
- Asner, G. P., Knapp, D. E., Kennedy-Bowdoin, T., Jones, M. O., Martin, R. E., Boardman, J., and Field, C. B., 2007, Carnegie Airborne Observatory: in-flight fusion of hyperspectral imaging and waveform light detection and ranging for three-dimensional studies of ecosystems: *Journal of Applied Remote Sensing*, v. 1, no. 1, p. 013536-013536-013521.
- Bates, D., Maechler, M., and Bolker, B., 2013, lme4: Linear mixed-effects models using S4 classes, R package version 1.1-8.

Boelman, N. T., Gough, L., McLaren, J. R., and Greaves, H., 2011, Does NDVI reflect variation in the structural attributes associated with increasing shrub dominance in arctic tundra?: *Environmental Research Letters*, v. 6, no. 3, p. 035501.

Breda, N. J. J., 2003, Ground-based measurements of leaf area index: a review of methods, instruments and current controversies: *Journal of Experimental Botany*, v. 54, no. 392, p. 2403-2417.

Buchhorn, M., Walker, D. A., Heim, B., Raynolds, M. K., Epstein, H. E., and Schwieder, M., 2013, Ground-based hyperspectral characterization of Alaska tundra vegetation along environmental gradients: *Remote Sensing*, v. 5, no. 8, p. 3971-4005.

Carlson, T. N., and Ripley, D. A., 1997, On the relation between NDVI, fractional vegetation cover, and leaf area index: *Remote Sensing of Environment*, v. 62, no. 3, p. 241-252.

Chander, G., Markham, B. L., and Helder, D. L., 2009, Summary of current radiometric calibration coefficients for Landsat MSS, TM, ETM+, and EO-1 ALI sensors: *Remote Sensing of Environment*, v. 113, no. 5, p. 893-903.

Chen, W., Li, J., Zhang, Y., Zhou, F., Koehler, K., LeBlanc, S., Fraser, R., Olthof, I., Zhang, Y., and Wang, J., 2009, Relating biomass and leaf area index to non-destructive measurements in order to monitor changes in arctic vegetation: *Arctic*, p. 281-294.

Douma, J. C., Van Wijk, M. T., Lang, S. I., and Shaver, G. R., 2007, The contribution of mosses to the carbon and water exchange of arctic ecosystems: quantification and relationships with system properties: *Plant, Cell & Environment*, v. 30, no. 10, p. 1205-1215.

Engstrom, R., Hope, A., Kwon, H., and Stow, D., 2008, The relationship between soil moisture and NDVI near Barrow, Alaska: *Physical Geography*, v. 29, no. 1, p. 38-53.

Gonsamo, A., Pellikka, P., and King, D. J., 2011, Large-scale leaf area index inversion algorithms from high-resolution airborne imagery: *International Journal of Remote Sensing*, v. 32, no. 14, p. 3897-3916.

Guan, X. J., Westbrook, C. J., and Spence, C., 2010, Shallow soil moisture - ground thaw interactions and controls - Part 1: Spatiotemporal patterns and correlations over a subarctic landscape: *Hydrology and Earth System Sciences*, v. 14, no. 7, p. 1375-1386.

Hallik, L., Kull, O., Nilson, T., and Peñuelas, J., 2009, Spectral reflectance of multispecies herbaceous and moss canopies in the boreal forest understory and open field: *Canadian Journal of Remote Sensing*, v. 35, no. 5, p. 474-485.

Harris, A., 2008, Spectral reflectance and photosynthetic properties of *Sphagnum* mosses exposed to progressive drought: *Ecohydrology*, v. 1, no. 1, p. 35-42.

Hinzman, L. D., Kane, D. L., Benson, C. S., and Everett, K. R., 1996, Energy balance and hydrological processes in an Arctic watershed, in Reynolds, J. F., and Tenhunen, J. D., eds., *Ecological Studies; Landscape function and disturbance in Arctic tundra*, Springer-Verlag; Springer-Verlag New York, Inc., p. 131-154.

Hunt, E. R., Hively, W. D., Fujikawa, S., Linden, D., Daughtry, C. S., and McCarty, G., 2010, Acquisition of NIR-Green-Blue Digital Photographs from Unmanned Aircraft for Crop Monitoring: *Remote Sensing*, v. 2, no. 1, p. 290-305.

Jia, G. J., Epstein, H. E., and Walker, D. A., 2006, Spatial heterogeneity of tundra vegetation response to recent temperature changes: *Global Change Biology*, v. 12, p. 42-55.

Jonckheere, I., Fleck, S., Nackaerts, K., Muys, B., Coppin, P., Weiss, M., and Baret, F., 2004, Review of methods for in situ leaf area index determination - Part I. Theories, sensors and hemispherical photography: *Agricultural and Forest Meteorology*, v. 121, no. 1-2, p. 19-35.

Johnson, B., 2014, Effects of pansharpening on vegetation indices: ISPRS International Journal of Geo-Information, v. 3, no. 2, p. 507-522.

McGuffie, K., and Henderson-Sellers, A., 1986, Technical note. Illustration of the influence of shadowing on high latitude information derived from satellite imagery: International Journal of Remote Sensing, v. 7, no. 10, p. 1359-1365.

McNamara, J. P., Kane, D. L., and Hinzman, L. D., 1998, An analysis of streamflow hydrology in the Kuparuk River basin, Arctic Alaska: A nested watershed approach: Journal of Hydrology, v. 206, no. 1-2, p. 39-57.

McNamara, J. P., Kane, D. L., and Hinzman, L. D., 1999, An analysis of an arctic channel network using a digital elevation model: Geomorphology, v. 29, p. 339-353.

Osterkamp, T. E., and Payne, M. W., 1981, Estimates of permafrost thickness from well logs in northern Alaska: Cold Regions Science and Technology, v. 5, no. 1, p. 13-27.

R Core Team, 2014, R: A Language and Environment for Statistical Computing: Vienna, Austria, R Foundation for Statistical Computing.

Raynolds, M. K., Comiso, J. C., Walker, D. A., and Verbyla, D., 2008, Relationship between satellite-derived land surface temperatures, arctic vegetation types, and NDVI: Remote Sensing of Environment, v. 112, no. 4, p. 1884-1894.

Richardson, A. J., and Everitt, J. H., 1992, Using spectral vegetation indices to estimate rangeland productivity: Geocarto International, v. 7, no. 1, p. 63-69.

Richter, R., and Schlapfer, D., 2011, Atmospheric/topographic correction for satellite imagery, ATCOR 2/3 User Guide.

Riedel, S. M., Epstein, H. E., and Walker, D. A., 2005, Biotic controls over spectral reflectance of arctic tundra vegetation: *International Journal of Remote Sensing*, v. 26, p. 2391-2405.

Rocha, A. V., and Shaver, G. R., 2009, Advantages of a two band EVI calculated from solar and photosynthetically active radiation fluxes: *Agricultural and Forest Meteorology*, v. 149, no. 9, p. 1560-1563.

Rousseeuw, P., Croux, C., Todorov, V., Ruckstuhl, A., Salibian-Barrera, M., Verbeke, T., Koller, K., and Maechler, M., 2014, robustbase: Basic Robust Statistics, R package version 0.92-5.

Shaver, G. R., Street, L. E., Rastetter, E. B., Van Wijk, M. T., and Williams, M., 2007, Functional convergence in regulation of net CO₂ flux in heterogeneous tundra landscapes in Alaska and Sweden: *Journal of Ecology*, v. 95, no. 4, p. 802-817.

Shippert, M. M., Walker, D. A., Auerbach, N. A., and Lewis, B. E., 1995, Biomass and leaf-area index maps derived from SPOT images for Toolik Lake and Imnavait Creek areas, Alaska: *Polar Record*, v. 31, no. 177, p. 147-154.

Stenberg, P., Rautiainen, M., Manninen, T., Voipio, P., and Smolander, H., 2004, Reduced simple ratio better than NDVI for estimating LAI in Finnish pine and spruce stands: *Silva Fennica*, v. 38, no. 1, p. 3-14.

Stow, D., Daeschner, S., Hope, A., Douglas, D., Petersen, A., Myneni, R., Zhou, L., and Oechel, W., 2003, Variability of the seasonally integrated normalized difference vegetation index across the north slope of Alaska in the 1990s: *International Journal of Remote Sensing*, v. 24, no. 5, p. 1111-1117.

Stoy, P. C., Williams, M., Disney, M., Prieto-Blanco, A., Huntley, B., Baxter, R., and Lewis, P., 2009, Upscaling as ecological information transfer: a simple framework with application to Arctic ecosystem carbon exchange: *Landscape Ecology*, v. 24, no. 7, p. 971-986.

Tang, S., Chen, J. M., Zhu, Q., Li, X., Chen, M., Sun, R., Zhou, Y., Deng, F., and Xie, D., 2007, LAI inversion algorithm based on directional reflectance kernels: *Journal of Environmental Management*, v. 85, no. 3, p. 638-648.

Tape, K., Sturm, M., and Racine, C., 2006, The evidence for shrub expansion in Northern Alaska and the Pan-Arctic: *Global Change Biology*, v. 12, p. 686-702.

Tape, K. D., Verbyla, D., and Welker, J. M., 2011, Twentieth century erosion in Arctic Alaska foothills: The influence of shrubs, runoff, and permafrost: *Journal of Geophysical Research-Biogeosciences*, v. 116, p. 1-11.

Te-Ming, T., Ching-Luh, H., Pin-Yi, T., and Ching-Hai, L., 2012, An Adjustable Pan-Sharpener Approach for IKONOS/QuickBird/GeoEye-1/WorldView-2 Imagery: *Selected Topics in Applied Earth Observations and Remote Sensing, IEEE Journal of*, v. 5, no. 1, p. 125-134.

Trochim, E.D., 2009, Modeling discharge using HBV in the Imnavait Basin, North Slope, Alaska. M.Sc. thesis (p. 137). Fairbanks: University of Alaska Fairbanks.

Trochim, E. D., 2015, Bridging Arctic pathways: Integrating hydrology, geomorphology and remote sensing in the north, Ph.D. diss., University of Alaska Fairbanks.

Tucker, C. J., 1977, Asymptotic nature of grass canopy spectral reflectance: *Applied Optics*, v. 16, no. 5, p. 1151-1156.

Van Wijk, M. T., and Williams, M., 2005, Optical instruments for measuring leaf area index in low vegetation: Application in Arctic ecosystems: *Ecological Applications*, v. 15, no. 4, p. 1462-1470.

Varadhan, R., University, J. H., Borchers, H. W., and Research, A. C., 2011, dfoptim: Derivative-free Optimization, R package version 2011.8-1.

Verbyla, D., 2008, The greening and browning of Alaska based on 1982-2003 satellite data: *Global Ecology and Biogeography*, p. 1-10.

Walker, D. A., and Maier, H. A., 2008, Vegetation in the vicinity of the Toolik Field Station, Alaska: Institute of Arctic Biology.

Walker, M. D., Walker, D. A., and Auerbach, N. A., 1994, Plant communities of a tussock tundra landscape in the Brooks Range Foothills, Alaska: *Journal of Vegetation Science*, v. 5, p. 843-866.

Watson, D. J., 1947, Comparative Physiological Studies on the Growth of Field Crops: I. Variation in Net Assimilation Rate and Leaf Area between Species and Varieties, and within and between Years: *Annals of Botany*, v. 11, no. 1, p. 41-76.

Weidong, L., Baret, F., Xingfa, G., Qingxi, T., Lanfen, Z., and Bing, Z., 2002, Relating soil surface moisture to reflectance: *Remote Sensing of Environment*, v. 81, no. 2, p. 238-246.

Williams, M., Bell, R., Spadavecchia, L., Street, L. E., and Van Wijk, M. T., 2008, Upscaling leaf area index in an Arctic landscape through multiscale observations: *Global Change Biology*, v. 14, no. 7, p. 1517-1530.

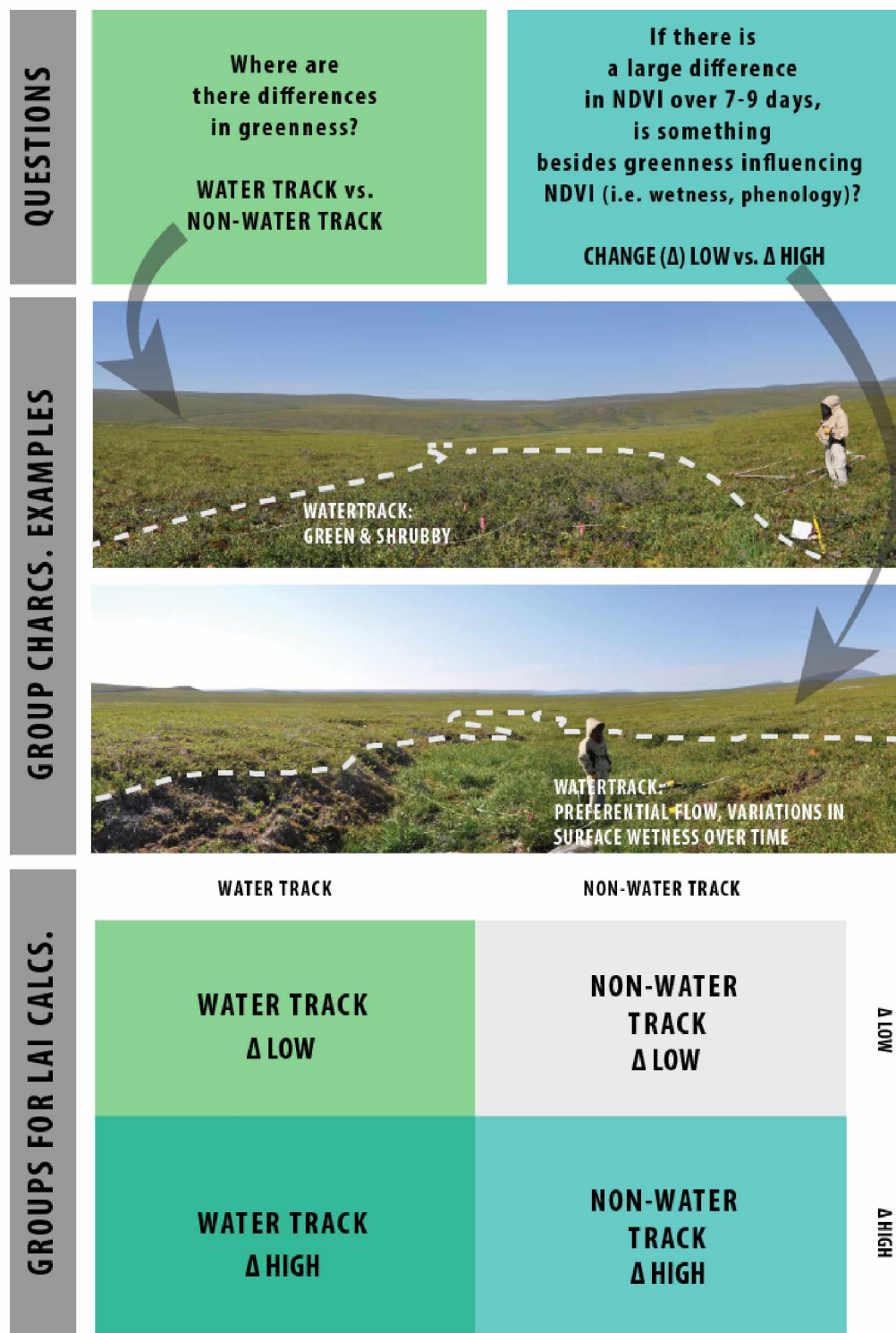


Figure 3.1: Development of groups to quantify effects of water tracks in the study area on the North Slope of Alaska.

Water tracks are discernable on the ground by their curvilinear structure and by differences in vegetation compared to the adjacent areas. Vegetation and surface wetness can vary between and within tracks. Photos: E.D. Trochim.

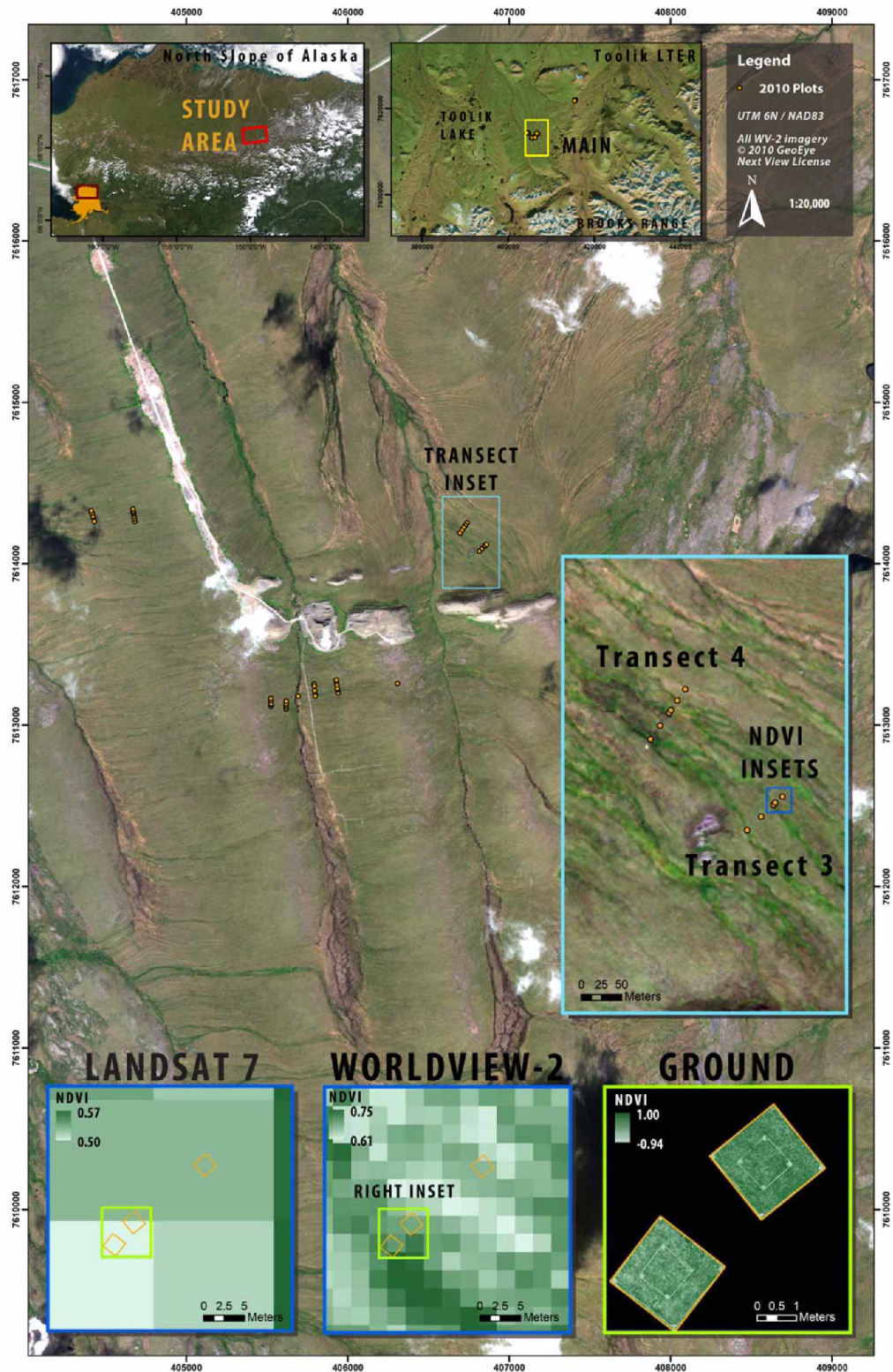


Figure 3.2: Study area location showing WorldView-2 imagery (Bands 431 as RGB) used as input and the location of LAI ground-based measurements.

Bottom insets contrast the NDVI values from the different imagery.

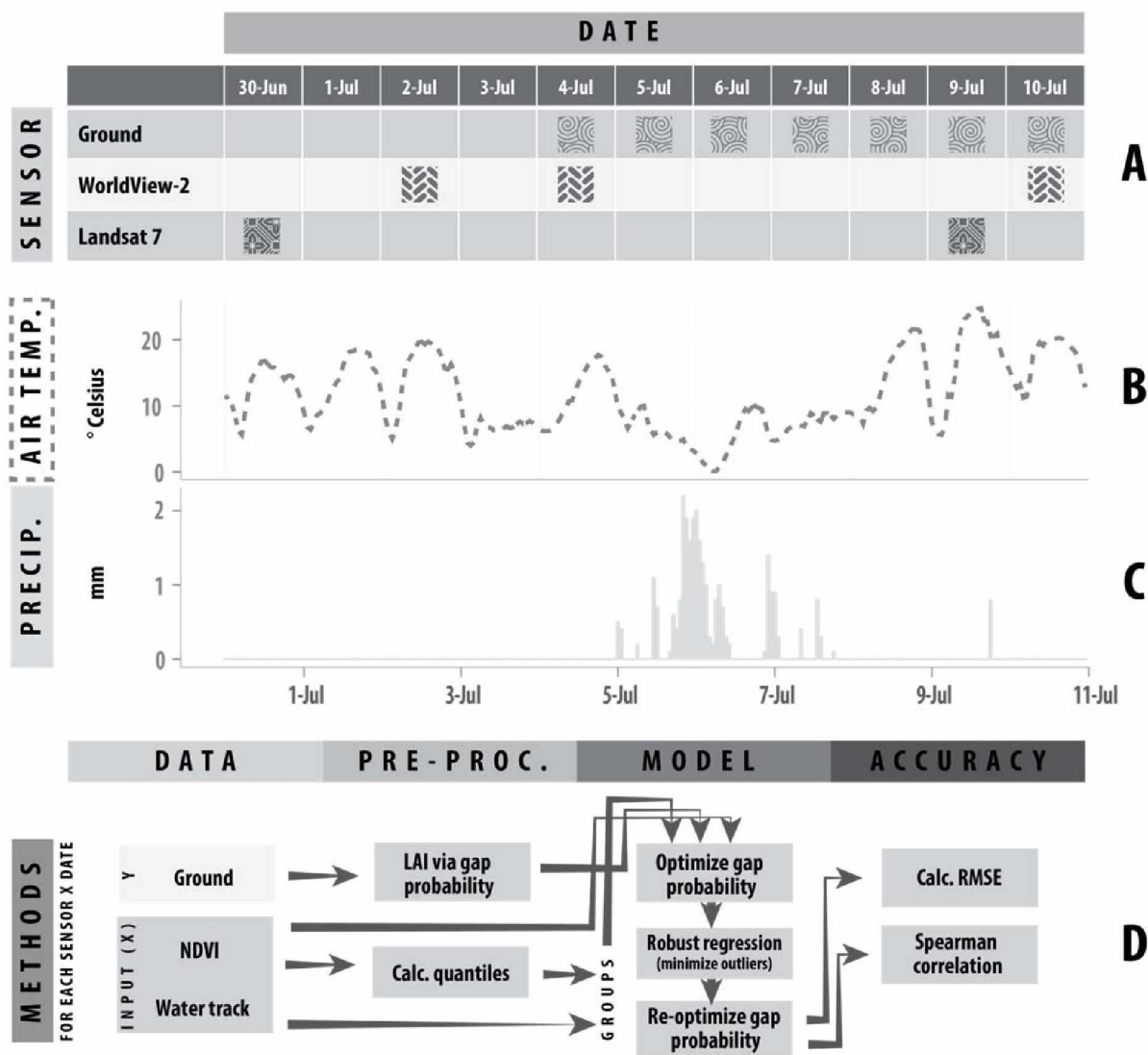


Figure 3.3: Summary of experimental design including input imagery and climatic variables.

A) Timing of collection of imagery from ground and satellite (WorldView-2 and Landsat 7) sources. B) & C) Air temperature at 1 m and precipitation collected at the Imnavait Basin Station (68° 36' 58.6" N, 149° 18' 13.0" W, elevation: 937 meters). There was a large precipitation event on July 5 and 6 which included both rain and snow. D) Flowchart of input data and methodology including pre-processing, model and accuracy steps.

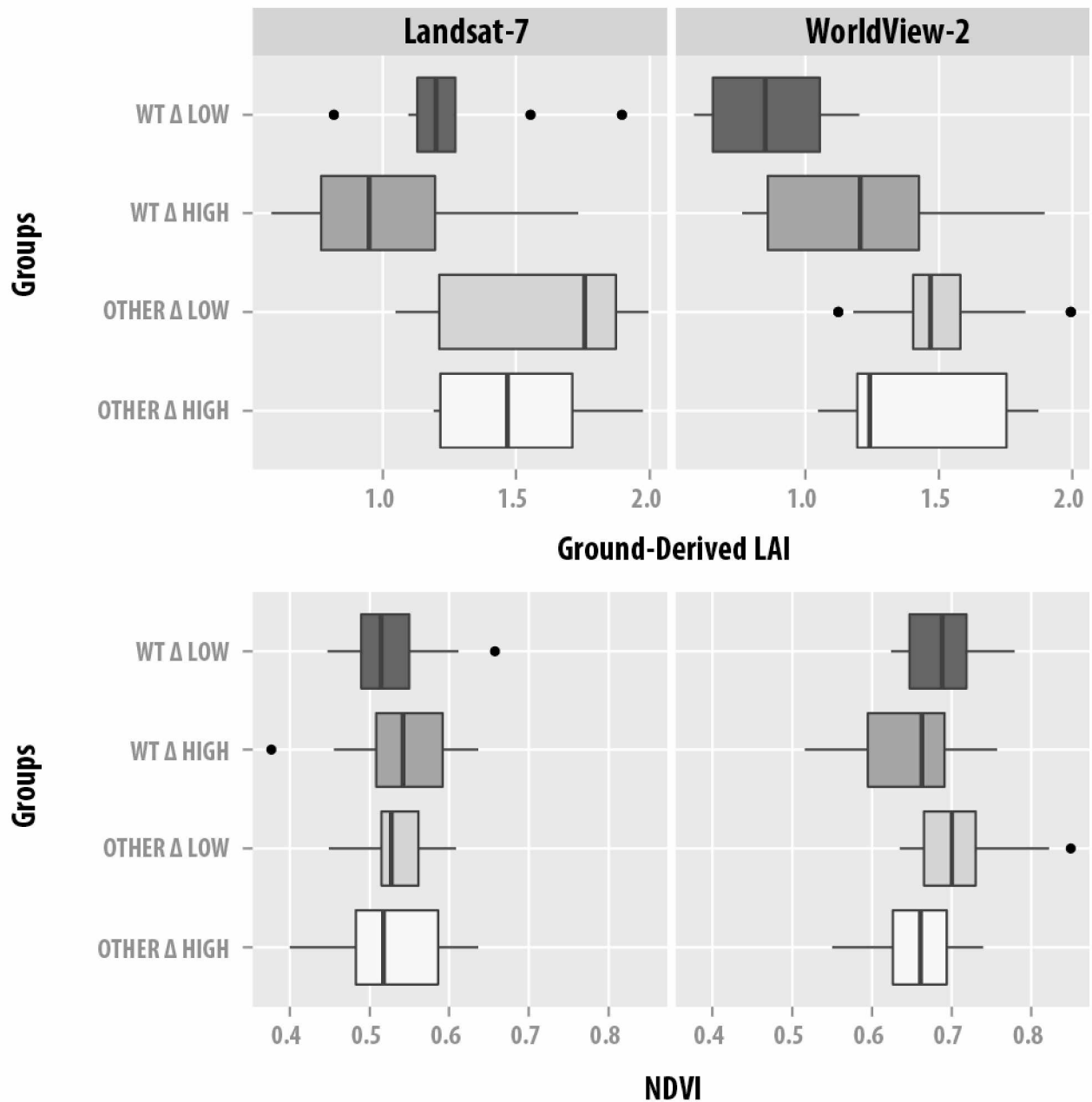


Figure 3.4: Comparing median values of ground-derived LAI and NDVI between different groups by data acquired from Landsat-7 and WorldView-2 satellites.

The upper and lower “hinges” of each box represent the 25th and 75th percentiles, while dots represent outliers.

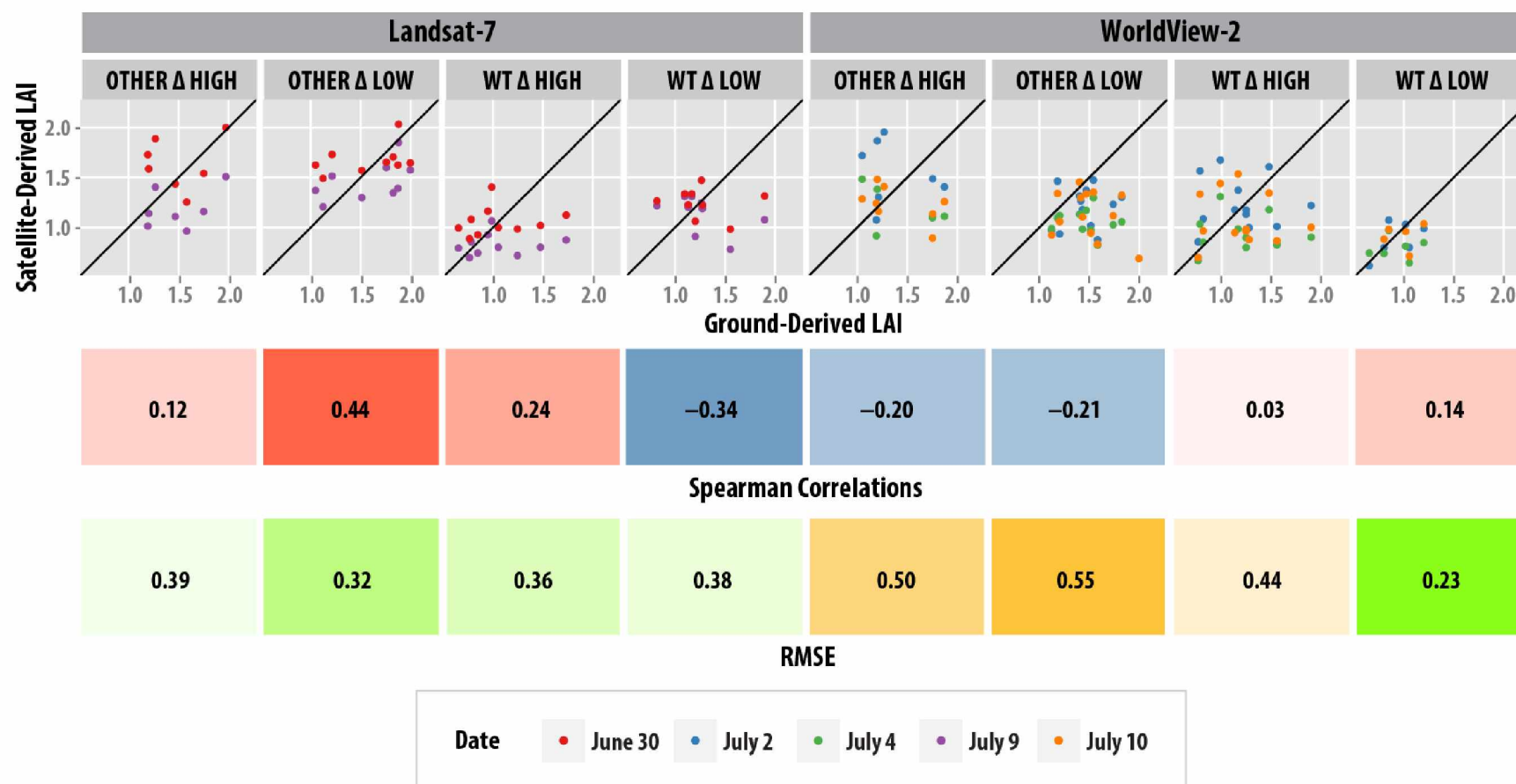


Figure 3.5: Analysis of gap probability LAI results by group.

Ground and satellite-derived LAI are compared where the most accurate results follow the 45° line indicating a perfect fit. Spearman correlation and RMSE values corresponding to each group are given below where strongly positive correlations (red) and low RMSE results (green) indicate the best results.

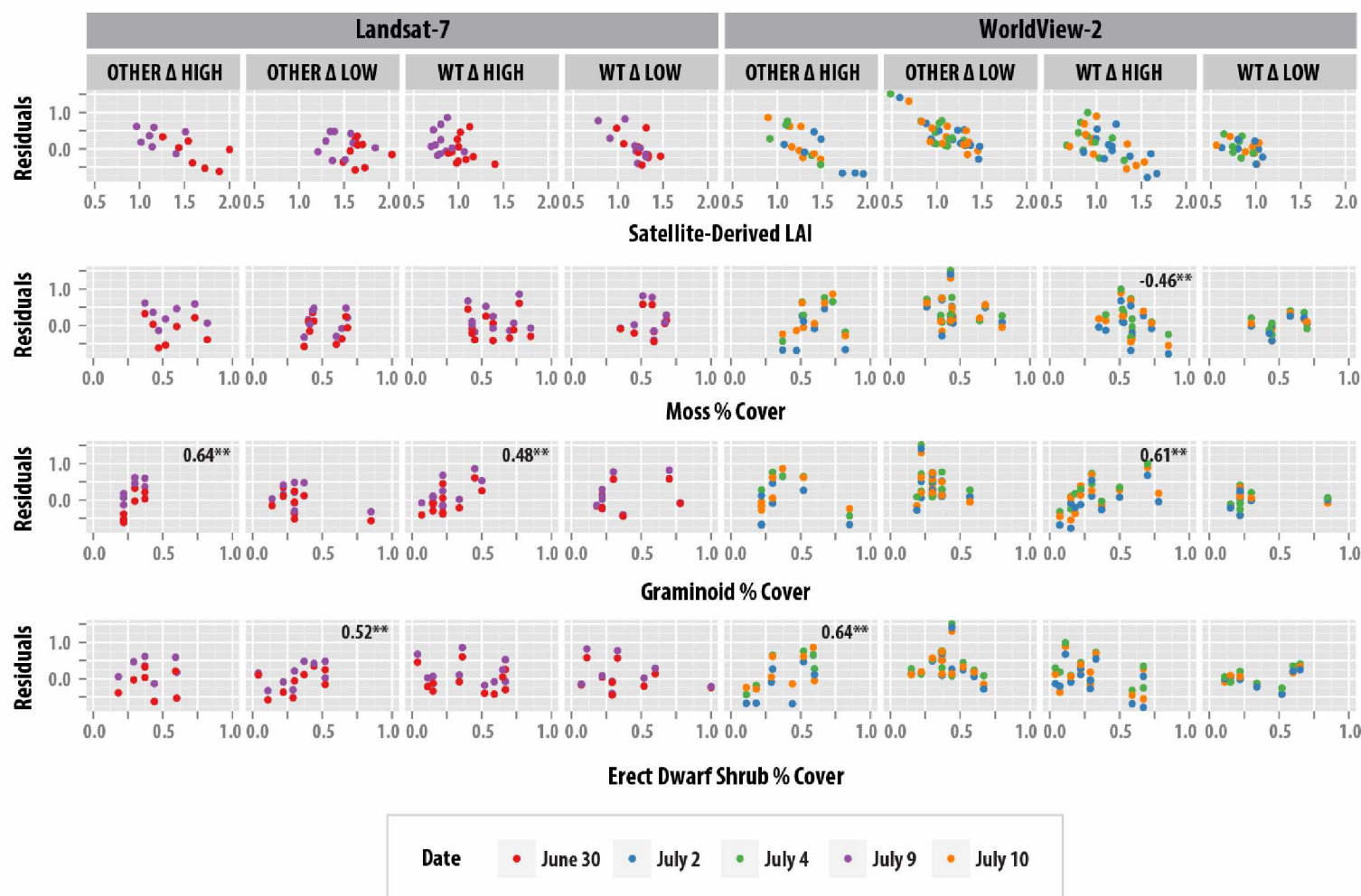


Figure 3.6: Residual results divided by group.

Homoscedasticity (random variation) and heteroscedasticity (trends) can be compared between the different groups for each of the variables. The percent cover of moss, graminoid and erect dwarf shrubs using the Braun-Blanquet approach (Mueller-Dombois and Ellenberg, 1974) were collected concurrently in the field during the ground-derived LAI calculations. Spearman correlation coefficients are listed on each plot if the relationship was significant ($p < 0.05$).

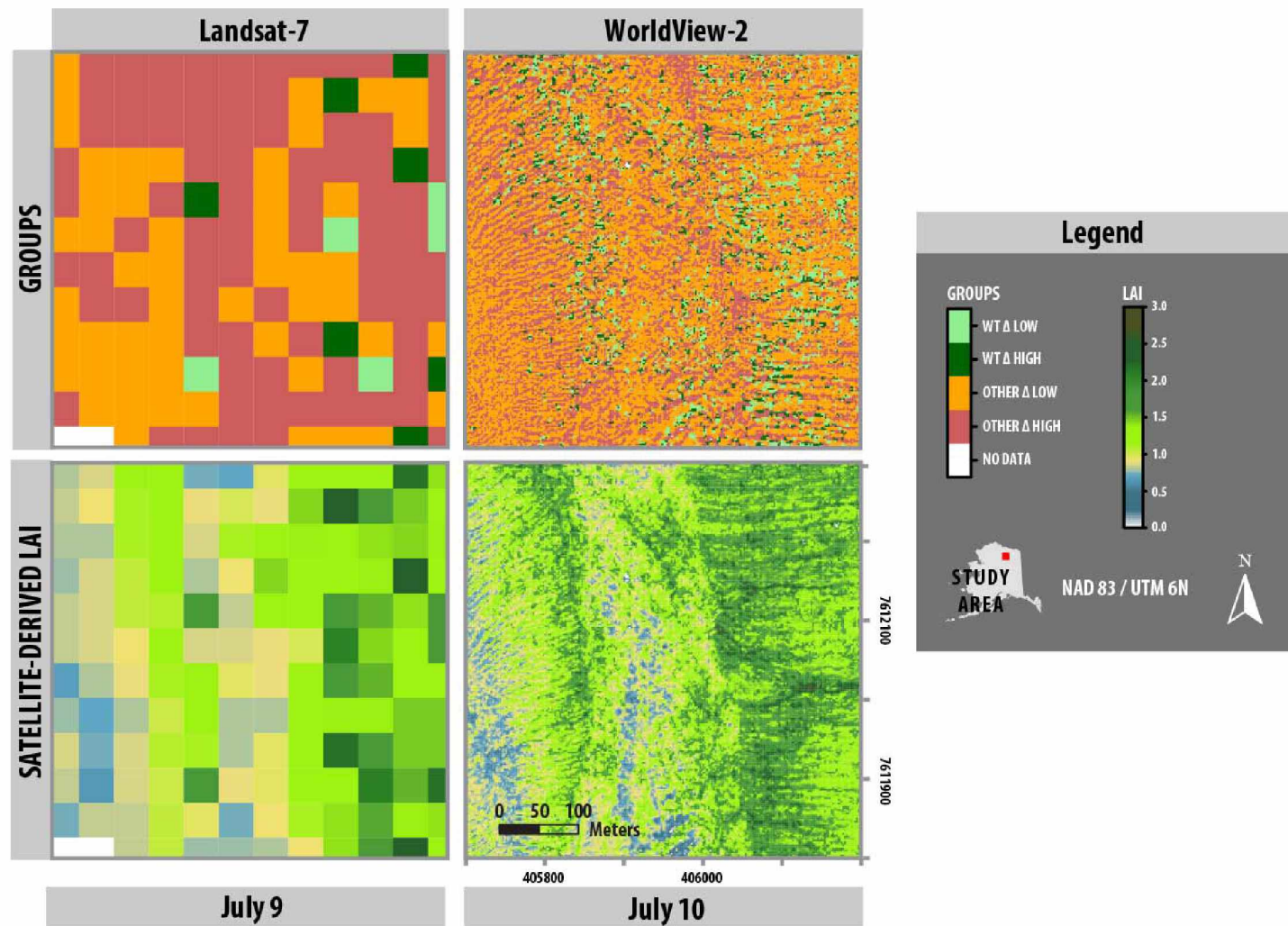


Figure 3.7: Location of each group compared to satellite-derived LAI values from each image date. LAI values are higher for the WorldView-2 imagery than Landsat-7 over similar dates.

Table 3.1: Radiometric, spatial, and spectral resolutions of the WorldView-2 and Landsat 7 satellite imagery used for this study.

Sensor	Radiometric resolution	Spatial resolution (m)	Total spectral bands	Selected bands	Name	Band range (nm)
WorldView-2	11-bit	1.84	8	B5	Red	630 – 690
				B7	NIR1	770 – 895
Landsat-7	8-bit	30	8	B3	Red	630 – 690
				B4	NIR	750 – 900
		15	1	B8	Panchromatic	520 – 900

Table 3.2: Final NDVI_g and $\text{NDVI}_{\text{back}}$ values for each group and sensor.

These were a result of optimization of the gap-method for calculating LAI. NDVI_g remains relatively constant while $\text{NDVI}_{\text{back}}$ resulted in higher parameterization.

Sensor	Group	NDVI_g	$\text{NDVI}_{\text{back}}$
L7	Water track Δ low	0.999999	-0.06113
	Water track Δ high	0.999999	-0.23488
	Other Δ low	0.999999	0.136768
	Other Δ high	0.999998	0.050766
WV2	Water track Δ low	0.999998	0.095434
	Water track Δ high	0.999999	0.145836
	Other Δ low	1	0.3
	Other Δ high	0.999994	0.278987

Chapter 4 Geophysical and cryostratigraphic investigations for road design in northern Alaska¹

4.1 Abstract

This study used combined geophysical and cryostratigraphic methods for permafrost characterization in Arctic road design and engineering. Two major study areas located in the continuous permafrost zone represented a range of terrain conditions including yedoma (syngenetically frozen ice-rich silts with large ice wedges) plateaus and hills, thaw-lake basins, river terraces, and modern floodplains. Direct-current resistivity - electrical resistivity tomography (DCR-ERT) using a Wenner array was applied over transects. Complementary site data including the results of drilling and active layer depths measurements were also obtained. The boreholes provided cryostratigraphic information on soil texture, cryostructures, massive ground ice, and gravimetric moisture content of frozen soils. The resistivity data supported evaluation of the presence/absence of permafrost; location and depth of the active and intermediate layers; and in some conditions changes in ice content. In contrast, the cryostratigraphic interpretation generally offered more nuanced analysis of the subsurface, but was limited in its ability to detect unconformities and the depth of drilling. Both techniques were enhanced by the availability of high-resolution geospatial information and can be used to optimize the location and density of the boreholes for road construction.

4.2 Introduction

Design, construction and maintenance of roads in Arctic Alaska requires identification of permafrost distribution and its properties. The nature and extent of permafrost, in turn, strongly influences route selection, mitigation techniques and cost. Ice content along with ground temperature, and soil stratigraphy and composition are fundamental parameters for planning, designing and evaluating engineering applications.

This study employs geophysical techniques and cryostratigraphic analysis to identify permafrost characteristics in a proposed road corridor connecting the Dalton Highway and Umiat

¹ Trochim, E.D., Schnabel, W.E., Kanevskiy, M., Munk, J., Shur, Y., Geophysical and cryostratigraphic investigations for road design in northern Alaska, submitted to *Cold Regions Science and Technology*.

on the Colville River in Northern Alaska. The proposed road corridor is located within the continuous permafrost zone and crosses the Itkillik, Anaktuvuk, Chandler, and potentially Colville rivers between the Dalton Highway and Umiat (Figure 4.1 and Figure 4.2). Thickness of permafrost in northern Alaska can range from 200 m in the foothills to 600 m on the coast (Osterkamp and Payne, 1981). Estimated ground ice distribution (Jorgenson et al., 2008) indicated that finer grained soils tended to be more ice rich, however features such as ice-wedge polygons occurred in a variety of environments. Silt-dominated ice-rich deposits more than 30 m thick with syngenetic ice-wedges formed in the late Pleistocene (Yedoma) have been documented in the adjacent area along the Itkillik River (Kanevskiy et al., 2011a; Kanevskiy et al., 2011b).

The main goal of a geophysical survey as part of a geotechnical investigation is evaluation of the homogeneity of a studied geological body and the uncovering of heterogeneities in it. Geophysical methods used in geotechnical investigations in the permafrost region—electrical, seismic, magnetic, and gravity—uncover differences between properties of geological bodies in the Earth's crust, and use of these methods is time- and cost-efficient. In general, geophysical methods are indirect. Direct evaluation of soil properties by geophysical methods is limited. To make a direct conclusion, geophysical data should be calibrated by using information on soil obtained by direct methods, such as trenching and drilling. The application of geophysical methods at a key site can be used for calibration, and the application of calibrated geophysical methods can be used for extrapolation of geotechnical data on similar landforms and for design of a drilling program. Geophysical methods can theoretically greatly reduce the number of boreholes.

Cryostratigraphy analysis is a main method of identification of genesis and properties of permafrost soils. This analysis and geophysics represent complimentary methods of collecting and interpreting information about permafrost characteristics. Cryostratigraphy is a branch of geocryology originally developed in Russia for analyzing the structures specific to permafrost and has been used to understand the particularities of permafrost environments and Arctic engineering applications (French and Shur, 2010). Previous studies in Alaska have indicated a strong relationship between cryostratigraphy and corresponding terrain units derived from

interpreting imagery via remote sensing (Jorgenson et al., 1998; Kanevskiy et al., 2014). The limitations to the cryostratigraphic technique include a high-level of localized permafrost knowledge being necessary to construct the interpretations and the time required to complete the analysis. The soils and permafrost data for cryostratigraphic analysis can be obtained from either boreholes or outcrops as available.

A variety of geophysical techniques have been used to delineate permafrost distribution and ice morphology (Kneisel et al., 2008). These include ground penetrating radar (GPR) and various types of electrical resistivity tomography (ERT) including: 1) direct-current resistivity (DCR-ERT) (Hilbich et al., 2008; Isaksen et al., 2011; Katasonov, 1978; Kneisel, 2010; Lewkowicz et al., 2011; McClymont et al., 2013; Overduin et al., 2012; Rodder and Kneisel, 2012; You et al., 2013), and 2) capacitive-coupled resistivity (CCR-ERT) (De Pascale et al., 2008; Fortier and Savard, 2010; Kuras et al., 2006; Timofeev et al., 1994). Others have used a combination of either GPR and DCR-ERT (Sjöberg et al., 2015) or CCR- and DCR-ERT (Oldenborger and LeBlanc, 2013). Ideally all investigations should be supported by subsurface data based on outcrops, boreholes, or excavation methods.

Interpreting geophysical data, in both permafrost and non-permafrost environments, greatly benefits from information derived from remotely sensed data and boreholes in order to increase the understanding of pertinent landscape characteristics (Hubbard et al., 2013). Cryostratigraphic analysis can be used to constrain geophysical models as described by Fortier et al. (2008) where they examined the ice-content of permafrost mounds. Translating these ideas into practices that can be reasonably applied over large scales where there can be substantial variation both within and between terrain units is important for Arctic road construction. This project used DCR-ERT to detect soil properties as resistivity (the reciprocal of conductivity). As soil particles and ice are both highly resistive compared to liquid water, the relative fractions of ice, soil particles, and liquid water strongly influence the resistivity of different soil strata or formations (Hauck, 2002). The changes in resistivity directly relate to changes in soil properties (Scherler et al., 2010). However, other factors influencing resistivity include texture, temperature, salinity, and cryogenic structure of the soil (Samouëlian et al., 2005). Consequently application of DCR-ERT, like all geophysical methods, requires field calibration for evaluating soil properties at key sites.

Boreholes can allow accurate characterization of soil stratigraphy, ice content, depth to bedrock and potential of fill material. Solid-stem drilling is relatively cheap, very fast and the most common approach in Alaska. This technique is limited to general information on ground ice distribution, soil texture and moisture content as auger cuttings cannot be used for detailed evaluation of permafrost structure and properties. Undisturbed samples of ice obtained by a SIPRE (Snow, Ice, and Permafrost Research Establishment) corer, or moderately disturbed samples of ice obtained by split spoons following solid-stem augering, or direct-push Geoprobe drilling are suitable for describing cryogenic structure, evaluating visible ice volume, and soil testing. Generally exploratory solid-stem boreholes are drilled first to contextualize the overall surficial geology. This is followed by additional drilling of regularly spaced solid-stem boreholes and ideally an area of hollow-stem auguring. The more detailed results from the undisturbed samples can clarify permafrost structure and origin (i.e. differentiating between tabular and wedge ice, or syngenetic and epigenetic permafrost) and help understand the variability of permafrost properties within the area. The total number of boreholes necessary is generally constrained by cost and complexity of the environment where the results depend on the spatial heterogeneity of materials over short distances, time required to drill per borehole and portability of the drilling equipment.

The goal of this project is to combine DCR-ERT and cryostratigraphic interpretations in delineating significant permafrost characteristics for Arctic road construction. There are few published best practices with respect to optimizing geophysical interpretation with boreholes in continuous permafrost areas. Producing reasonable cryostratigraphic interpretations of permafrost conditions requires a substantial amount of accumulated knowledge about the subsurface conditions. It rests on the assumptions that similar surficial conditions in an area should have comparable subsurface stratigraphy. In this study, we evaluate the effectiveness of the two techniques for improving site characterization.

4.3 Methods

Regional setting and identification of terrain units

The study area is located within the physiographic province of the Arctic Foothills (Wahrhaftig, 1965). At Umiat (69°22'N, 152°08'W, 81 meters above sea level) mean annual air

temperature is -11.8 °C, mean annual precipitation and snow depth are 229 mm and 136 mm correspondingly (based on National Climate Data Center records from 1971 to 2000). 5-Model Projected Average, Mid-Range Emissions (A1B) predict mean annual temperature to warm to -11.0 °C and mean annual precipitation to decrease slightly to 222 mm for the interval of 2010 to 2019 (Scenarios Network for Alaska Planning, 2015). The major ecosystems consist of upland low birch-willow shrub tundra and upland shrubby tussock tundra, where *Betula nana* and *Salix pulchra* serve as canopy cover, and overlapping understory species include *Vaccinium uliginosum*, *Vaccinium vitis-idaea*, *Epilobium nigrum*, *Equisetum arvense*, and *Sphagnum* spp. On alluvial plains the ecosystem transforms to riverine low willow shrub tundra, where *Salix aleutica*, *S. arbusculoidea*, and *S. glauca* are the main tall shrubs in frequently flooded areas, and *Salix lanata richardsonii* and *S. pulchra* dominate the inactive areas (Jorgenson and Heiner, 2008). Based on an interpretation of aerial and satellite images, aerial reconnaissance, and observations on the ground we identified five major terrain units: (1) low hills with gentle slopes and flat plateaus formed by ice-rich yedoma deposits, (2) flat thaw-lake basins connected by erosional patterns, (3) shallow thermokarst depressions connected by erosional patterns, (4) river terraces, and (5) modern floodplains.

Site selection

The analysis focused on two major areas: **AR6** (Anaktuvuk River Bridge Crossing) and **AL2** (Alignment Hole #2) (Figure 4.2). Site selection was based on potential bridge alignment sites and characterization of ice-rich permafrost with ice wedge polygons. Inclusion of sites representing the area of 2008 Anaktuvuk tundra fire (Jones et al., 2009) was a secondary consideration. These sites represent a range of conditions including tussock tundra (both unburned and burned conditions), high and low centered ice-wedge polygons and active thermokarst features. Fieldwork for this study was completed by September 10, 2010, when the depth of seasonal thawing was close to maximum.

Electrical resistivity tomography

DCR-ERT transects were completed in conjunction with the drilling of boreholes in the study area. The DCR-ERT surveys were acquired using an Earth Resistivity/IP Meter SUPER STING R1 IP (AGI Advanced Geosciences Inc.). The spacing of the electrodes and total length of the

survey varied by transect, and are detailed in Table 4.1. Both of these characteristics determined the depth which could be effectively resolved using the DCR-ERT methodology. A Wenner array was used due to its ability to discriminate changes in the vertical dimension and high signal-to-noise ratio (Loke, 2010). It is suitable for imaging permafrost structures such as the location of the permafrost table (Fortier et al., 2008). The software package RES2DINV (Loke and Barker, 1995) generates a two dimensional resistivity cross-section, that seeks to minimize the root-mean-square error (RMSE) between the measured and simulated apparent resistivities, with the simulated data derived from the 2-D model.

Borehole and geospatial data

Fourteen boreholes were drilled using a SIPRE corer (7.5 cm inside diameter) with Tanaka power head to a maximum depth of 3.9 m (Figure 4.3). Two boreholes, 6-m deep AL2 (TH10-631) and 4-m deep AL1 (TH10-632), were drilled by the Alaska Department of Transportation and Public Facilities (AKDOT & PF). A total of 58 samples were obtained to determine gravimetric water content of frozen soils. The borehole data were contextualized by active layer depths at each electrode, vegetation descriptions and site photographs. Aerial photographs and airborne light detection and ranging (LiDAR) data were collected in August 2008. Elevation data were derived from the LiDAR with cell size of 0.9 m and a vertical accuracy of 0.5 m. The aerial imagery had a 0.3 m (1 foot) spatial resolution. The elevation data were incorporated as part of the inversion process in obtaining the calculated resistivity cross-sections and incorporated into plots showing variations in active layer depths. Landform analysis of surficial geology was based on the aerial photographs. The elevation data and aerial photographs were also draped in 3-D to assist with visualization.

Permafrost description

In the areas of ice-rich permafrost, specific methods of geotechnical investigations have been successfully applied (Kanevskiy et al., 2012; Kanevskiy et al., 2013; Stephani et al., 2010), including the cryostratigraphy methods and especially cryofacies analysis (French and Shur, 2010; Katasonov, 1969; Katasonov, 1978) which was used for this study. It is based on the close relationship between shape, size, and spatial pattern of ice inclusions in soils (i.e., cryostructures) and specific terrain units, which reveals the nature of permafrost formation. For cryostratigraphic

descriptions, we used a classification of cryostructures (patterns formed by ice inclusions in the frozen soil), which has been adapted from several Russian and North American classifications (French and Shur, 2010; Gasanov, 1963; Katasonov, 1969; Katasonov, 1978; Shur and Jorgenson, 1998; Zhestkova, 1982). The ice content of frozen soil was evaluated by oven-drying (90°C, 72 h) samples. Gravimetric moisture contents (GMC) were calculated on a dry-weight basis.

4.4 Results

Site – AL2

The AL2 study site is comprised of two major terrain units: low hills with gentle slopes formed by ice-rich yedoma deposits and flat thaw-lake basins connected by erosional patterns (Figure 4.2). Transects 1 and 3 were located on yedoma deposits (Figure 4.4) which consist of silt with large syngenetic ice wedges formed in the late Pleistocene. Transect 4 was located on deposits of thaw-lake basins which consist of ice-rich peat and organic-rich silt, with modern ice wedges underlain by relatively ice-poor lacustrine and taberal (thawed and refrozen) silt. The cryostratigraphy and gravimetric water content of soils from the boreholes are summarized in Figure 4.5.

The content of wedge ice in yedoma is presumably very high: four of five boreholes from transects 1 and 3 at the AL2 site drilled in yedoma deposits encountered ice wedges. Ice wedges were also encountered by two boreholes (TH10-631 and TH10-632) drilled in this area by AKDOT & PF. Ice wedges were encountered at depths from 0.9 m to 2.2 m. The gravimetric moisture content of the ice-rich silt layer above the ice wedges, known as intermediate layer (Kanevskiy et al., 2011a; Shur, 1988) varied from 56–223% (average 112%, n=14). A single borehole without wedge ice (AL2-4) was drilled from the top of a baidzharakh (thermokarst mound), which formed due to thawing of the surrounding ice wedges. The GMC of yedoma silt in this borehole varied from 59 to 82% (average 71%, n=5).

AL2 transect 1 is gently sloped toward the lake and has been affected by recent fire. All three boreholes drilled within transect 1 (AL2-1, AL2-2 and AL2-3) indicated the presence of ice wedges. Active layer depths on AL2 transect 1 averaged 55 cm with a standard deviation of 10

cm. The lowest modeled resistivities of just under $300\ \Omega\ \text{m}$ were detected in the active layer of highly burned well-drained surfaces (Figure 4.6). High surface modeled resistivities of approximately $1.0\ \text{k}\Omega\ \text{m}$ were located in areas with water-filled thermokarst troughs above degrading ice wedges. Higher resistivities of $19.8\ \text{k}\Omega\ \text{m}$ were found in the upper part of permafrost. Toward the maximum resolution depth of 25 m, resistivities decreased approximately in half to $10.8\ \text{k}\Omega\ \text{m}$.

The transition between recently burned tussock tundra and the thermokarst lake was examined in AL2 transect 3 (Figure 4.6). The center of the survey was positioned next to the boundary between the burned tussock tundra on the main yedoma surface and actively sliding material on the slope adjacent to the thermokarst lake to maximize the DCR-ERT vertical resolution. The average active layer was 62 cm, and the standard deviation was 20 cm due to large differences between the slope and main yedoma surface. For example, active-layer thickness in the exposed soil on top of baidzharakh reached 1.5 m (borehole AL2-4). The lowest modeled resistivities of just over $60\ \Omega\ \text{m}$ corresponded to wet silt in the active layer. On the slope affected by surficial thermokarst and thermal erosion activity, modeled permafrost resistivity values of $5.8\ \text{k}\Omega\ \text{m}$ were found approximately 5 m below the surface, while under the main yedoma surface the low-resistivity layer was much thinner (Figure 4.6). The resistivity in yedoma increased with depth to $12.3\ \text{k}\Omega\ \text{m}$.

Thaw-lake basin deposits were studied in AL2 transect 4 (Figure 4.6) and borehole AL2-5 (Figures 4.4 and 4.5). The deposits consist of ice-rich peat almost 1.5 m thick and gray silt more than 2.5 m thick, which contains layers and inclusions of peat. The GMC of the peat varied from 180% to more than 300%, and the GMC of the shallow-water lacustrine silt with peat inclusions varied from 80 to 170%. Ice-poor deep-water lacustrine and taberal (thawed and refrozen) silt with peat layers was detected from 2.55 to 3.89 m (Figure 5, borehole AL2-5). The GMC of silt varied from 33–61%. Though the peat layer contained almost no visible ice, its GMC was 234%. In borehole AL2-6, wedge ice was encountered right below the active layer at a depth of less than 0.5 m (Figure 4.5).

At the AL2 transect 4 an electrode spacing was reduced to 1 m to better delineate the ice content in the upper permafrost. The average active-layer depth was 50 cm, with a standard deviation of 11 cm. Resistivities of approximately 120 Ω m were measured near the surface in the area with low-centered polygons (around electrode 1) and where the surface transitioned back to tussock tundra near the base of the yedoma slope (toward electrode 84) that was more severely burned during the tundra fire (Figure 4.6). Higher modeled resistivity values, around 20.0 k Ω m, were found 2.5 m below the surface around both boreholes. At the central part of the transect, modeled resistivity values decreased to 430 Ω m at 6 m below the surface. This low-resistivity area formed a circular structure approximately 8 m in diameter. Two smaller areas with relatively low resistivity values of 2.8 k Ω m were encountered at similar depths on both sides of this structure.

Site – AR6

The AR6 study site is made up of three major terrain units: (1) low hills with gentle slopes formed by ice-rich yedoma deposits, (2) river terrace (abandoned floodplain), and (3) modern floodplain. The height of the yedoma hills is 30–50 m, and the height of the river terrace is approximately 5 m above the surface of the Anaktuvuk River floodplain. The river terrace and yedoma hills were affected by the recent fire (Figure 4.2). On the east side of the Anaktuvuk River, AR6 transect 1 bisected the large flat floodplain adjacent to the main channel (Figure 4.7). AR6 transects 2 and 3 focused on the ground ice distribution on the river terrace. Summarized in Figure 4.8 are the cryostratigraphy and gravimetric water content of soils from the boreholes in this area.

The AR6 transect 1 had a sandy unit supported shrub growth and overlaying the river gravels. The presence of *Salix alaxensis* indicated a more recent history of active flooding. Multiple smaller subchannels contained coarser surficial gravels and cobbles. Surficial investigations indicated an active layer depth of greater than 1.5 m and absence of ice-rich permafrost. However the presence of gravels confounded our efforts to obtain core samples and to reach the permafrost table. The DCR-ERT configuration used for this transect, on the other hand, allowed us to image to approximately 13 m depth. The AR6 transect 1 had modeled resistivities with minimum and maximum values of approximately 300 Ω m and 8.8 k Ω m

(Figure 4.9). The surficial channels are indicated by the lowest resistivity values, ranging from 300 to 500 Ω m. A high-resistivity area was detected from depths of 2 to 4 m.

The AR6 transect 2 examined the transition between high-centered ice-wedge polygons at the river terrace and the lower-lying floodplain while the AR6 transect 3 investigated the high-centered ice-wedge polygons in greater detail. The boreholes AR6-1, AR6-2, and AR6-3 were located within the low river terrace. All boreholes reached gravel at depths of 0.9–1.9 m. The upper permafrost at this location consisted of ice-rich peat, silt, and silty sand 0.6–1.3 m thick underlain by sand and gravel. The GMC of the peat, silt, and silty sand deposits varied from 117 to 444% (average 293%, $n=5$). The GMC of the underlying sand deposits varied from 33 to 112% (average 64%, $n=5$). High-centered ice-wedge polygons were framed by troughs up to 1 m deep and 1.5 m wide, developed above thawing ice wedges. The vertical extent of ice wedges in the river terrace is not expected to exceed 3 m because gravel is located close to the surface. As a side note, borehole AR6-2 was drilled through the small ice wedge up to 0.3 m wide (Figure 4.10).

The average active layer depth for AR6 transect 2 was 54 cm with a standard deviation of 13 cm. On the western end of the transect (the section lying within the floodplain), active layer depths exceeded the 1 m extent of our probe. The highest modeled resistivities of 21.0 k Ω m were found under the river terrace with ice-wedge polygons at depths from 4 to 15 m; the lowest were present under the floodplain with approximate values between 270 and 500 Ω m. Modeled resistivities for all three boreholes at depth 1.5 were approximately 3.2 k Ω m.

The AR6 transect 3 average active layer depths were 48 cm with a standard deviation of 7 cm. Resistivities of between 117 and 220 Ω m were found close to the surface in the centers of ice-wedge polygons with higher values around 400 Ω m in the polygon depressions and in the vicinity of cracks in the soil resulting from tundra fire. Gravel deposits correspond to modeled resistivity values ranging from 5197 to 7490 Ω m.

4.5 Analysis

Terrain units and permafrost properties

Low hills with gentle slopes and flat plateaus formed by yedoma deposits. The structure and properties of this unit were evaluated based on similarity with Yedoma silt deposits studied in the adjacent area at the Itkillik River exposures (Kanevskiy et al., 2011a; Kanevskiy et al., 2011b). This deposit is Pleistocene syngenetic permafrost characterized by extremely high ice content and large ice wedges. The thickness of yedoma deposits varies from several meters to more than 35 m. There are two different generations of ice wedges (depicted in Figure 4.6): active Holocene ice wedges (usually encountered at depths from 0.6–1.0 m) and inactive late Pleistocene ice wedges (usually encountered at depths from 1.5–2.5 m). Most late-Pleistocene ice wedges penetrate through the whole yedoma stratum, and are separated from the active layer by the ice-rich intermediate layer (Kanevskiy et al., 2011a; Shur, 1988). The volume of Holocene wedge ice in the upper permafrost (within the intermediate layer) usually varies from 10–30%, and the volume of Pleistocene wedge ice varies from 40–70%. The GMC of the intermediate layer varies from 80% to more than 200%, while the GMC of Pleistocene yedoma deposits typically varies from 50 to 80%. The borehole data proved the similarity of the unit to yedoma deposits and intermediate layer previously studied by Kanevskiy and co-authors at the Itkillik River exposure (Kanevskiy et al., 2011a).

Flat thaw-lake basins connected by erosional patterns. The depth of thaw-lake basins varies from several meters to more than 20 m. Deposits of thaw-lake basins consist of ice-rich peat and organic-rich lacustrine silt (GMC varies from 80% to more than 300%) with modern active ice wedges underlain by relatively ice-poor lacustrine and taberal (thawed and refrozen) silt (GMC typically varies from 30–40%). Active ice wedges are very close to the bottom of the active layer and usually up to 3 m wide with a vertical extent of up to 5 m. The thickness of peat usually varies from 1 to 3 m, and the thickness of ice-rich lacustrine silt typically does not exceed 2 m. The thickness of ice-poor thawed and refrozen silt depends on the initial (prior to thawing) thickness and ice content of yedoma deposits and can reach 10 m and more.

Shallow thermokarst depressions connected by erosional patterns. The depth of shallow thermokarst depressions does not exceed several meters. We believe these landforms are related

mostly to thawing of relatively thin yedoma strata. In some cases, shallow thermokarst depressions form when thawing of yedoma under thermokarst lakes is interrupted by sudden lake drainage. Lack of drilling data prevents us from characterizing the structure and properties of deposits of shallow thermokarst depressions. Landforms transitional from thaw-lake basins to shallow thermokarst depressions can be observed.

River terraces (abandoned floodplain). Deposits of low alluvial terraces include ice-rich peat and organic-rich silt and silty sand up to 2 m thick (GMC varies from 100 to more than 400%) with active ice wedges; the terraces are underlain by sand (up to 1 m thick; GMC decreases with depth from more than 100% to 40%) and gravel, which is mostly ice-poor.

Modern floodplains. Several levels of floodplain can be detected. The younger (lower) levels are formed by unfrozen gravel (the depth of closed talik is unknown) or by presumably ice-poor gravel beneath the more than 2-m thick active layer. The older (higher) levels have permafrost, which is indicated by ice-wedge polygons. Lack of drilling data in the study area prevents us from characterizing the structure and properties of the floodplain deposits.

Combined cryostratigraphic and geophysical interpretations

Direct comparison of the cryostratigraphic and geophysical interpretations of various terrain units (Figure 4.11 and Figure 4.12) allows the two techniques to be contrasted and evaluated in their usefulness for delineating permafrost characteristics. In the AL2 transects 1 and 3 the general thickness and areal distribution of the active layer and intermediate layer were similar between the two techniques. Knowledge derived from both the adjacent boreholes and soils of similar nature suggested the presence of inactive Late Pleistocene ice wedges interspersed with yedoma silt. The interpretation derived from the geophysics perceived this unit as a homogenous frozen mass where resistivity values varied between 9 and 15 k Ω m depending on depth due to the spacing of the electrodes. The relatively small active Holocene ice wedges identified by the borehole results and interpolated into the cryostratigraphic analysis based on pre-existing landscape knowledge were not detected by geophysical data, because these wedges are associated mainly with the ice-rich intermediate layer with high resistivity. No distinct ice-

wedge polygons were visible in the areas of transect 1 and 3, which is typical of the yedoma surface, but at some places, shallow troughs about degrading ice wedges could be observed.

On the AL2 transect 3, the elevation of the yedoma hill above the lake suggested that a thickness of yedoma exceeds 12 m, which is matched in the geophysical interpretation. The geophysical results can be used to clearly delineate extent of the thermokarst processes (including potential underground piping) near the edge of the lake where resistivity values fall below 200 Ω m. They also suggest that the intermediate layer is thicker than what is estimated by the cryostratigraphic analysis. Alternatively, it may also indicate a thicker active layer as the tundra fire resulted in substantial thermokarst especially in the intermediate layer.

There were some significant differences between the cryostratigraphic and geophysical analysis for AL2 transect 4. The cryostratigraphic interpretation identified ice wedges based on the borehole results and aerial photographs which corresponded to deeper active layer areas in the geophysics. The interpretability of the geophysics is affected by the choice of a Wenner array which is generally better at resolving vertical resistivity variations, while the dipole-dipole has improved lateral resolution. The Wenner array also has greater depth capabilities and for that reason we chose it. Time permitting we would have performed both. In this case, the resistivity results do show reasonable correlation to the estimated ice-wedge distribution but they are not distinct in terms of value or separable from the near surface.

In the central part of AL2 transect 4, in a drained lake basin, the geophysics reveal a zone with electric resistivity lower than 1 k Ω m, which could be interpreted as an isolated talik formed due to partial freezing of the closed talik which had formed under the thermokarst lake before its drainage. Deeper borehole drilling would be necessary to confirm the nature of this low-resistivity zone. Features like taliks are important considerations for permafrost engineering and Arctic road construction. Geophysical techniques like DCR-ERT are very useful for guiding boreholes to document the nature and extent of taliks and can significantly reduce the number of boreholes which are required to delineate talik zones.

The AR6 transect 1 cryostratigraphic interpretation was not possible because the SIPRE corer is not suitable for drilling in coarser material such as gravel. Active channels were delineated using the aerial photography. The geophysical data supported the location and extent of the channels, and also indicated similarity to the adjacent channels. The base of the active layer was interpreted to be consistent with the boundary of the 3 k Ω m layer identified as frozen sand. Soils with values in excess of 8 k Ω m at depth were considered to be frozen gravel.

On the AR6 transect 2, analysis of the DCR-ERT data was able to differentiate the margin between the active layer on lower-lying modern floodplain (less than 600 Ω m) and the frozen gravel (\sim 5.0 – 10.0 k Ω m). This gravel layer under the floodplain is less resistive than deposits of the river terrace containing ice wedges. A transitional layer between the gravel and the active layer was identified as the peat and silt layer based on the borehole results. In comparison to the cryostratigraphic analysis, the Holocene ice wedges, alluvial sand and the peat and silt layer could not be clearly separated from each other by the geophysics. This transect benefited greatly from the elevation data for topographic correction.

The AR6 transect 3 geophysical analysis identified both the active layer and frozen peat and silt layer in the near-surface of the ground. They matched the cryostratigraphic interpretation very closely. The alluvial sand layer could not be differentiated from the alluvial gravel with mean values of 8.6 k Ω m. There were distinct wedge or channel shapes with slightly lower resistivity mean values of 6.3 k Ω m. The positioning of the mass on the left side of the transect suggests that it might be a buried ice wedge as it aligns with the cryostratigraphic interpretation. However, the 6.3 k Ω m distribution on the right does not match the location of ice-wedge polygons suggested by the borehole. The surface pattern indicates an ice-wedge polygon located directly above the transect. Since the current from an injection point integrates over an area perpendicular to the transect, an ice wedge directly adjacent could influence the resistivity results. Further examination of the ice-wedge polygons would benefit from the use of quasi-3D resistivity imaging (Rodder and Kneisel, 2012).

Overall, the geophysical and cryostratigraphic interpretations for most transects greatly benefited one from the other. The geophysical analysis was superior for identifying potential

unconformities in the subsurface such as the potential talik in AL2 transect 4. The DCR-ERT results using a Wenner array were particularly useful in delineating the shape and depth of the active and intermediate layers. It should be noted that delineating the intermediate layer is not as simple as simply measuring the active layer at one period, as it is based on the soil and ice properties in the cryostratigraphic interpretation. The cryostratigraphic analysis produced detailed subsurface representations, however they are based on a wealth of subsurface knowledge from previous studies (Kanevskiy et al., 2011a; Kanevskiy et al., 2011b) and rest on the assumption that these transects are similar to others studied in detail via exposed outcrops.

Suitability of cryostratigraphic and geophysical methods for Arctic road construction and alternatives

Evaluating the effectiveness of the DCR-ERT geophysics and cryostratigraphy for examining permafrost characteristics for road construction in the Arctic should account for multi-criteria including: time, effort, experience, cost and accuracy. In the preliminary stages, producing permafrost distribution and characteristics through either DCR-ERT or cryostratigraphy is time and labor intensive. Both techniques benefit from pre-existing knowledge of regional characteristics, and they should be preceded by differentiation of terrain units to characterize the landscape. Identifying the areal extent of these units can assist in targeting drilling programs which are the backbone of soil and permafrost characterization for roads. The locations of geophysical transects can and should be pre-selected in many cases to maximize the potential results (e.g., at the boundaries of different terrain units). In the case of DCR-ERT it can be beneficial to model the expected resistivity results in order to select the best electrode spacing and array type. Both methods are bolstered by the availability of ancillary data such as high-resolution visible imagery and good-quality DEMs.

The location and spacing of boreholes strongly shapes the cryostratigraphic analysis. As the primary source of information and verification, boreholes can be located at either regular intervals (driving up costs) or located to discriminate between terrain units (requires landscape interpretation experience). In contrast, geophysical interpretation is often most effective when the data is collected first and then boreholes are situated where they maximize information. In this study, the deeper boreholes were drilled either before or concurrently to the fieldwork. The

shallower boreholes and DCR-ERT transects were acquired simultaneously, while the geospatial data were obtained afterward due to limitations in field logistics. The most effective order would be to acquire the geospatial information first to optimize the locations of the geophysical transects. The DCR-ERT data would then be collected and preliminarily analyzed before using all available data to select the location of the boreholes. This would maximize the inference from the datasets and improve interpretation of both the geophysical and cryostratigraphic results. In many instances, this could lead to a reduced number of boreholes required. Geophysics can also be used to assist in interpolating between boreholes in an alignment, regardless of when or where the boreholes are drilled.

The three main advantages of DCR-ERT for examining permafrost characteristics for road construction are: 1) the type of array can be varied from the Wenner array; 2) multiple arrays can be used in the inversion process and 3) the spacing of the electrodes can be easily varied to control the resolution and depth of investigation. Time permitting, we would have also used the dipole-dipole array (Van Dam, 2012) on our transects, which is more sensitive to changes in vertical structure in the near surface (Dahlin and Zhou, 2004). One disadvantage of DCR-ERT is that the technique requires a moderate amount of time and effort in order to get good contact between the electrode stakes and ground. CCR-ERT (De Pascale et al., 2008; Hauck and Kneisel, 2006; Kuras et al., 2006) is a reasonable alternative to DCR-ERT as the technique does not require staking.

The biggest limitation to cryostratigraphic analysis of permafrost for road construction is the base of knowledge required to produce accurate representations of the subsurface. Semi-automating the construction of the cryostratigraphic interpretations for transects could produce significant savings in effort. Integrating remotely quantified information such as wedge-ice volumes (Ulrich et al., 2014) for planning and designing road construction would be a good addition. The cryostratigraphic method provides intricate estimates of soil-ice volume in addition to the subsurface distribution of ground ice. These estimates of the ground-ice content are critical for geosystems approaches to permafrost engineering for road construction (Stephani et al., 2014).

4.6 Conclusions

This study found DCR-ERT transects with a Wenner array and cryostratigraphy analysis produced sufficient information on permafrost characteristics pertinent to road construction in northern Alaska. There was consistency between the geophysical interpretations and the terrain units, confirming that terrain units are a good indicator of the subsurface conditions. Optimizing the electrode spacing to adjust the vertical depth and resolution of transects allowed the geophysical results to highlight differences in presence/absence of permafrost and estimate active and intermediate layer depths. The major drawback was the 2 m electrode spacing was relatively ineffective in delineating ice-rich from ice-poor layers at depths greater than 10 m. Subsurface heterogeneity was most detectable when there were significant differences in landcover such as the transition from floodplain to river terrace.

Both the geophysical and cryostratigraphic results and interpretations were improved by availability of high-resolution geospatial (aerial photographs & DEMs) data. Given the planning and financial resources that go into constructing roads in continuous permafrost, data collection should begin with geospatial information and geophysical data collected at key sites. Boreholes would preferably be drilled in areas where they maximize the interpretation from the geophysics. This approach also capitalizes on the time, effort and expertise required to process and analyze the results. Future improvements in geospatial and geophysical methods and techniques will eventually make it easier to estimate permafrost characteristics; however, borehole data remain the baseline source of subsurface information.

4.7 Acknowledgements

This project was supported by Alaska University Transportation Center (Project Number 410018), in cooperation with the U.S. Department of Transportation Research and Innovative Technology Administration (RITA), and the Alaska Department of Transportation & Public Facilities. It was part of work overseen by Billy Conner, P.E., Director of AUTC. Expert advice and technical coordination was provided by Steve Masterman of the AKDOT & PF Northern Region Design and Engineering Services. Processed LiDAR data was graciously shared by Benjamin Crosby.

4.8 References

- Dahlin, T. and Zhou, B., 2004. A numerical comparison of 2D resistivity imaging with 10 electrode arrays. *Geophysical Prospecting*, 52(5): 379-398.
- De Pascale, G.P., Pollard, W. H. and Williams, K. K., 2008. Geophysical mapping of ground ice using a combination of capacitive coupled resistivity and ground-penetrating radar, Northwest Territories, Canada. *Journal of Geophysical Research: Earth Surface*, 113(F2): F02S90.
- Fortier, R., LeBlanc, A. M., Allard, M., Buteau, S. and Calmels, F., 2008. Internal structure and conditions of permafrost mounds at Umiujaq in Nunavik, Canada, inferred from field investigation and electrical resistivity tomography. *Canadian Journal of Earth Sciences*, 45(3): 367-387.
- Fortier, R. and Savard, C., 2010. Engineering geophysical investigation of permafrost conditions underneath airfield embankments in northern Quebec (Canada), Sixth Canadian Conference on Permafrost, GEO2010, Calgary, Alberta, Canada, pp. 1307–1314.
- French, H. and Shur, Y., 2010. The principles of cryostratigraphy. *Earth-Science Reviews*, 101(3–4): 190-206.
- Gasarov, S.S., 1963. Morphogenetic classification of cryostructures of frozen sediments. *Trudy SVKNII*(3): 53–62.
- Hauck, C., 2002. Frozen ground monitoring using DC resistivity tomography. *Geophysical Research Letters*, 29(21): 12-1-12-4.
- Hauck, C. and Kneisel, C., 2006. Application of capacitively-coupled and DC electrical resistivity imaging for mountain permafrost studies. *Permafrost and Periglacial Processes*, 17(2): 169-177.

Hilbich, C., Hauck, C., Hoelzle, M., Scherler, M., Schudel, L., Völksch, I., Vonder Mühll, D. and Mäusbacher, R., 2008. Monitoring mountain permafrost evolution using electrical resistivity tomography: A 7-year study of seasonal, annual, and long-term variations at Schilthorn, Swiss Alps. *Journal of Geophysical Research: Earth Surface*, 113(F1): F01S90.

Hubbard, S.S., Gangodagamage, C., Dafflon, B., Wainwright, H., Peterson, J., Gusmeroli, A., Ulrich, C., Wu, Y., Wilson, C., Rowland, J., Tweedie, C. and Wulschleger, S. D., 2013. Quantifying and relating land-surface and subsurface variability in permafrost environments using LiDAR and surface geophysical datasets. *Hydrogeology Journal*, 21(1): 149-169.

Isaksen, K., Ødegård, R. S., Etzelmüller, B., Hilbich, C., Hauck, C., Farbrot, H., Eiken, T., Hygen, H. O. and Hipp, T. F., 2011. Degrading Mountain Permafrost in Southern Norway: Spatial and Temporal Variability of Mean Ground Temperatures, 1999–2009. *Permafrost and Periglacial Processes*, 22(4): 361-377.

Jones, B. M., Kolden, C.A., Jandt, R., Abatzoglou, J. T., Urban, F. and Arp, C. D., 2009. Fire Behavior, Weather, and Burn Severity of the 2007 Anaktuvuk River Tundra Fire, North Slope, Alaska. *Arctic Antarctic and Alpine Research*, 41(3): 309-316.

Jorgenson, M. T. and Heiner, M., 2008. *Ecosystems of Northern Alaska*. ABR Inc. and the Nature Conservancy.

Jorgenson, M. T., Shur, Y. L. and Osterkamp, T. E., 2008. Thermokarst in Alaska. In: D.L. Kane and K.M. Hinkel (Editors), *Ninth International Conference on Permafrost*. Institute of Northern Engineering, Fairbanks, AK, pp. 869-876.

Jorgenson, M. T., Shur, Y.L. and Walker, H. J., 1998. Evolution of a permafrost-dominated landscape on the Colville River Delta, northern Alaska, *Proc. 7 Int. Permafrost Conf*, pp. 523-529.

Kanevskiy, M., Jorgenson, T., Shur, Y., O'Donnell, J. A., Harden, J. W., Zhuang, Q. and Fortier, D., 2014. Cryostratigraphy and Permafrost Evolution in the Lacustrine Lowlands of West-Central Alaska. *Permafrost and Periglacial Processes*, 25(1): 14-34.

Kanevskiy, M., Shur, Y., Connor, B., Dillon, M., Stephani, E. and O'Donnell, J., 2012. Study of the ice-rich syngenetic permafrost for road design (Interior Alaska). In: K.M. Hinkel (Editor), Tenth International Conference on Permafrost, June 25-29, 2012, . The Northern Publisher, Salekhard, Russia, pp. 191-196.

Kanevskiy, M., Shur, Y., Fortier, D., Jorgenson, M. T. and Stephani, E., 2011a. Cryostratigraphy of late Pleistocene syngenetic permafrost (yedoma) in northern Alaska, Itkillik River exposure. *Quaternary Research*, 75(3): 584-596.

Kanevskiy, M., Shur, Y., Jorgenson, M. T., Ping, C. L., Fortier, D., Stephani, E. and Dillon, M., 2011b. Permafrost of Northern Alaska, Twenty-first International Offshore and Polar Engineering Conference, Maui, Hawaii, USA, pp. 1179–1186.

Kanevskiy, M., Shur, Y., Krzewinski, T. and Dillon, M., 2013. Structure and properties of ice-rich permafrost near Anchorage, Alaska. *Cold Regions Science and Technology* 93: 1-11.

Katasonov, E. M., 1969. Composition and cryogenic structure of permafrost. In: N.R.C.o. Canada (Editor), Ottawa, pp. 25–36.

Katasonov, E. M., 1978. Permafrost-facies analysis as the main method of cryolithology, Permafrost: The USSR Contribution to the Third International Conference. National Academy of Sciences, Washington, D.C., pp. 171–176.

Kneisel, C., 2010. Frozen ground conditions in a subarctic mountain environment, Northern Sweden. *Geomorphology*, 118(1-2): 80-92.

Kneisel, C., Hauck, C., Fortier, R. and Moorman, B., 2008. Advances in geophysical methods for permafrost investigations. *Permafrost and Periglacial Processes*, 19(2): 157-178.

Kuras, O., Beamish, D., Meldrum, P. I. and Ogilvy, R. D., 2006. Fundamentals of the capacitive resistivity technique. *Geophysics*, 71(3): G135-G152.

Lewkowicz, A. G., Etzelmüller, B. and Smith, S. L., 2011. Characteristics of Discontinuous Permafrost based on Ground Temperature Measurements and Electrical Resistivity Tomography, Southern Yukon, Canada. *Permafrost and Periglacial Processes*, 22(4): 320-342.

Loke, M., 2010. Rapid 2-D Resistivity & IP inversion using the least-squares method (RES2DINV ver. 3.59 for Windows XP/Vista/7, manual). Geotomo Software, Malaysia, pp. 53.

Loke, M. H. and Barker, R. D., 1995. Least-square deconvolution of apparent resistivity pseudosections. *Geophysics*, 60(6): 1682-1690.

McClymont, A. F., Hayashi, M., Bentley, L. R. and Christensen, B. S., 2013. Geophysical imaging and thermal modeling of subsurface morphology and thaw evolution of discontinuous permafrost. *Journal of Geophysical Research: Earth Surface*, 118(3): 1826-1837.

Oldenborger, G. A. and LeBlanc, A. M., 2013. Capacitive resistivity inversion using effective dipole lengths for line antennas. *Journal of Applied Geophysics*, 98(0): 229-236.

Osterkamp, T. E. and Payne, M. W., 1981. Estimates of permafrost thickness from well logs in northern Alaska. *Cold Regions Science and Technology*, 5(1): 13-27.

Overduin, P. P., Westermann, S., Yoshikawa, K., Haberlau, T., Romanovsky, V. and Wetterich, S., 2012. Geoelectric observations of the degradation of nearshore submarine permafrost at Barrow (Alaskan Beaufort Sea). *Journal of Geophysical Research: Earth Surface*, 117(F2): F02004.

Rodder, T. and Kneisel, C., 2012. Permafrost mapping using quasi-3D resistivity imaging, Murtel, Swiss Alps. *Near Surface Geophysics*, 10(2): 117-127.

Samouëlian, A., Cousin, I., Tabbagh, A., Bruand, A. and Richard, G., 2005. Electrical resistivity survey in soil science: a review. *Soil and Tillage research*, 83(2): 173-193.

Scenarios Network for Alaska Planning, 2015. Community Charts, https://www.snap.uaf.edu/sites/all/modules/snap_community_charts/charts.php#community=433&dataset=1&scenario=a1b&units=standard&variability=0 (accessed April 10, 2015).

Scherler, M., Hauck, C., Hoelzle, M., Stähli, M. and Völksch, I., 2010. Meltwater infiltration into the frozen active layer at an alpine permafrost site. *Permafrost and Periglacial Processes*, 21(4): 325-334.

Shur, Y., 1988. The upper horizon of permafrost soils, Fifth International Conference on Permafrost, Tapir Publishers, Trondheim, Norway, pp. 867-871.

Shur, Y. and Jorgenson, M. T., 1998. Cryostructure development on the floodplain of the Collville River Delta, northern Alaska, Proceedings of the Seventh International Conference on Permafrost. Laval University, Yellowknife, Canada, pp. 993–999.

Sjöberg, Y., Marklund, P., Pettersson, R. and Lyon, S., 2015. Geophysical mapping of palsa peatland permafrost. *The Cryosphere*, 9(2): 465-478.

Stephani, E., Fortier, D. and Shur, Y., 2010. Applications of cryofacies approach to frozen ground engineering - Case study of a road test site along the Alaska Highway (Beaver Creek, Yukon, Canada), 63rd Canadian Geotechnical Conference & 6th Canadian Permafrost Conference, Calgary, AB, Canada, pp. 476-483.

Stephani, E., Fortier, D., Shur, Y., Fortier, R. and Dore, G., 2014. A geosystems approach to permafrost investigations for engineering applications, an example from a road stabilization experiment, Beaver Creek, Yukon, Canada. *Cold Regions Science and Technology*, 100: 20-35.

Timofeev, V. M., Rogozinski, A. W., Hunter, J. A. and Douma, M., 1994. A new ground resistivity method for engineering and environmental geophysics, *Symposium on the Application of Geophysics to Engineering and Environmental Problems. EEGS*, pp. 701-15.

Ulrich, M., Grosse, G., Strauss, J. and Schirrmeister, L., 2014. Quantifying Wedge-Ice Volumes in Yedoma and Thermokarst Basin Deposits. *Permafrost and Periglacial Processes*, 25(3): 151-161.

Van Dam, R. L., 2012. Landform characterization using geophysics—Recent advances, applications, and emerging tools. *Geomorphology*, 137(1): 57-73.

Wahrhaftig, C., 1965. *Physiographic Divisions of Alaska*. United States Government Printing Office, Washington, pp. 52.

You, Y., Yu, Q., Pan, X., Wang, X. and Guo, L., 2013. Application of electrical resistivity tomography in investigating depth of permafrost base and permafrost structure in Tibetan Plateau. *Cold Regions Science and Technology*, 87(0): 19-26.

Zhestkova, T. N., 1982. *Formation of the Cryogenic Structure of Ground*. Nauka, Moscow, 209 pp.



Figure 4.1: Stream meandering along ice wedges of high center ice-wedge polygons with the high bank of the Colville River in the background

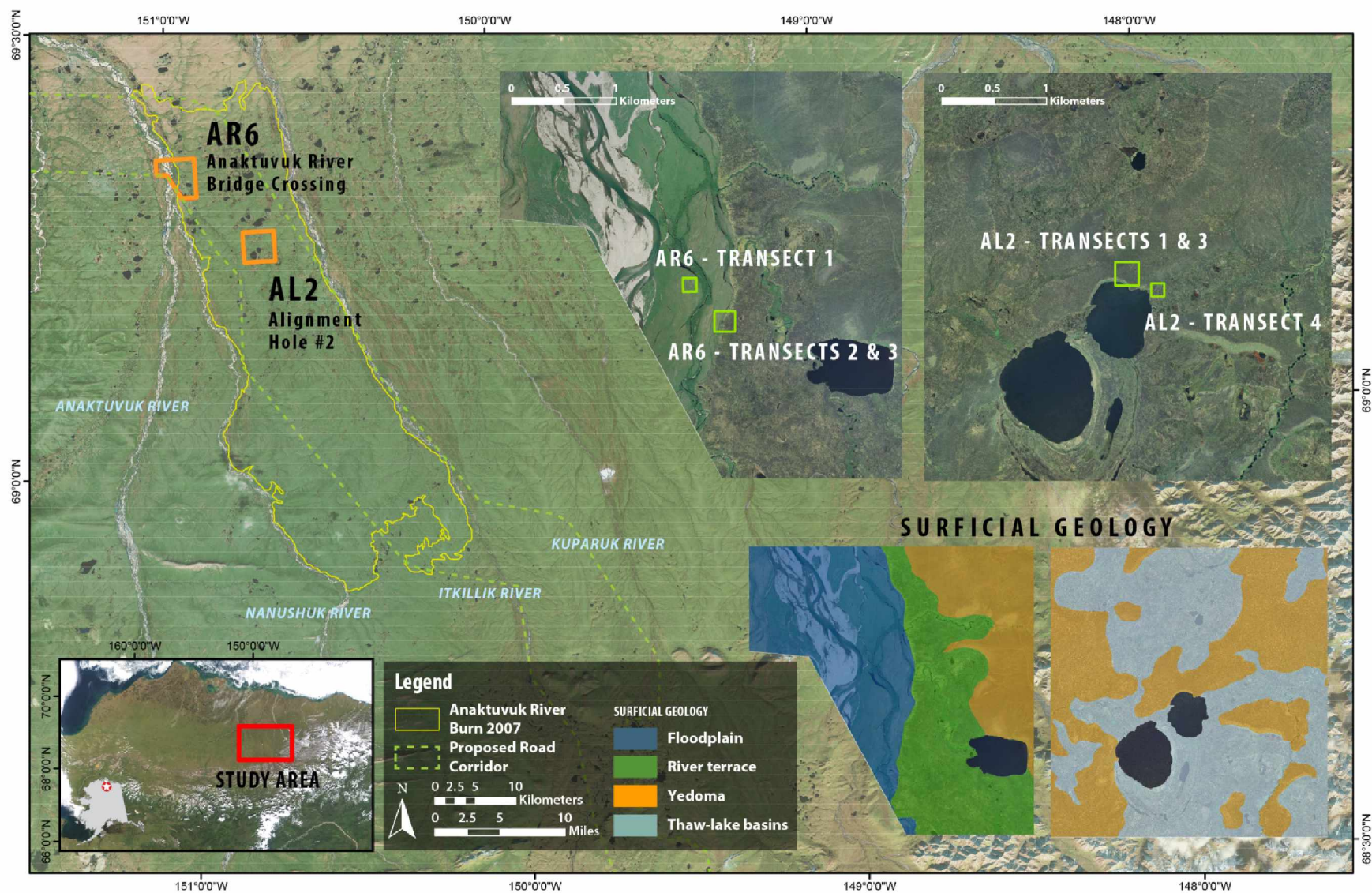


Figure 4.2: Study area showing field sites AR6 and AL2 with inset versions of aerial photographs and surficial geology



Figure 4.3: Drilling with SIPRE corer at site AL4-2 in burned tussock tundra

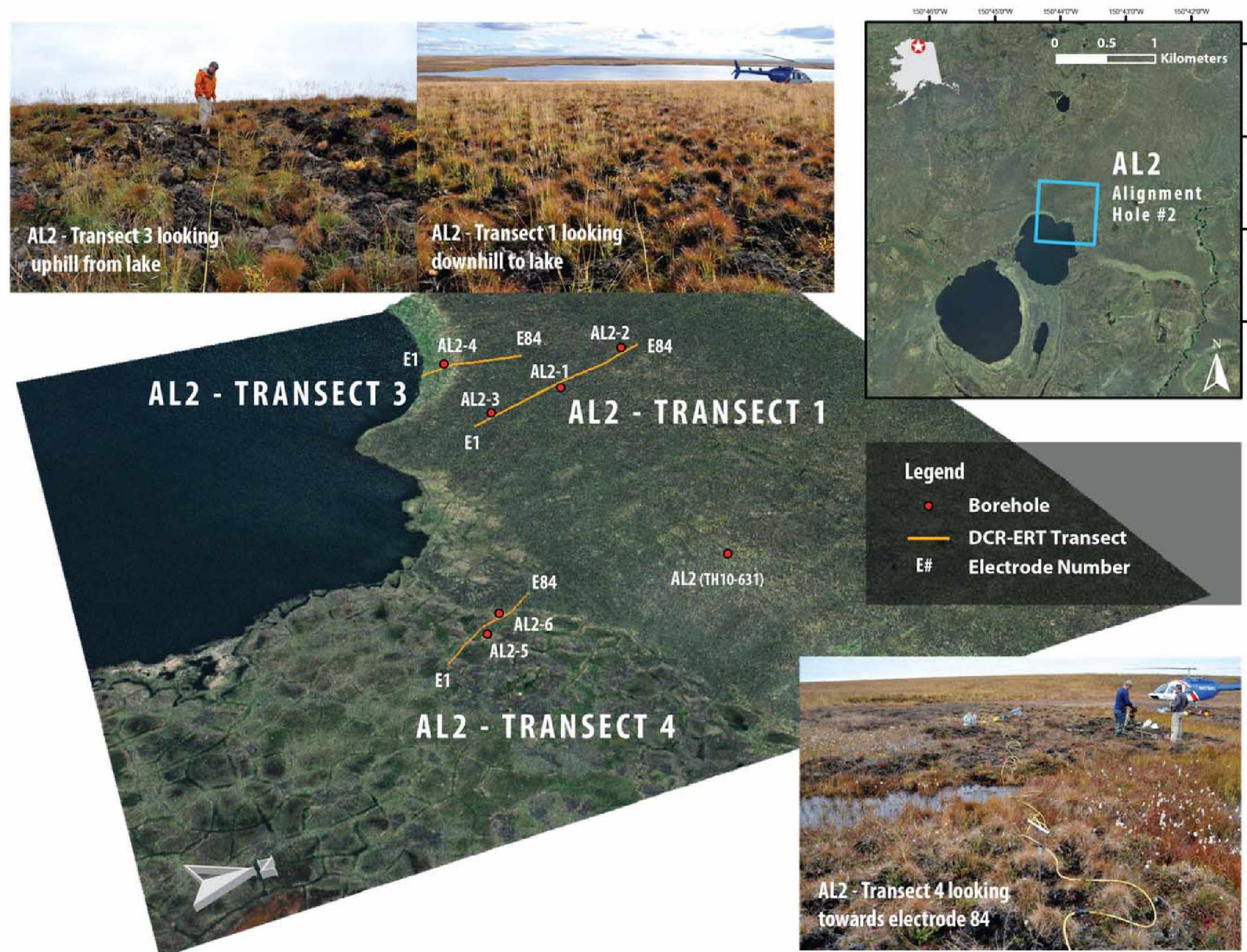


Figure 4.4: AL2 transect 1, 3 and 4 showing aerial photograph draped with 2 times vertical exaggeration and site photographs

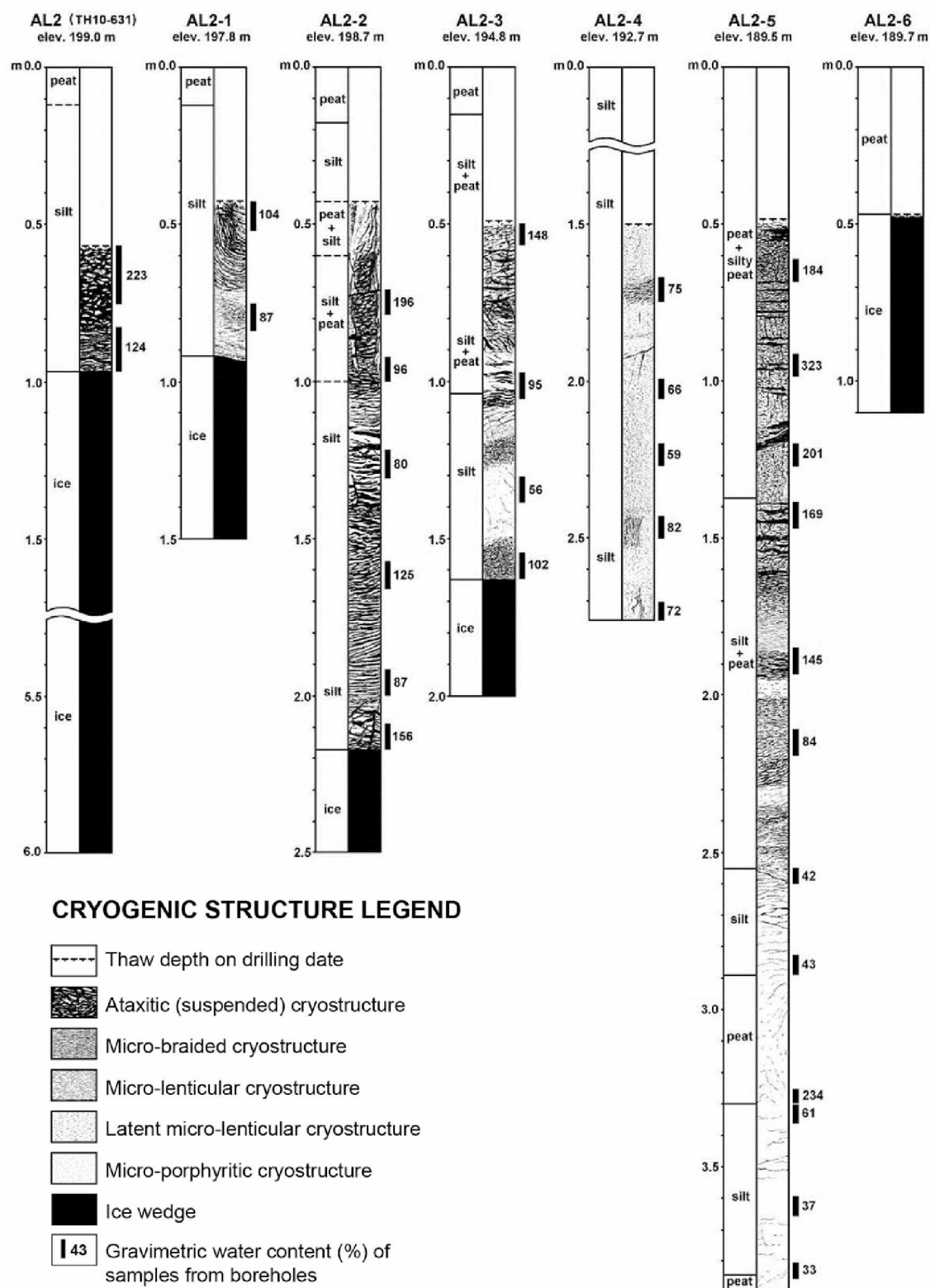


Figure 4.5: Cryostratigraphy and gravimetric water content (%) of frozen soils, site AL2.
 Borehole AL2 was drilled on September 1, 2010; all other boreholes – on September 8-9, 2010.

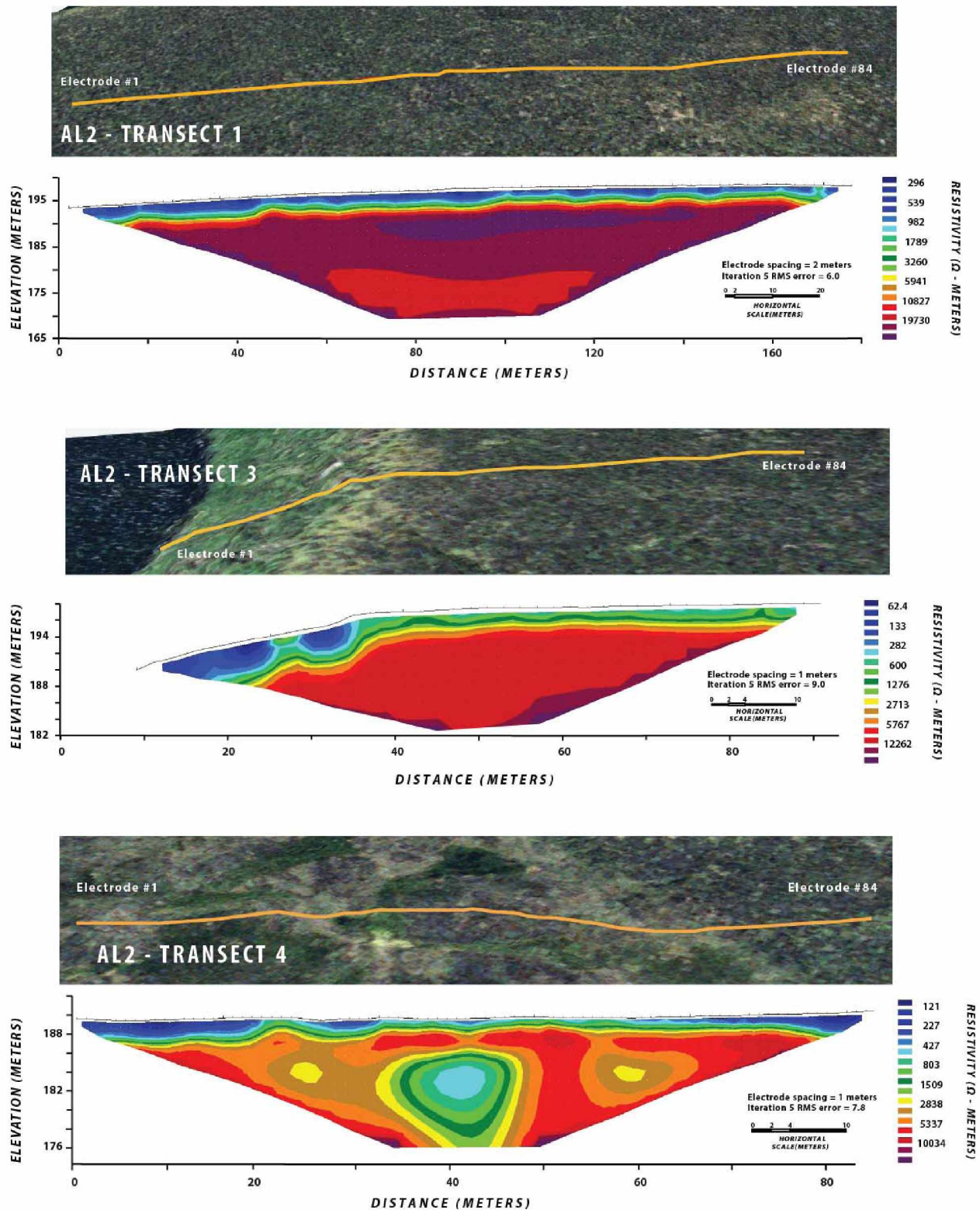


Figure 4.6: Draped aerial photographs of AL2 transects 1, 3 and 4 with their corresponding DCR-ERT modeled resistivity (Ω m) below each

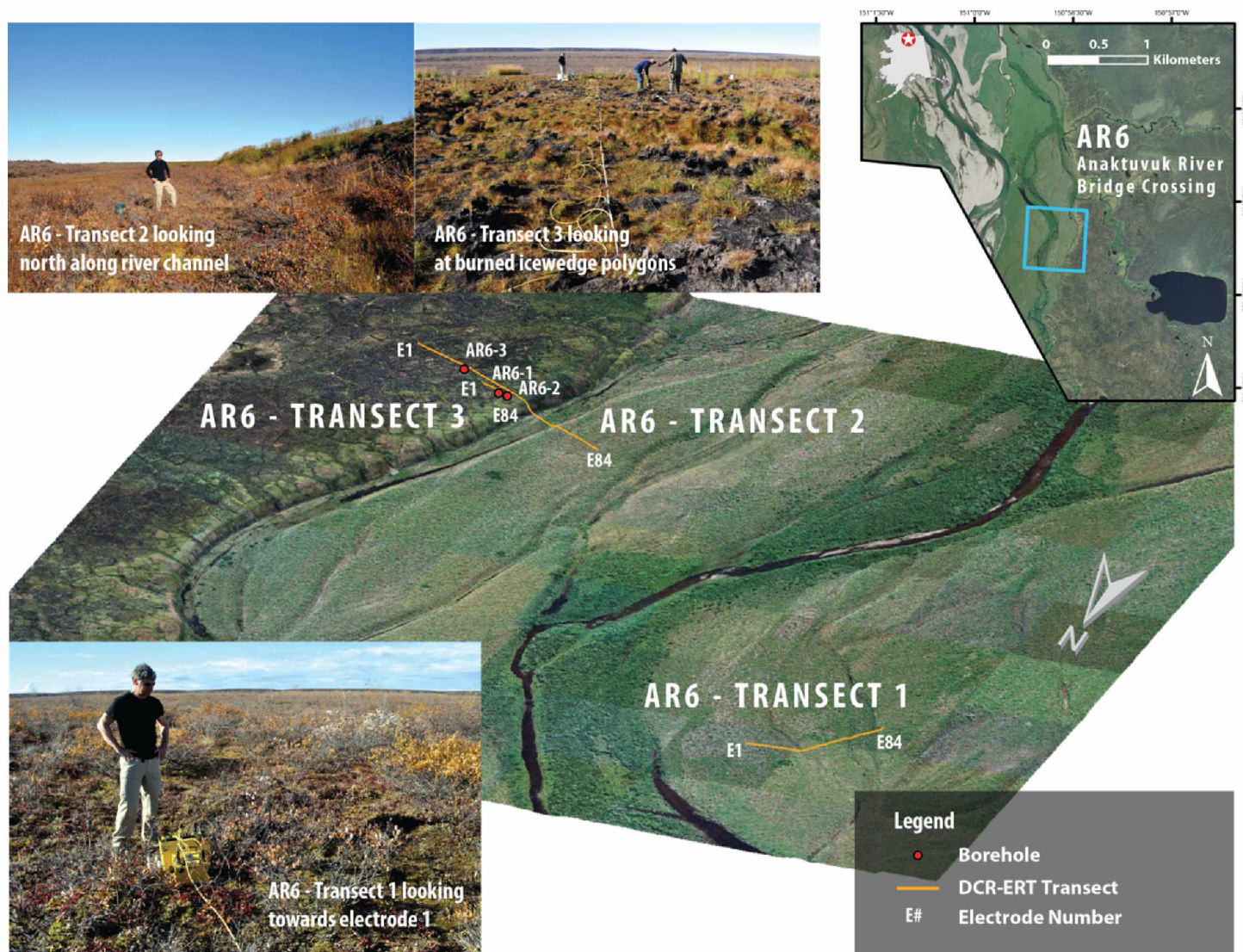


Figure 4.7: AR6 transect 1, 2 and 3 showing aerial photograph draped with 2 times vertical exaggeration and site photographs

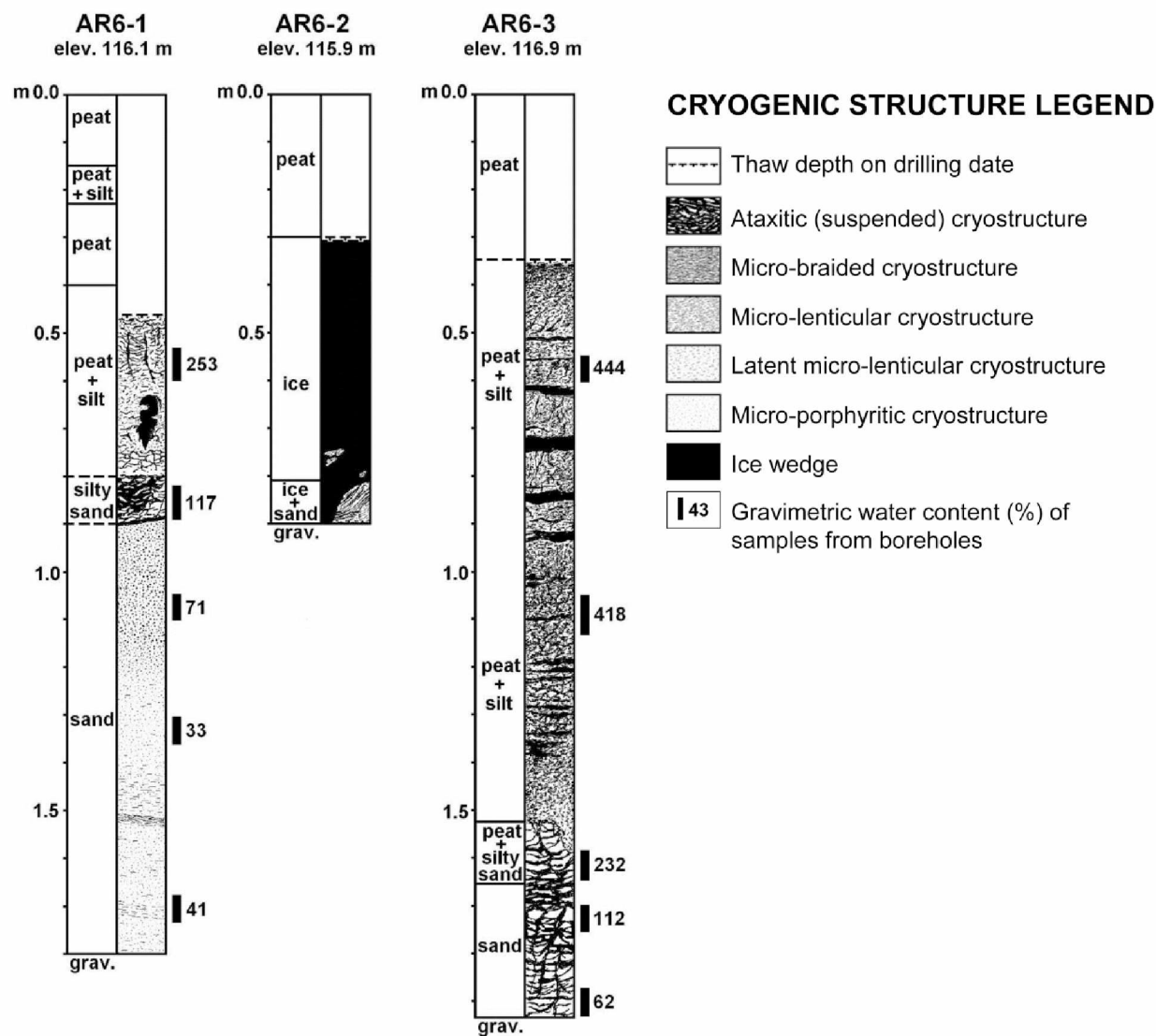


Figure 4.8: Cryostratigraphy and gravimetric water content (%) of frozen soils, site AR6 (Bridge).
All boreholes were drilled on September 10, 2010.

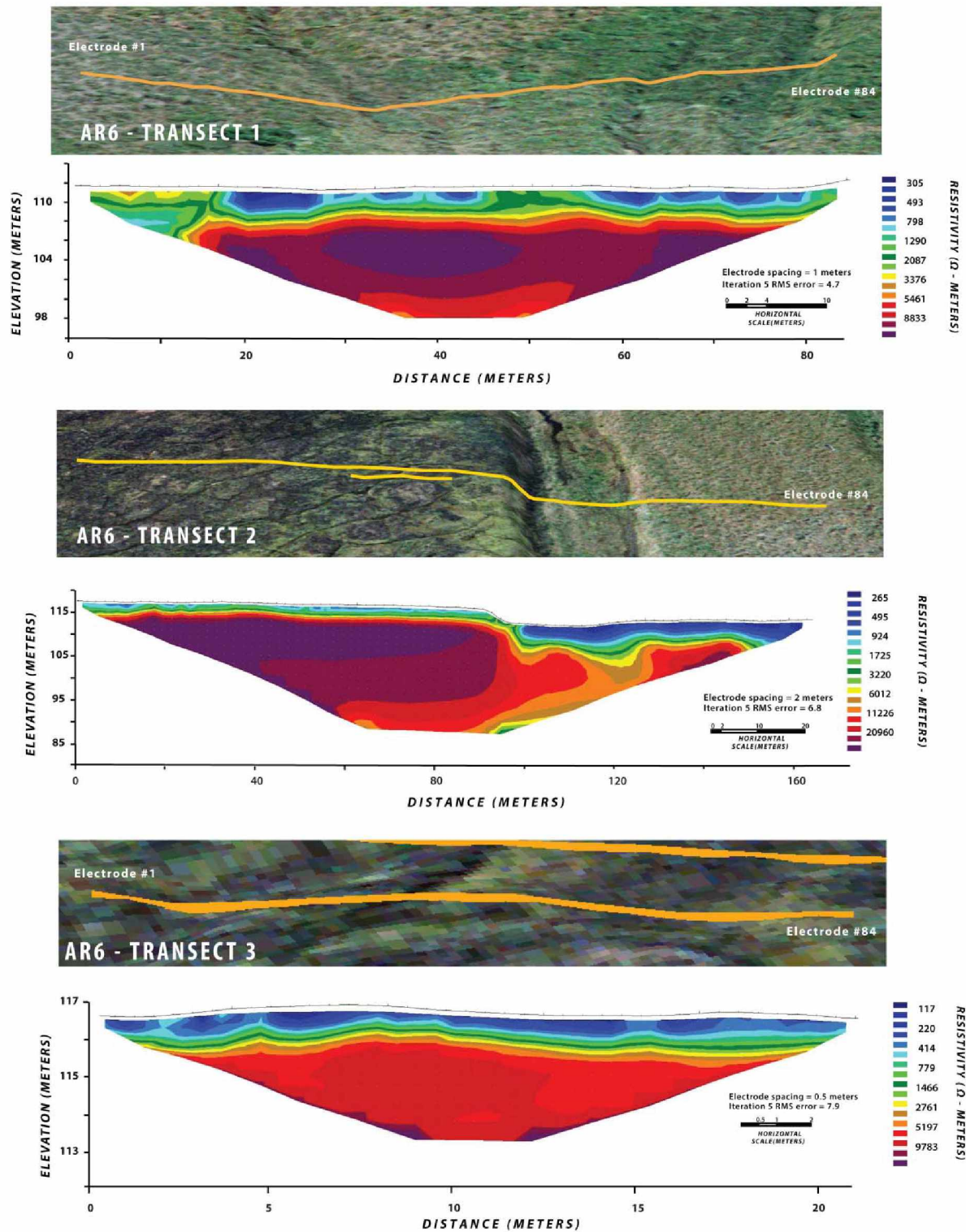


Figure 4.9: Draped aerial photographs of AR6 transects 1, 2 and 3 with their corresponding DCR-ERT modeled resistivity ($\Omega \cdot \text{m}$) below each



Figure 4.10: Top surface of the small ice wedge, borehole AR6-2

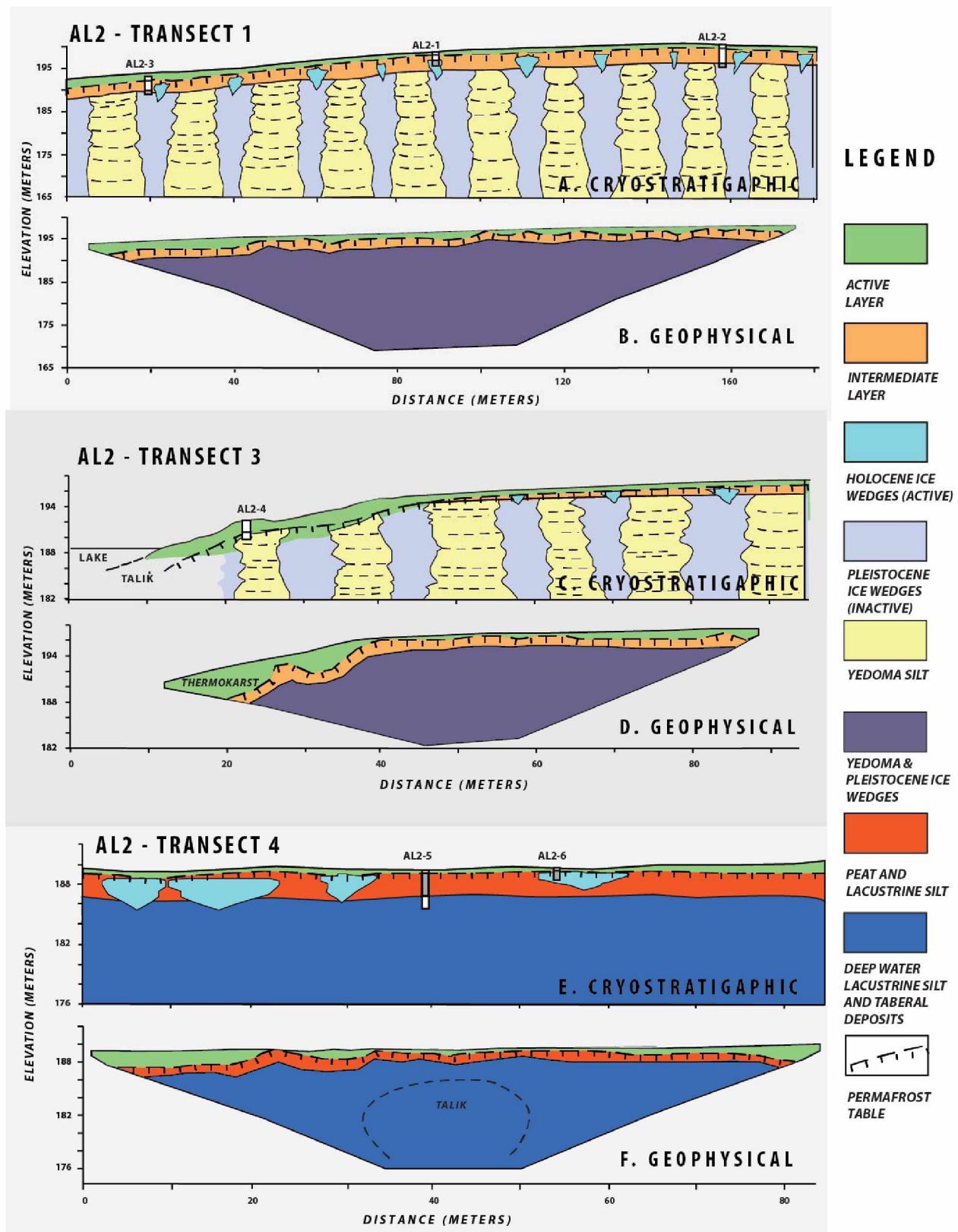


Figure 4.11: : Comparison of subsurface characteristics derived from cryostratigraphic analysis (A, C & E) vs. geophysical interpretation (B, D & F) for AL2 transects 1, 3 and 4

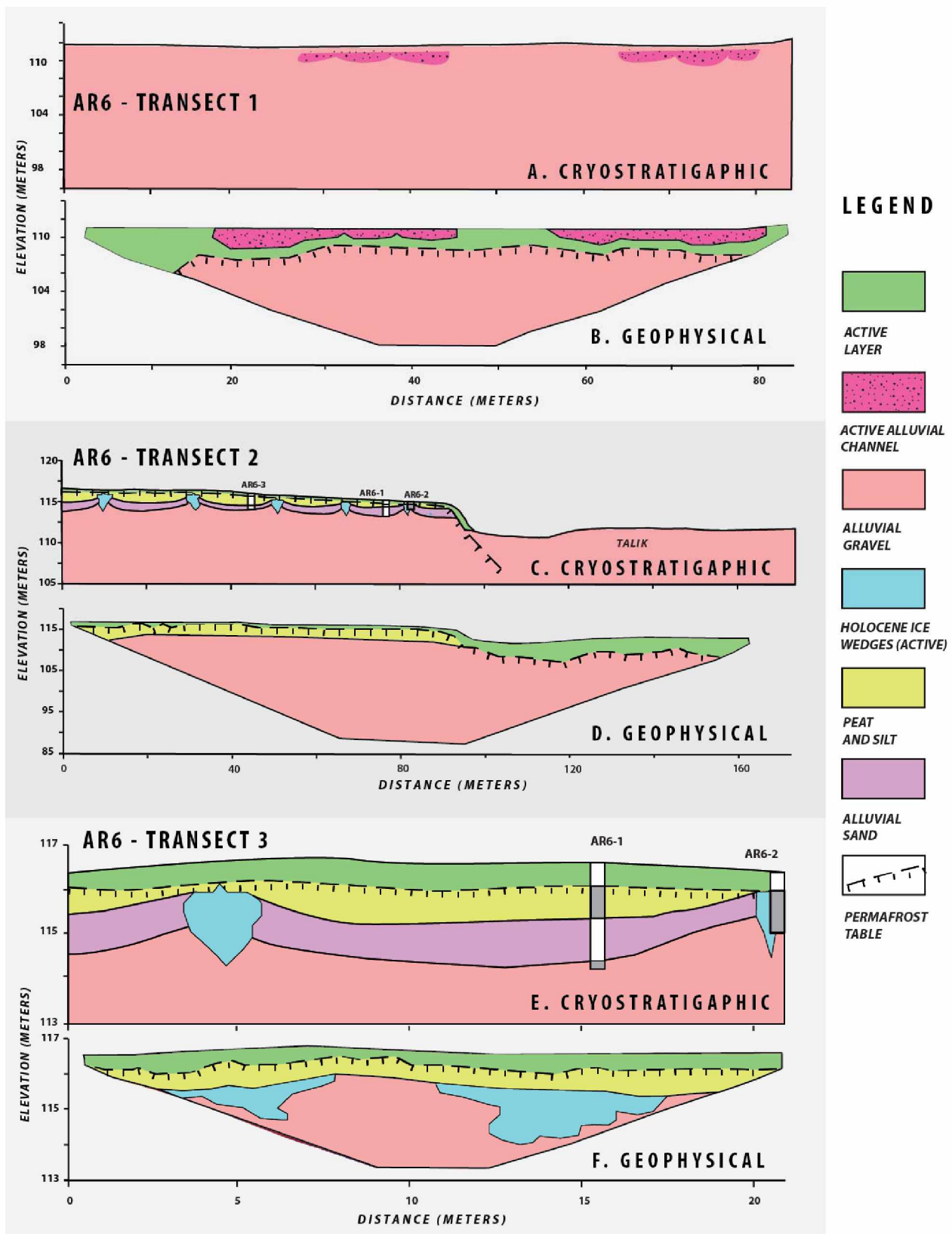


Figure 4.12: Comparison of subsurface characteristics derived from cryostratigraphic analysis (A, C & E) vs. geophysical interpretation (B, D & F) for AR6 transects 1, 2 and 3

Table 4.1: Site characteristics and descriptions of DCR-ERT, active layer depths and ice

Site	Description	Electrodes	Electrode Spacing (m)	Maximum Resolution Depth (m)	Resistivity (Ω m)		Average Active Layer Depth (cm)
					Min.	Max.	
AR6 #1	Anaktuvuk River Alluvial Plain	42	2	13	305	8833	--
AR6 #2	Burned Tussock Tundra to Flood Plain	84	2	25	265	20960	54
AR6 #3	Burned Tussock Tundra and Degrading High Centered Polygons	42	0.5	3.5	117	9703	48
AL2 #1	Burned Tussock Tundra on Gentle Slope	84	2	25	296	19370	55
AL2 #3	Burned Tussock Tundra and Thermokarst	42	2	14.5	62.4	12262	62
AL2 #4	Low & High Centered Polygons	84	1	13.5	121	10034	50

Conclusion

The motivation for this thesis was to advance how we examine the interactions between hydrology, geomorphology, ecology and permafrost on Arctic landscapes. Using robust, repeatable methods which are spatially scalable is a critical foundation for engaging in interdisciplinary research. I created a classification for water tracks to understand the geomorphic and biophysical properties of water tracks within the Kuparuk River basin and adjacent areas. I then used these water track classes as the basis for finding their spatial distribution using high-resolution remotely sensed imagery. I examined the effects of drainage networks in calculating LAI based on NDVI and how the accuracy and trends varied depending on the spatial resolution of the input imagery. I also used a combination of cryostratigraphic and geophysical data to characterize permafrost for Arctic road design and engineering.

In order to accomplish my objectives, I combined knowledge from a variety of fields including hydrology, remote sensing, engineering, permafrost, ecology and geomorphology. By unifying complimentary principles from a variety of fields, more complex questions could be answered while examining them through lenses of scale and laws of proximity. The key was to identify the primary driving forces so that questions and areas of emphasis could be targeted at specific areas using purposeful steps. These created frameworks to illuminate how location, timing and magnitude influence data and the interactions of the main patterns and processes. Ultimately this allowed complex, interdisciplinary questions to be answered with greater certainty and accuracy.

Five water track classes were developed using robust statistical methods which effectively partitioned a wide range of biophysical factors. This methodology represented a unique solution to minimize bias and maximize reliability for organizing, analyzing and interpreting complex data to obtain new information for classifying water tracks. Our interpretation revealed that water tracks are controlled primarily by surficial geology, although we found interactions among a wide range of factors. Water tracks represented a range of preferential flow paths in periglacial landscapes. Understanding how water tracks differ within a region in terms of their geomorphology is a critical factor in study designs for hydrology, ecology and permafrost investigations.

Both water track presence and different water track classes were identified mostly using WorldView-2 imagery. The mineral-flark, steep and narrow water tracks displayed a curvilinear shape and repeating pattern perpendicular to the hill slope. The highest accuracy and best ROC values were found for the organic-rich and wide water track classes. The biggest underlying issue was the complexity of the water track classes. Although they represent the geomorphic properties, they were classified using a combination of variables including vegetation, soil moisture, and surficial geology. The ability to map known water track geomorphic conditions provides a critical baseline for further investigations of landscape dynamics within a region. Given the complex interactions of these factors within the context of a changing Arctic climate, deriving and quantifying different water track classes offers a substantial step towards interpretation.

LAI was calculated using satellite-derived NDVI values by using optimization in the gap-probability model. The results showed that groups based on the presence/absence of water tracks and the magnitude of variation in NDVI over time had distinct LAI values even with variability over time. The effects of the groups were compared between WorldView-2 and Landsat-7 imagery where the LAI values were higher in the WorldView-2 results. This did not result in more accurate LAI estimates, as the Landsat-7 imagery had lower RMSE values. We concluded that the spatial resolution had an overall effect on the LAI values by substantially changing the nonlinear spectral mixing inputs. Future studies should be cognizant of the advantages and limitations offered by the increased spatial resolution on LAI calculations based on NDVI and modify their project design accordingly.

DCR-ERT transects with a Wenner array were a useful tool when combined with cryostratigraphy information for examining continuous permafrost characteristics pertinent to road construction in northern Alaska. The resistivity cross-sections derived using DCR-ERT were consistent with the terrain units, suggesting that terrain is a good indicator of the subsurface. Optimizing the electrode spacing to adjust the vertical depth and resolution of transects allowed the geophysical results to highlight differences in presence/absence of permafrost and estimate active and intermediate layer depths. Acquiring and compiling

geospatial (aerial photographs & DEMs) data with geophysical results permitted maximum contextualization of borehole data, and the order of acquisition may allow future projects to leverage data more effectively.

Both disciplinary and interdisciplinary research is rarely linear in execution. This thesis is a cumulative step forward towards understanding how and why water moves on Arctic landscapes. It required a broad approach as measuring water in streams or rivers is only a fraction of the knowledge required to scale between a channel and landscape dynamics. I also incorporated techniques like remote sensing and geophysics which could be reasonably applied over large areas. This was important not only for monitoring and evaluating for climate affects but also for engineering applications and future planning scenarios. The development of complementary approaches for Artic landscape characterization creates more realistic scenarios for the application of highly sophisticated numerical models where the physical parameters used accurately reflect those found on the landscape.

It is my hope that my research will contribute to a better understanding of the patterns and processes which connect Arctic science and engineering, and also contribute to improving methods for answering interdisciplinary research questions in Alaska and beyond.

References

- Bliss, L. C., Heal, O. W., Moore, J. J. and Programme, I. B., 1981. *Tundra Ecosystems: A Comparative Analysis*. Cambridge University Press.
- Blok, D., Heijmans, M. M. P. D., Schaepman-Strub, G., Ruijven, J., Parmentier, F. J. W., Maximov, T. C. and Berendse, F., 2011. The Cooling Capacity of Mosses: Controls on Water and Energy Fluxes in a Siberian Tundra Site. *Ecosystems*, 14(7): 1055-1065.
- Callaghan, T. V., Bjorn, L. O., Chernov, Y., Chapin, T., Christensen, T. R., Huntley, B., Ima, R. A., Johansson, M., Jolly, D., Jonasson, S., Matveyeva, N., Panikov, N., Oechel, W., Shaver, G., Schaphoff, S. & Sitch, S., 2004. Effects of changes in climate on landscape and regional processes, and feedbacks to the climate system. *Ambio*, 33(7): 10.
- Drury, W. H., 1956. Bog flats and physiographic processes in the upper Kuskokwim River region, Alaska. *Contributions from the Gray Herbarium of Harvard University*: 1-130.
- Ferrians, O. J., Kachadoorian, R. and Greene, G. W., 1969. Permafrost and related engineering problems in Alaska. In: U.S. Government of the Interior (Editor), *Geological Survey Professional Paper 678*. U.S. Government Printing Office, Washington, pp. 42.
- Fortier, D., Allard, M. and Shur, Y., 2007. Observation of rapid drainage system development by thermal erosion of ice wedges on Bylot island, Canadian Arctic Archipelago. *Permafrost and Periglacial Processes*, 18(3): 229-243.
- French, H. and Thorn, C. E., 2006. The changing nature of periglacial geomorphology. *Géomorphologie: relief, processus, environnement*(3/2006).
- French, H. M., 2000. Does Lozinski's periglacial realm exist today? A discussion relevant to modern usage of the term 'periglacial'. *Permafrost and Periglacial Processes*, 11(1): 35-42.

Golde, C. M. and Gallagher, H. A., 1999. The challenges of conducting interdisciplinary research in traditional doctoral programs. *Ecosystems*, 2(4): 281-285.

Hauck, C. and Kneisel, C., 2006. Application of capacitively-coupled and DC electrical resistivity imaging for mountain permafrost studies. *Permafrost and Periglacial Processes*, 17(2): 169-177.

Hinzman, L. D., Deal, C. J., McGuire, A. D., Mernild, S. H., Polyakov, I. V. and Walsh, J. E., 2013. Trajectory of the Arctic as an integrated system. *Ecological Applications*, 23(8): 1837-1868.

Hinzman, L. D., Gieck, R. E. and Kane, D. L., 2008. Spatial and temporal variation of soil temperatures and arctic hydrology in the Kuparuk River Basin, Alaska. In: D.L. Kane and K.M. Hinkel (Editors), Ninth International Conference on Permafrost. Institute of Northern Engineering, Fairbanks, AK, U.S., pp. 711-716.

Hobbie, J., 1997. History of Limnology in Alaska: Expeditions and Major Projects. In: A. Milner and M. Oswood (Editors), *Freshwaters of Alaska*. Ecological Studies. Springer New York, pp. 45-60.

Homan, J. W. and Kane, D. L., 2015. Arctic snow distribution patterns at the watershed scale. *Hydrology Research*, 46(4), pp. 507-520.

Jorgenson, M. T., Shur, Y. L. and Osterkamp, T. E., 2008. Thermokarst in Alaska. In: D. L. Kane and K. M. Hinkel (Editors), Ninth International Conference on Permafrost. Institute of Northern Engineering, Fairbanks, AK, pp. 869-876.

Lachenbruch, A. H. and Marshall, B. V., 1986. Changing Climate: Geothermal Evidence from Permafrost in the Alaskan Arctic. *Science*, 234(4777): 689-696.

McNamara, J. P., Kane, D. L. and Hinzman, L. D., 1999. An analysis of an arctic channel network using a digital elevation model. *Geomorphology*, 29: 339-353.

Munger, C. A., Walker, D. A., Maier, H. A. and Hamilton, T. D., 2008. Spatial analysis of glacial geology, surficial geomorphology, and vegetation in the Toolik Lake region: Relevance to past and future land-cover changes. In: D. L. Kane and K. M. Hinkel (Editors), Ninth International Permafrost Conference. Institute of Northern Engineering, Fairbanks, AK, pp. 1255-1260.

Osterkamp, T. E., 2007. Characteristics of the recent warming of permafrost in Alaska. *Journal of Geophysical Research-Earth Surface*, 112(F2).

Osterkamp, T. E., 2008. Thermal state of permafrost in Alaska during the fourth quarter of the twentieth century. In: D. L. Kane and K. M. Hinkel (Editors), Ninth International Conference on Permafrost. Institute of Northern Engineering, Fairbanks, AK, U.S., pp. 1333-1338.

Prowse, T. D., Wrona, F. J., Reist, J. D., Gibson, J. J., Hobbie, J. E., Levesque, L. M. J. and Vincent, W. F., 2006. Climate change effects on hydroecology of Arctic freshwater ecosystems. *Ambio*, 35(7): 347-358.

Schramm, I., Boike, J., Bolton, W. R. and Hinzman, L. D., 2007. Application of TopoFlow, a spatially distributed hydrological model, to the Imnavait Creek watershed, Alaska. *Journal of Geophysical Research-Biogeosciences*, 112(G4): 1-14.

Serreze, M. C., Walsh, J. E., Chapin, F. S., Osterkamp, T., Dyurgerov, M., Romanovsky, V., Oechel, W. C., Morison, J., Zhang, T. and Barry, R. G., 2000. Observational evidence of recent change in the northern high-latitude environment. *Climatic Change*, 46(1-2): 159-207.

Slaymaker, O., 2011. Criteria to distinguish between periglacial, proglacial and paraglacial environments. *Quaestiones Geographicae*, 30(1): 85-94.

Stoeckeler, E. G., 1949. Identification and evaluation of Alaskan vegetation from airphotos with reference to soil, moisture and permafrost conditions, U.S. Army Corps of Engineers, St. Paul, Minnesota, St. Paul District.

Walker, D., Hamilton, T., Ping, C., Daanen, R. and Streever, W., 2008. Dalton Highway Field Trip Guide for the Ninth International Conference on Permafrost. Alaska Division of Geological & Geophysical Surveys, Guidebook, 9.

Walker, M. D., Walker, D. A. and Auerbach, N. A., 1994. Plant communities of a tussock tundra landscape in the Brooks Range Foothills, Alaska. *Journal of Vegetation Science*, 5: 843-866.

White, D., Hinzman, L., Alessa, L., Cassano, J., Chambers, M., Falkner, K., Francis, J., Gutowski, W.J., Holland, M., Holmes, R.M., Huntington, H., Kane, D., Kliskey, A., Lee, C., McClelland, J., Peterson, B., Rupp, T.S., Straneo, F., Steele, M., Woodgate, R., Yang, D., Yoshikawa, K. and Zhang, T., 2007. The arctic freshwater system: Changes and impacts. *Journal of Geophysical Research-Biogeosciences*, 112(G4): 21.